Article

Current Biology

Store-independent activation of STIM1-ORAI1 by SPCA2 determines the basal CFTR activity in secretory epithelial cells

Graphical abstract

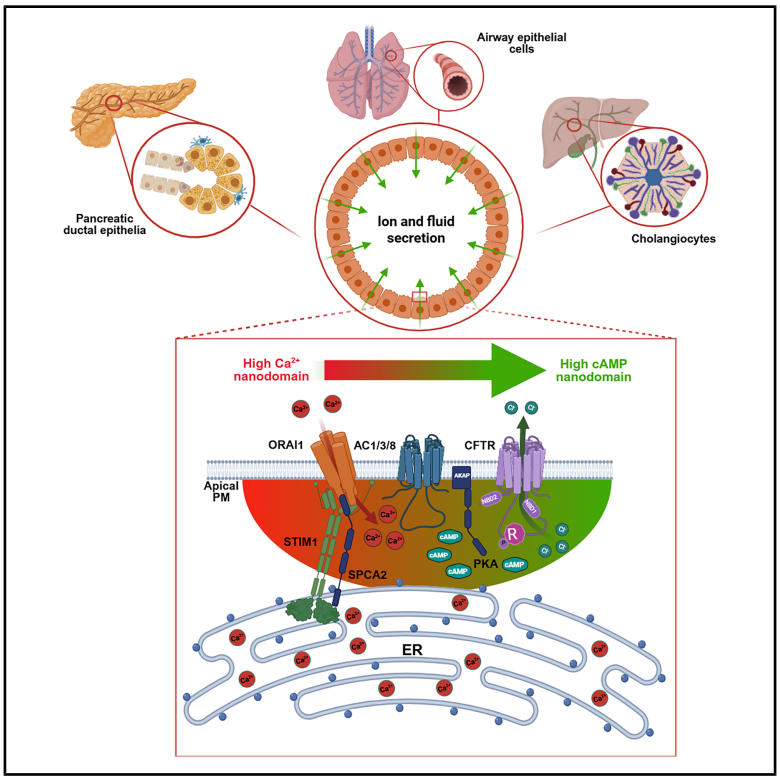

Highlights

- An apical nanodomain in epithelial cells includes SPCA2, STIM1/ORAI1, ACs, and CFTR
- SPCA2 maintains constitutive Ca^{2+} entry via ORAI1 in secretory epithelial cells
- SPCA2 increases the ORAI1 current and enhances the interaction between STIM11 and ORAI1
- SICE regulates basal, unstimulated CFTR activity in secretory epithelial cells

Authors

Aletta Kiss, Árpád Varga, Marietta Görög, ..., Miklós Erdélyi, Shmuel Muallem, József Maléth

Correspondence

jozsefmaleth1@gmail.com or maleth.jozsef@med.u-szeged.hu

In brief

Kiss et al. identify an apical membrane nanodomain containing SPCA2, STIM1/ORAI1, adenylyl cyclases, and CFTR in secretory epithelial cells, where SPCA2 drives constitutive, store-independent yet STIM1-dependent ORAI1 Ca^{2+} influx that converts local Ca^{2+} signals into cAMP to maintain basal CFTR activation and ion secretion in unstimulated cells.

Kiss et al., 2025, Current Biology *35*, 1–18
October 20, 2025
https://doi.org/10.1016/j.cub.2025.09.006

CellPress

Please cite this article in press as: Kiss et al., Store-independent activation of STIM1-ORAI1 by SPCA2 determines the basal CFTR activity in secretory epithelial cells, Current Biology (2025), https://doi.org/10.1016/j.cub.2025.09.006

Current Biology

CellPress
OPEN ACCESS

Article

Store-independent activation of STIM1-ORAI1 by SPCA2 determines the basal CFTR activity in secretory epithelial cells

Aletta Kiss,[1,2,3,9] Árpád Varga,[1,2,3,9] Marietta Görög,[1,2] Tamara Madácsy,[1,2,3] Woo Young Chung,[4] Petra Pallagi,[1,2,3] Viktória Szabó,[1,2,3] Petra Susánszki,[1,2] Enikő Kúthy-Sutus,[1,2,3] Dániel Varga,[5] Péter Bíró,[5] Ingrid Hegnes Sendstad,[1,2,3] Tim Crul,[1,2,3] Boldizsár Jójárt,[1,2,3] Bálint Tél,[1,2,6] Zsófia Horváth,[1,2] Szintia Barnai,[1,2] Anita Balázs,[7] György Lázár,[8] Miklós Erdélyi,[5] Shmuel Muallem,[4] and József Maléth[1,2,3,10,*]

[1]Department of Medicine, University of Szeged, Szeged 6720, Hungary
[2]HAS-USZ Momentum Epithelial Cell Signaling and Secretion Research Group, University of Szeged, Szeged 6720, Hungary
[3]HCEMM-SZTE Molecular Gastroenterology Research Group, University of Szeged, Szeged 6720, Hungary
[4]National Institute of Dental and Craniofacial Research, National Institutes of Health, Bethesda, MD 20892, USA
[5]Department of Optics and Quantum Electronics, Faculty of Science and Informatics, University of Szeged, Szeged 6720, Hungary
[6]First Department of Pediatrics, Semmelweis University, Budapest 1085, Hungary
[7]Department of Pediatric Pulmonology, Immunology and Intensive Care Medicine, Charité – Universitätsmedizin Berlin, Berlin 13353, Germany
[8]Department of Surgery, University of Szeged, Szeged 6720, Hungary
[9]These authors contributed equally
[10]Lead contact
*Correspondence: jozsefmaleth1@gmail.com or maleth.jozsef@med.u-szeged.hu
https://doi.org/10.1016/j.cub.2025.09.006

SUMMARY

Cystic fibrosis transmembrane conductance regulator (CFTR) determines epithelial ion secretion, which is fundamental in various organs. The synergy between cyclic AMP (cAMP) and Ca^{2+} signaling fine-tunes CFTR-mediated secretion; however, the organization of such signaling complexes and their physiological impact remained largely unknown. Here, we identified an apical membrane signaling complex consisting of secretory pathway Ca^{2+}-ATPase (SPCA2), stromal interaction molecule 1 (STIM1)/ORAI1, adenylyl cyclases, and CFTR. In this complex, SPCA2 facilitates constitutive, store-independent but STIM1-dependent ORAI1-mediated Ca^{2+} influx by activating ORAI1 and promoting STIM1/ORAI1 interaction, which is essential for basal CFTR function. Analysis by super-resolution dSTORM revealed constitutive organization of the proteins in a nanodomain on the apical membrane, which translates local Ca^{2+} increases to cAMP elevation and CFTR activation in unstimulated cells required for ion secretion. The same system operates in the pancreas, airways, and liver. Our findings reveal an essential, self-directing regulatory mechanism of CFTR-mediated ion secretion in secretory epithelial cells, independent from neurohormonal stimuli.

INTRODUCTION

Secretory epithelial cells are essential orchestrators of organ physiology by determining the composition and volume of bodily fluids via vectorial transport of ions and water. This tightly regulated secretion is achieved by the polarized expression of secretory and regulatory proteins[1] and is primarily determined by the interplay between the Ca^{2+} and cyclic AMP (cAMP) signaling.[2] In non-excitable cells, the receptor-evoked Ca^{2+} signaling incorporates the release of the endoplasmic reticulum (ER) Ca^{2+} stores via inositol 1,4,5-trisphosphate (IP_3) receptors (IP_3Rs) followed by the influx of the extracellular Ca^{2+} through store-operated Ca^{2+} entry (SOCE). SOCE is initiated by the ER Ca^{2+} sensor stromal interaction molecule 1 (STIM1), which changes conformation upon the release of the Ca^{2+} ions from the N-terminal EF hands, leading to multimerization and localization of STIM1 at the ER/plasma membrane (PM) contact sites.[3] This triggers the assembly and activation of the PM Ca^{2+} channel ORAI1, leading to extracellular Ca^{2+} influx,[4] which provides Ca^{2+} to refill the ER stores via the sarco/ER Ca^{2+}-ATPase (SERCA) pumps. By being one of the most versatile signal transduction pathways, SOCE can participate directly in regulating physiological processes. As an example, ORAI1-mediated extracellular Ca^{2+} influx was recently described as a critical regulator of the agonist-induced Cl^- secretion by anoctamin 1 (ANO1)—a Ca^{2+}-activated Cl^- channel—in eccrine sweat glands[5] and activation of the NFAT gene program in virtually all cells.[6] Although STIM1 is the primary activator of ORAI1, there is evidence that Ca^{2+} influx, perhaps by ORAI1 activation in a STIM1-independent manner or activation of ORAI1 that is not initiated by STIM1 clustering. For example, pathogenic gain-of-function mutations can activate ORAI1 independently of STIM1.[7] Additionally, the interaction of ORAI1 with other proteins, such as the secretory pathway Ca^{2+}-ATPase 2 (SPCA2), can initiate STIM1-independent ORAI1 activation.[8–10]

Please cite this article in press as: Kiss et al., Store-independent activation of STIM1-ORAI1 by SPCA2 determines the basal CFTR activity in secretory epithelial cells, Current Biology (2025), https://doi.org/10.1016/j.cub.2025.09.006

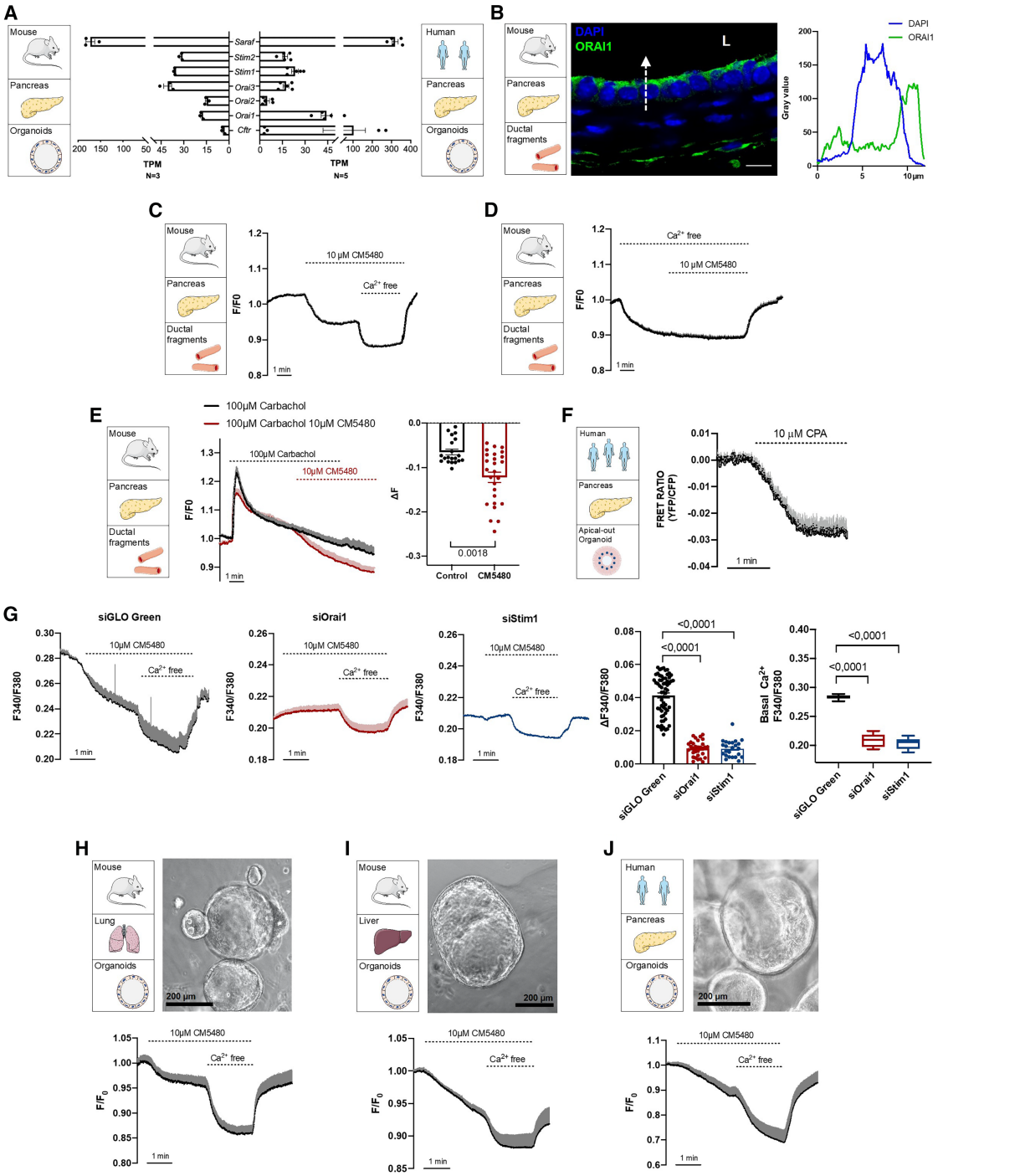

Figure 1. ORAI1 Ca^{2+} channel is constitutively active in primary polarized pancreatic ductal epithelial cells

Q11 (A) Expression level of SOCE-related genes in mouse ($N = 3$) and human ($N = 5$) pancreas organoids. All data are given in TPM. The TPM values of the human *CFTR* gene were published previously.[28]

(B) Representative confocal image and line profile analysis of ORAI1 protein in primary isolated pancreatic ductal fragments (scale bar: 10 μm).

(C) Intracellular Ca^{2+} levels were monitored using Fura 2-AM in unstimulated murine ductal fragments where treatment with 10 μM CM5480, a pharmacological inhibitor of ORAI1, resulted in a marked decrease in basal Ca^{2+} levels.

(D) Removal of extracellular Ca^{2+} resulted in a decreased intracellular Ca^{2+} level in isolated ductal fragments, which was not reduced further by subsequent treatment with 10 μM CM5480.

(E) 100 μM carbachol was applied to induce a peak-plateau Ca^{2+} signal. The administration of 10 μM CM5480 disrupted the plateau phase of the signal as demonstrated by average traces and bar chart.

(legend continued on next page)

Please cite this article in press as: Kiss et al., Store-independent activation of STIM1-ORAI1 by SPCA2 determines the basal CFTR activity in secretory epithelial cells, Current Biology (2025), https://doi.org/10.1016/j.cub.2025.09.006

This STIM1-independent mechanism raises the possibility that Orai1 can be activated by SPCA2 alone; however, it does not rule out the existence of STIM1-dependent pathways for SPCA2-mediated activation. Therefore, the potential mechanism of ORAI1 activation that is not initiated by STIM1 has yet to be understood. Even if proteins like SPCA2 directly activate ORAI1, the function of STIM1 in triggering the change in ORAI1 localization might be required. Furthermore, recent studies have identified a functional complex consisting of SPCA2, the Kv10.1 potassium channel, and ORAI1. In this complex, SPCA2 enhances the membrane expression of Kv10.1 and ORAI, and the activity of all three proteins is necessary to mediate store-independent Ca^{2+} entry (SICE) that maintains the activation of the pro-survival pathway in breast cancer cells.[11,12] Cross et al. reported that the massive basolateral Ca^{2+} influx into mammary epithelia is mediated by SICE, which supports the large Ca^{2+} transport requirements for milk secretion.[9] Moreover, the potential role of SPCA2-mediated ORAI1 activation was reported in cell proliferation.[10] However, the physiological role of SICE that is not initiated by STIM1 clustering is only partially known. One of the goals of the present work is to address these questions.

The ion transport processes in secretory epithelial cells are primarily determined by the activity of the cystic fibrosis transmembrane conductance regulator (CFTR) Cl^- channel, which represents the rate-limiting step for anion (Cl^- and HCO_3^-) secretion.[13] Therefore, CFTR regulates both the amount and composition of epithelial secretions such as airway surface liquid, pancreatic juice, bile, and sweat, which play vital physiological roles in the innate defense of the lungs,[14] digestion of food,[15] and body temperature regulation.[16] The crucial importance of proper CFTR function is further emphasized by diseases associated with CFTR dysfunction, such as cystic fibrosis or cholera.[17] CFTR activation involves the phosphorylation of the R domain by protein kinase A (PKA),[18–21] which is followed by the ATP binding and conformational change of the nucleotide-binding domains (NBDs), leading to channel opening.[22] The activity of PKA is determined by the local cAMP concentration, which is generated by adenylyl cyclases (ACs) and hydrolyzed by phosphodiesterases (PDEs). Recent studies suggest that ACs and PDEs organize into nanodomains, ensuring the compartmentalization of the cAMP signals and thus the specificity of the agonist-evoked response.[23] It is also well established that in secretory epithelial cells, the cAMP/PKA pathway interacts at multiple levels with the intracellular Ca^{2+} signaling to control and tune the activity of each other, which facilitates maximal response but also prevents the overshoot of the signaling that could lead to cell damage.[2,24] Previously, a direct interaction was identified between the Ca^{2+}-stimulated adenylyl cyclase 8 (AC8) and ORAI1 via the N termini of the proteins, which determined the activity and subcellular distribution of AC8 in HEK293 cells.[25] Additionally, the co-localization of CFTR and ORAI1 in overlapping PM microdomains was suggested based on indirect evidence.[26] These reports shed light on the sophisticated organization of the signaling complexes to coordinate synergism between Ca^{2+} and cAMP signals that determine the activity of epithelial ion secretion. However, the precise organization and temporal dynamics of such signaling complexes in primary polarized cells and their impact on epithelial cell physiology remained largely unknown.

In this study, we aimed to understand the physiological role of the ORAI1-mediated Ca^{2+} influx in polarized epithelial cells and understand the complex regulation of epithelial ion secretion with a particular focus on controlling CFTR activity by the intracellular Ca^{2+} signaling. Remarkably, we demonstrated that ORAI1-mediated Ca^{2+} entry is constitutively active in secretory epithelial cells derived from the pancreas, lung, and liver, independently from the depletion of the intracellular Ca^{2+} stores. The constitutive, STIM1-dependent ORAI1 activity is maintained by SPCA2, which increases the STIM1-ORAI1 clustering and ORAI1 current in unstimulated cells. We demonstrate that ORAI1 co-localizes with CFTR in nanodomains of the apical PM and determines the activity of CFTR in secretory epithelial cells. Finally, we showed that the regulation of CFTR by ORAI1 involves Ca^{2+}/calmodulin-stimulated AC1, 3, and 8, located in the same protein nanodomain as CFTR and ORAI1.

RESULTS

ORAI1-mediated extracellular Ca^{2+} entry is constitutively active in primary polarized epithelial cells

To establish the role of SOCE in secretory epithelial cells, we first determined the expression of key signaling components using RNA sequencing of human and mouse pancreatic ductal organoids.[27] Transcriptome analysis, confirmed by endpoint PCR, revealed expression of all 3 *Orai* family members (*Orai1/2/3*), the ER Ca^{2+} sensors *Stim1* and *Stim2* and the regulator protein *Saraf* (Figures 1A and S2A). ORAI1 was primarily localized on the apical PM with a low level in the basolateral membrane of pancreatic ductal cells, as demonstrated in cross-sections of mouse isolated ductal fragments (Figure 1B). Interestingly, administration of the selective ORAI1 inhibitor CM5480 in the presence of 1 mM extracellular Ca^{2+} to mouse isolated ductal fragments markedly reduced the intracellular Ca^{2+} concentration ($[Ca^{2+}]_i$) of epithelial cells without prior ER Ca^{2+} store depletion (Figure 1C). On the other hand, removing the extracellular Ca^{2+} triggered a marked drop of $[Ca^{2+}]_i$, which was not further decreased by CM5480 (Figure 1D). This constitutive activity was not observed in pancreatic acinar cells, although the ER Ca^{2+} depletion triggered the ORAI1-mediated extracellular Ca^{2+} influx as expected (Figures S2B and S2C). CM5480 and GSK-7975A, which is another selective ORAI1 inhibitor,

(F) Average traces of 3 individual FRET experiments after D1ER sensor transfection into apical-out human pancreatic organoids demonstrate that the Ca^{2+} stores are not depleted, as indicated by the decreasing FRET ratio (YFP/CFP) in response to 10 μM CPA.
(G) The effect of 10 μM CM5480 was abolished by *siOrai1* and *siSim1* treatment. The same genetic perturbations decreased the basal Ca^{2+} level significantly.
(H–J) Average traces of 3–5 experiments are demonstrated in each indicated Ca^{2+} measurement. Transmitted light microscopy images of cystic organoids in mouse lung (H), mouse liver (I), and human pancreatic cultures (J). ORAI1 inhibition significantly decreased the resting intracellular Ca^{2+} level in mouse lung (H), mouse liver (I), and human pancreatic organoid cultures (OCs) (J). Average traces of 3–4 experiments were carried out on each biological sample types.
See also Figure S2.

Please cite this article in press as: Kiss et al., Store-independent activation of STIM1-ORAI1 by SPCA2 determines the basal CFTR activity in secretory epithelial cells, Current Biology (2025), https://doi.org/10.1016/j.cub.2025.09.006

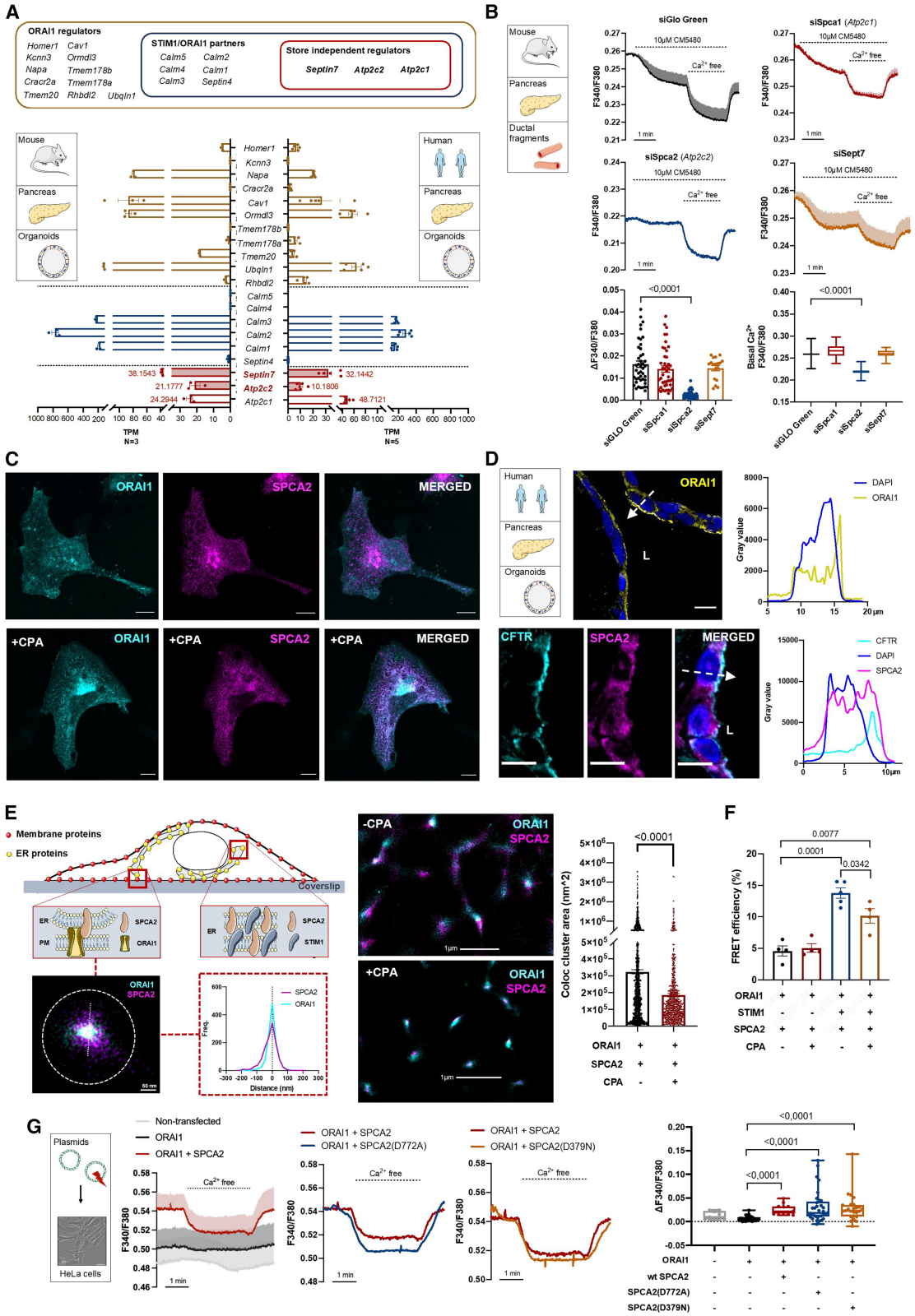

Figure 2. SPCA2 regulates constitutive ORAI1 activity in primary polarized epithelial cells

(A) Expression profile of ORAI1 regulators (brown), STIM1/ORAI1 interacting partners (blue), and store-independent ORAI1 regulators (red) in mouse ($N = 3$) and human ($N = 5$) pancreas OCs.

(legend continued on next page)

Please cite this article in press as: Kiss et al., Store-independent activation of STIM1-ORAI1 by SPCA2 determines the basal CFTR activity in secretory epithelial cells, Current Biology (2025), https://doi.org/10.1016/j.cub.2025.09.006

significantly impaired the $[Ca^{2+}]_i$ increase in response to carbachol stimulation when administrated during the plateau phase of the signal in ductal epithelial cells (Figures 1E and S2D–S2F). To rule out that the ER Ca^{2+} stores were artificially depleted, we directly measured the ER Ca^{2+} store content by transfecting the primary epithelial cells in human pancreatic apical-out organoids with the genetically encoded Ca^{2+} sensor D1ER (Figure S2G).[28,29] We detected a rapid decrease in the D1ER fluorescence resonance energy transfer (FRET) ratio upon ER store depletion with 10 μM CPA (Figure 1F); in contrast, 10 μM CM5480 had no detectable effect (Figure S2H). To further confirm this, isolated ductal fragments and mouse and human apical-in and human apical-out organoids loaded with Mag-Fluo-4 showed a rapid decrease upon treatment with 25 μM CPA or 10 μM ionomycin in Ca^{2+}-free solution (Figure S2I). These control experiments provided confirmation that the ER Ca^{2+} stores of the primary epithelial cells were not depleted. Importantly, gene knockdown by siOrai1 and siStim1 abolished the response to CM5480 in the primary ductal cells and reduced the basal $[Ca^{2+}]_i$ that was significantly impaired in both cases, compared with the siGLO green transfected controls (Figure 1G). The residual reduction in $[Ca^{2+}]_i$ in response to extracellular Ca^{2+} removal was retained in siStim1- and siOrai1-treated cells. To test if constitutive ORAI1 activity is specific to pancreatic cells or common among secretory epithelia, we generated airway and liver organoids from mice and pancreatic organoids from human cadaver donors. Ductal epithelial identity was confirmed by cytokeratin 19 (CYT19) immunofluorescence (Figure S2J). In unstimulated mouse lung (Figure 1H) and liver (Figure 1I) and in human pancreatic organoids (Figure 1J), the inhibition of ORAI1 with 10 μM CM5480 resulted in a prominent decrease of $[Ca^{2+}]_i$. These experiments revealed that the ORAI1-mediated extracellular Ca^{2+} influx is constitutively active in primary mouse and human secretory epithelial cells that significantly contribute to the maintenance of basal $[Ca^{2+}]_i$.

SPCA2 maintains constitutive ORAI1 activity in primary epithelial cells

In the next step, we examined the whole transcriptome of mouse and human pancreatic organoids for unbiased analysis of the potential regulatory components that maintain the constitutive activity of ORAI1. The sequencing identified transcripts of several STIM1/ORAI1-interacting proteins in pancreatic organoids, and among these, three different store-independent regulators—*Spca1–2* (also known as *Atp2c1–2*) and *Septin7*—were determined (Figure 2A). A previous study described a possible role of SPCA2—a member of the SPCA family—in a store-independent ORAI1-mediated Ca^{2+} entry in breast cancer cells.[10] SEPTIN7 emerged as a potential store-independent negative modulator of part of the extracellular Ca^{2+} influx.[30] Of note, previous studies identified a pancreatic acinar cell-specific isoform of SPCA2 (termed SPCA2C),[31,32] which was not found in pancreatic ductal cells. According to the Human Proteome Atlas, pancreatic ductal cells express the full-length SPCA2.[33] In addition, previous studies suggested that both the N′- and C′-terminal domains of SPCA2 have important functions in the protein-protein interactions.[12] Therefore, in this study, we focused on the full-length SPCA2. To test the role of these proteins in primary epithelial cells, we treated mouse ductal fragments with small interfering RNA (siRNA), for *Spca1*, *2*, and *Septin7*, and measured the changes in $[Ca^{2+}]_i$. In these series of experiments, siSPCA2 treatment lowered the basal $[Ca^{2+}]_i$ and significantly decreased the constitutive ORAI1-mediated extracellular Ca^{2+} influx in unstimulated mouse primary ductal epithelial cells, whereas siSPCA1 or siSEPT7 had no effect when compared with the siGLO green transfected control (Figure 2B). To understand the role of SPCA2 in the regulation of ORAI1, we analyzed the intracellular distribution of SPCA2 and ORAI1 in transiently transfected HeLa cells. In these cells, ORAI1 showed partial puncta formation, whereas SPCA2 showed a reticular ER-like expression pattern in unstimulated cells (Figure 2C). Notably, this expression pattern was not changed by the depletion of the ER Ca^{2+} stores with 10 μM CPA. SPCA2 showed a marked co-localization with ORAI1 and SERCA2 and with the ER marker calreticulin (Figure S3A). Whereas with the Golgi (golgin) and vesicular (Lamp1) markers, the co-localization was markedly lower, suggesting that SPCA2 is localized to the ER. For immunolocalization of ORAI1 and SPCA1 and 2 in primary epithelial cells, human pancreatic organoids were used. ORAI1 displayed an apical membrane localization as described previously.[34] SPCA1 localized in intracellular compartments, likely the perinuclear Golgi, supporting that SPCA1 does not regulate SICE. SPCA1 localized in distinct intracellular compartments, presumably in the perinuclear Golgi, consistent with previous findings[8] (Figure S3B). On the other hand, SPCA2 displayed both an intracellular expression pattern with significant apical presence. Owing to antibody incompatibility, the co-staining of ORAI1 and SPCA2 was not possible, therefore CFTR Cl^- channel was used as an apical membrane marker (Figure 2D). This expression pattern of SPCA2 was also

(B) Average traces and plots show the effect of siRNA perturbation (*Spca1*, *Spca2*, *Sept7*) on the resting intracellular Ca^{2+} level in mouse pancreatic ductal fragments.
(C) Representative confocal image demonstrates the localization and distribution of ORAI1 and SPCA2 in co-transfected HeLa cells with and without 10 μM CPA treatment (white color represents the overlapping areas).
(D) Representative confocal image and line profile analysis demonstrate the localization of ORAI1 and of CFTR and SPCA2 in human pancreatic organoids (scale bar: 10 μm; L, luminal/apical side).
(E) Schematic figure and dSTORM images and histogram demonstrate the physical proximity of ORAI1-SPCA2 in the focal plane of the PM. Super-resolution images and high-throughput cluster analysis show significantly decreased cluster area values upon 10 μM CPA treatment.
(F) The calculated FRET efficiency from FLIM measurements between ORAI1 and SPCA2 is presented in a bar chart.
(G) HeLa cells were transfected with wild-type ORAI1 and wild-type or mutant (D772A or D379N) SPCA2-carrying plasmids. Average traces and bar charts demonstrate that ORAI1 alone resulted in lower basal Ca^{2+} levels compared with co-transfected cells. None of the introduced SPCA2 mutations altered the significantly increased basal Ca^{2+} levels and Ca^{2+} influx caused by the co-transfection. Average traces of 3–4 experiments are demonstrated in each indicated measurement.
See also Figure S3.

Please cite this article in press as: Kiss et al., Store-independent activation of STIM1-ORAI1 by SPCA2 determines the basal CFTR activity in secretory epithelial cells, Current Biology (2025), https://doi.org/10.1016/j.cub.2025.09.006

confirmed in 2D adherent cell culture generated from the 3D organoids (Figure S3C). To further assess the co-localization of ORAI1 and SPCA2, we used super-resolution microscopy. dSTORM images confirmed partial co-localization of the SPCA2-ORAI1 clusters in resting and stimulated cells as well (Figures 2E and S3D). Of note, the clusters of SPCA2 displayed a reticular expression pattern, whereas ORAI1 clusters were more compact in unstimulated cells. In cells stimulated with 10 μM CPA, the co-cluster area significantly decreased. The criteria for co-clusters were defined based on the extent of the ER-PM contact sites.[35] Clusters of two proteins of interest were counted as co-clusters if the individual clusters were located within a maximal size of 300 nm. This observation was further investigated by fluorescent lifetime measurement (FLIM) based on the determination of FRET efficiency using SPCA-GFP (donor) and ORAI1-mCherry (acceptor). These experiments revealed that the fluorescent lifetime of the donor molecule increased after photobleaching the acceptor (Figures S3E and S3F). Moreover, the measurements revealed that SPCA2 and ORAI1 are in physical proximity in unstimulated cells (FRET efficiency: 4.61%), which was not increased further by CPA stimulation (Figure 2F). In contrast, the presence of STIM1 was sufficient to remarkably increase the FRET between ORAI1 and SPCA2, which was again not increased further by CPA stimulation. In the latter case, we even detected a moderate decrease in the FRET, which could be explained by the competition of STIM1 with SPCA2 for the binding sites of ORAI1. As SPCA2 does not participate in SOCE, it is not unexpected that CPA stimulation does not increase the SPCA2-ORAI1 interaction. To determine whether the effect of SPCA2 on the constitutive Ca^{2+} influx is dependent on its ATPase or Ca^{2+} pumping ability, we tested SPCA2(D379N) (that lacks ATPase activity) and SPCA2(D772A) (that has disrupted the Ca^{2+}-binding site)[10] (Figure S3G). Expression of ORAI1 and SPCA2 generated a constitutively active Ca^{2+} influx, which was not affected by the SPCA2 mutants (Figure 2G). These results suggest that SPCA2 regulates the SICE via ORAI1 independently from SPCA2 Ca^{2+} pumping ability, leading to constitutive extracellular Ca^{2+} influx in epithelial cells.

SPCA2 increases the ORAI1 current in the absence and presence of STIM1

It is assumed that SPCA2 activates ORAI1 in a STIM1-independent manner.[10] However, similar inhibition of the constitutive Ca^{2+} influx by siSTIM1 and siSPCA2 suggests that SPCA2 can also enhance the ORAI1-mediated Ca^{2+} influx when activated by STIM1. We tested this directly by measuring the ORAI1 current in HEK293T cells. Co-expression of ORAI1 with SPCA2 was reported to show a small Ca^{2+} influx, about 10% of the Ca^{2+} influx measured after store depletion.[10] In initial experiments, when expressing ORAI1 alone or ORAI1 with SPCA2, we failed to detect any current, likely because of the very low ORAI1 conductance and inhibition of the native store-operated Ca^{2+} influx when ORAI1 alone is expressed.[36] Therefore, we tested if SPCA2 can also act on the STIM1-ORAI1 complexes, and Figures 3A–3D show that SPCA2 did increase the STIM1-ORAI1 current density and caused a delayed increase in the rate of current inactivation. Next, we used the constitutively active ORAI1(V102C) mutant to test the effect of SPCA2 on the current. Figures 3E–3H show that SPCA2 increased the current density of ORAI1(V102C) and again revealed slow current inactivation. Thus, SPCA2 can activate ORAI1 when not regulated by STIM1 but can also influence the activity of ORAI1 when ORAI1 is activated by STIM1. Notably, the increased slow current inactivation is observed with a pipette solution containing 10 mM BAPTA when inactivation is minimal to not occurring.[37] In a previous study, we showed that this form of slow ORAI1 current inactivation is mediated by the SERCA pump and is due to the assembly of ORAI1, STIM1, and SERCA complexes.[38,39] Next, we assessed whether the effect of SPCA2 on the ORAI1 current is dependent on the Ca^{2+} ATPase activity of SPCA2. Our results showed that both mutant SPCA2 forms increased the STIM1-ORAI1 current density and significantly increased the rate of current inactivation (Figures 3I–3L). Interestingly, the measured parameters were higher in the mutant SPCA2 transfected cells compared with the wild-type SPCA2, especially the rate of inactivation. Taken together, these findings further support the modulatory role of SPCA2 in Orai1 channel activity. Q10

SPCA2 increases the interaction between STIM11 and ORAI1

Our data indicate that SPCA2 can activate ORAI1-mediated, store-independent extracellular Ca^{2+} entry; however, the findings also point to the involvement of STIM1 in this process. Therefore, we wanted to understand how SPCA2 affects STIM1-ORAI1 interactions. In unstimulated HeLa cells, the overexpressed SPCA2 and STIM1 showed a reticular ER expression pattern (Figure 4A), and STIM1 showed no significant punctation. To gain higher spatial resolution, we used dSTORM, which revealed that STIM1 and SPCA2 overlapped in the focal plane of the ER (Figure 4B). The SPCA2-induced puncta formation of ORAI1 was further quantified in STIM1-ORAI1 co-transfected cells. In the absence of Ca^{2+} store depletion, only a minimal number of STIM1/ORAI1 co-clusters were observed (Figures 4C and S4A). Co-transfection of ORAI1-STIM1 with SPCA2 resulted in a profound increase in spontaneous puncta formation in cells with filled Ca^{2+} stores, which was further increased by store depletion. To quantify STIM1-ORAI1 cluster overlap with and without SPCA2, using dSTORM, we co-transfected cells with STIM1 and ORAI1 ± SPCA2. Without ER Ca^{2+} store depletion, STIM1-ORAI1 co-localization was negligible but markedly increased after CPA-induced store depletion (Figures 4D, S4B, and S4C). Importantly, SPCA2 significantly increased the number of STIM1-ORAI1 co-clusters in cells with filled stores. This observation was further investigated by FLIM-FRET, using Stim1-YFP (donor) and ORAI1-mCherry (acceptor), revealing that the fluorescent lifetime of the donor molecule was increased after photobleaching the acceptor (Figures S4D and S4E). Therefore, the calculated FRET efficiency was significantly increased by SPCA2, compared with the group without SPCA2 transfection (Figure 4E). As expected, CPA treatment further increased FRET efficiency. The constitutive Ca^{2+} influx and increased STIM1-ORAI1 clustering may be caused by enhanced Ca^{2+} leakage and reduced ER Ca^{2+} stores in SPCA2-expressing cells. To exclude the possibility that STIM1-ORAI1 clustering is caused by the leakage of the ER Ca^{2+} stores, we measured the ER Ca^{2+} store content in HeLa cells transfected with D1ER and treated with 10 μM CPA. These experiments showed no effect of SPCA2 on the ER Ca^{2+} content (Figure 4F). A previous study

Please cite this article in press as: Kiss et al., Store-independent activation of STIM1-ORAI1 by SPCA2 determines the basal CFTR activity in secretory epithelial cells, Current Biology (2025), https://doi.org/10.1016/j.cub.2025.09.006

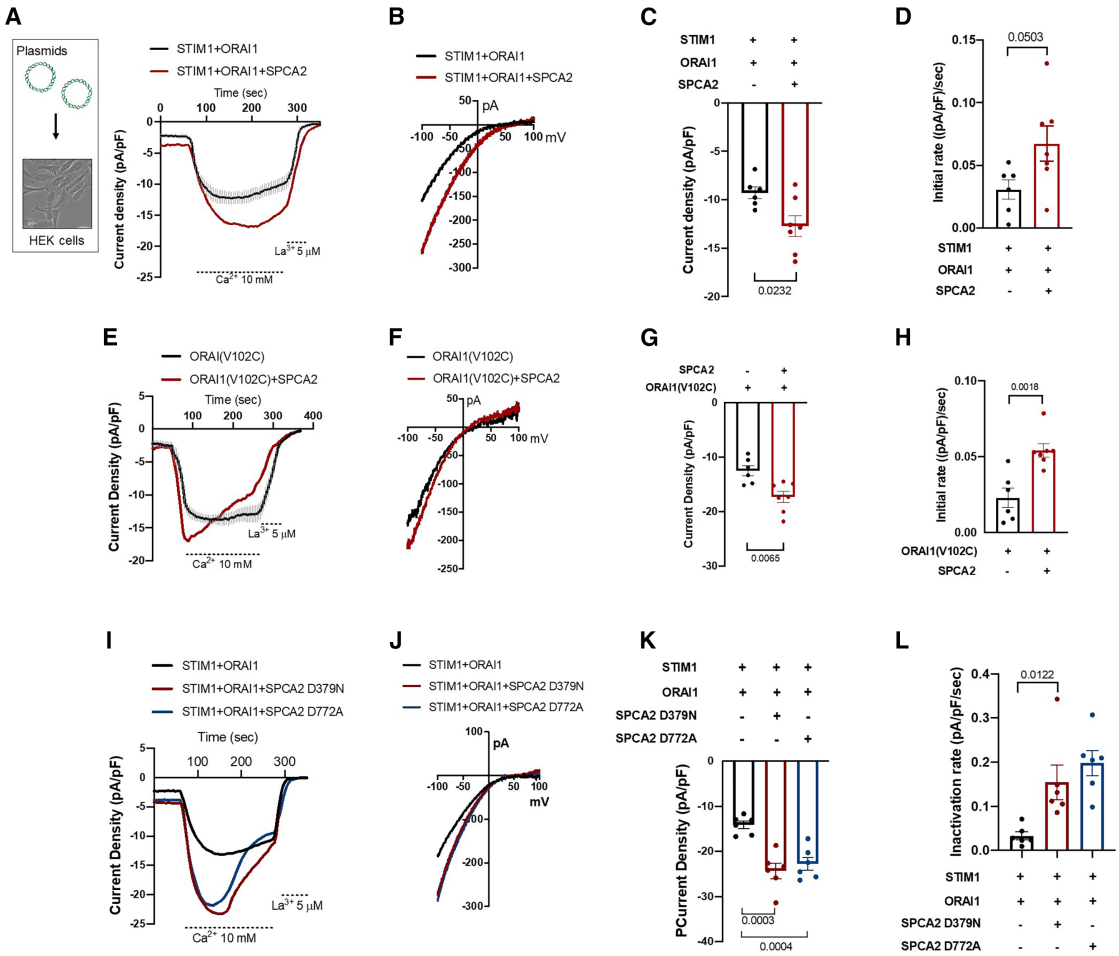

Figure 3. SPCA2 activates ORAI1 independent of STIM1 and when bound to STIM1

(A–D) HEK cells were transfected with ORAI1 and STIM1 alone (black) or with SPCA2 (red). (A) Shows the time course, (B) example I/V, (C) maximal current density, and (D) the current slow inactivation rate.

(E–L) (E) HEK cells were transfected with the constitutively active ORAI1(V102C) alone (black) or with SPCA2 (red) and were used to measure ORAI1 Ca^{2+} current. (E) Shows the time course, (F) example I/V, (G) maximal current density, and (H) the current slow inactivation rate. HEK cells were also transfected with STIM1, ORAI1 (black), and SPCA2 D379N (red) or D772A (blue) mutants to measure ORAI1 Ca^{2+} current. (I) shows the time course, (J) example I/V, (K) maximal current density, and (L) the current slow inactivation rate.

suggested that SPCA2 is required for the PM trafficking of ORAI1.[9] Therefore, we quantified the expression of ORAI1 by western blot and cell surface biotinylation assay, which revealed that the total expression of ORAI1 is not changed significantly in the presence of SPCA2 (Figures 4G and S5A). Although, ORAI1 cell surface expression was moderately decreased in the SPCA2 transfected cells, the difference was not significant (Figures 4H and S5B). The silencing of SPCA2 in ORAI1-overexpressing HeLa cells had no significant effect on ORAI1 surface levels, as revealed by capillary western blotting (Figures 4H and S5C). To further validate the proposed complex, we performed co-immunoprecipitation (coIP) using hemagglutinin (HA)-tagged ORAI1 in HeLa cells co-expressing STIM1-GFP and SPCA2-Myc. Both STIM1 and SPCA2 were detected in the HA pull-down fraction (Figures 4I and S5C), confirming their biochemical association with ORAI1. Notably, the increased basal STIM1-ORAI1 clustering by SPCA2 in the absence of apparent ER Ca^{2+} depletion that could not be observed when STIM1 and SPCA2 were co-expressed in the absence of ORAI1 suggests that SPCA2 acts on ORAI1 first, and when clustering ORAI1, it stabilized clustering of STIM1, as it is known that ORAI1 reduces STIM1 mobility to stabilize STIM1 clustering.[40] However, for the constitutive Ca^{2+} influx, the presence of STIM1 in the complex is also crucial.

ORAI1-mediated SICE regulates CFTR activity and fluid secretion in pancreatic ductal epithelial cells

The physiological role of spontaneous Ca^{2+} influx activated by SPCA2 via ORAI1 is unknown. We investigated whether it regulates epithelial ion and fluid secretion, mediated largely by the CFTR Cl^- channel. Thus, we first clearly demonstrated CFTR and ORAI1 co-localization on the apical membrane of mouse pancreatic ductal organoids (Figure 5A). The CFTR-ORAI1 co-localization was further confirmed by capturing dSTORM images of transfected HeLa cells and 2D adherent primary ductal cells generated from human pancreatic organoids, which

Please cite this article in press as: Kiss et al., Store-independent activation of STIM1-ORAI1 by SPCA2 determines the basal CFTR activity in secretory epithelial cells, Current Biology (2025), https://doi.org/10.1016/j.cub.2025.09.006

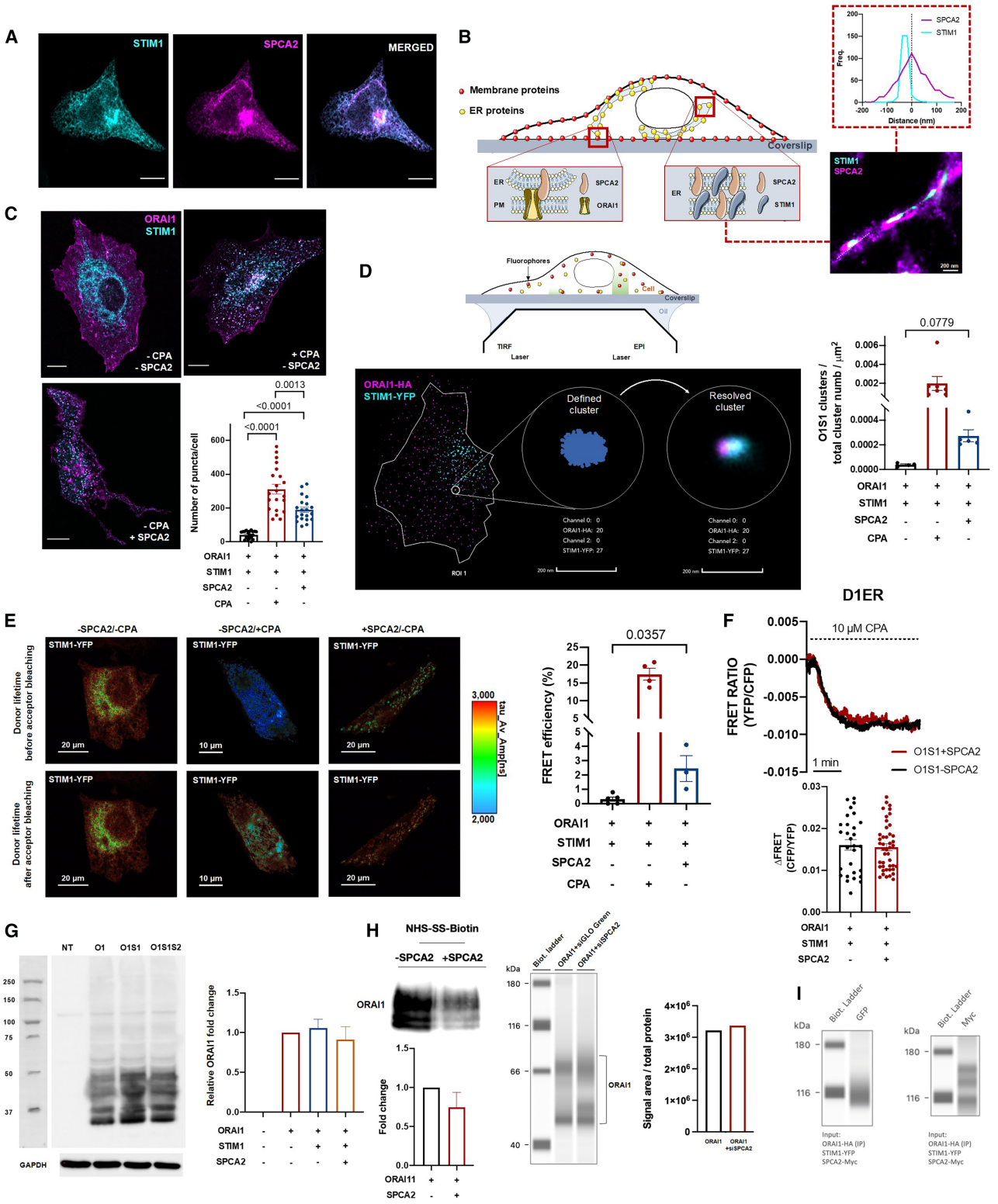

Figure 4. The presence of SPCA2 increases ORAI1-STIM1 interactions

(A) Confocal pictures demonstrate the intracellular co-localizing distribution of the reticular STIM1 and SPCA2 proteins in co-transfected HeLa cells (scale bar: 10 µm).

(B) Schematic figure and dSTORM images demonstrate the physical proximity of ORAI1-SPCA2 in the ER membrane. The frequency of blinking events was plotted as a function of the distance from the indicated white dashed lines.

(legend continued on next page)

Please cite this article in press as: Kiss et al., Store-independent activation of STIM1-ORAI1 by SPCA2 determines the basal CFTR activity in secretory epithelial cells, Current Biology (2025), https://doi.org/10.1016/j.cub.2025.09.006

endogenously expressed the two proteins (Figures 5B, 5C, S4F, and S4G). The combined localization *ex vivo* and dSTORM analysis suggest that CFTR and ORAI1 are located in the same PM nanodomain. To examine the role of SICE in CFTR activity, we measured CFTR-mediated Cl^- extrusion in pancreatic ductal fragments using the Cl^--sensitive dye MQAE, whose fluorescence increases upon Cl^- efflux.[27] Removal of extracellular Cl^- from the HCO_3^-/CO_2-buffered solution resulted in a decrease in $[Cl^-]_i$, which was abolished by 10 μM of the selective CFTR inhibitor CFTR(inh)-172 (Figure 5D). Notably, treating the ductal cells with 10 μM CM5480 or pre-incubation with 40 μM BAPTA-AM to chelate and buffer $[Ca^{2+}]_i$ resulted in a similar inhibition of Cl^- efflux (Figure 5D). Moreover, the knockdown of ORAI1 or STIM1 with siRNA resulted in a marked decrease in the Cl^- efflux (Figure 5E). On the other hand, the higher forskolin-stimulated maximal CFTR Cl^- efflux was not affected by the inhibition of ORAI1 with CM5480, suggesting that the stimulated secretion is independent of SICE (Figure 5F). These findings indicate that the spontaneous ORAI1-mediated SICE has a specific and major impact on the basal CFTR activity in ductal epithelial cells. To confirm the role of SPCA2 in regulating CFTR activity, the expression of SPCA1 and 2 and SEPTIN7 were knocked down in mouse pancreatic ductal fragments. In accord with the intracellular Ca^{2+} measurements, the activity of CFTR was significantly impaired by siSPCA2, while siSPCA1 and siSEPT7 had no effect (Figure 5G). A recent study indicated that SPCA2-mediated Ca^{2+} entry supports cellular respiration and mitochondrial membrane potential,[41] processes critical for epithelial secretion.[42] To explore SPCA2's role in mitochondrial function, we measured ATP content, mitochondrial membrane potential, and oxygen consumption in mouse pancreatic ductal organoids treated with the ORAI1 inhibitor CM5480 (Figures S2K–S2M). The inhibitor moderately reduced ATP levels and mitochondrial membrane potential but did not significantly affect oxygen consumption, suggesting that spontaneous extracellular Ca^{2+} influx contributes to mitochondrial functions to some extent but does not completely determine it. To verify physiological relevance, we assessed CFTR-dependent pancreatic ductal HCO_3^- and epithelial fluid secretion. Pancreatic ductal epithelial cells take up and extrude HCO_3^- in HCO_3^-/CO_2 buffered solution, which was significantly impaired by 10 μM CM5480 (Figure 5H). In addition, the spontaneous swelling of the untreated ductal fragments in HCO_3^-/CO_2 buffered solution was significantly impaired by ORAI1 inhibition (Figure 5I), suggesting the inhibition of the basal, unstimulated fluid secretion. Finally, to confirm our findings *in vivo*, the pancreatic fluid secretion was measured in control and CM5480-treated mice, which revealed that the inhibition of ORAI1 significantly inhibited the *in vivo* pancreatic ductal fluid secretion (Figure 5J). Our results demonstrate that SICE via the SPCA2/STIM1/ORAI1 complex determines basal CFTR activity and thus ion and fluid secretion in pancreatic ductal cells.

SICE via ORAI1 regulates CFTR activity in secretory epithelial cells

To determine whether the co-localization of ORAI1 and CFTR and the regulatory role of constitutive SICE by ORAI1 are ubiquitous features in secretory epithelia, we utilized organoid cultures from mouse airway, liver, and human pancreas. Immunofluorescent labeling in the organoids confirmed the co-localization of CFTR and ORAI1 on the apical membrane of epithelial cells (Figures 6A–6C). In addition, inhibition of ORAI1 with 10 μM CM5480 in unstimulated mouse lung (Figure 6A) and liver (Figure 6B) and human pancreatic organoids (Figure 6C) resulted in a decrease of the CFTR-mediated Cl^- efflux upon removal of extracellular Cl^-. Notably, the CFTR-mediated Cl^- efflux was almost completely abolished in airway organoids when the spontaneous Ca^{2+} influx was inhibited. The findings with various epithelia emphasize that regulating CFTR activity by SICE is a common regulatory mechanism in secretory epithelia in both mice and humans.

SICE by ORAI1 regulates CFTR activity via Ca^{2+}-dependent ACs

Synergism between cAMP and Ca^{2+} signaling is a major form of regulating CFTR activity.[43] To assess the role of SICE via ORAI1 in the regulation of local cAMP nanodomains, we first analyzed the adenyl cyclase genes (Adcy) transcriptome of the mouse and human pancreatic ductal organoids. The transcript/million (TPM) values demonstrated the expression of *Adcy3*, *6*, *8*, and *9* in mice with low but detectable transcript levels of *Adcy1* (Figure 7A). ADCY3, 6, and 9 were expressed in human pancreatic organoids, with low but detectable transcript levels of *ADCY1*, *4*, *5*, *7*, and *8*. AC9 showed a basolateral expression

(C) Confocal images (split channel images are available in Figure S4) and bar chart demonstrate significant differences in puncta formation between the three indicated experimental groups (ORAI1 + STIM1, ORAI1 + STIM1 + 10 μM CPA, ORAI1 + STIM1 + SPCA2).

Q12 (D) Schematic illustration of the dSTORM cluster analysis and experimental setup using total internal reflection fluorescence (TIRF) resulted in the determination of the ORAI1-STIM1 co-localizing cluster ratio in the focal plane of the PM. The bar chart shows the maximum number of ORAI1-STIM1 co-localizing clusters normalized to μm^2 membrane area.

(E) Confocal images and the calculated FRET efficiency between Stim1-YFP (donor) and ORAI1-mCherry (acceptor) plotted on a bar chart of the FLIM measurements.

(F) Average traces of 3–4 FRET experiments demonstrate no significant difference upon 10 μM CPA treatment in Ca^{2+} extrusion from the ER in the presence or absence of SPCA2 in STIM1-ORAI1 (O1S1) co-transfected HeLa cells by using D1ER FRET sensor.

(G) Western blot shows no change of the expression of ORAI1 (normalized to GAPDH intensity) in whole-cell lysate with STIM1 (O1S1) and STIM1-SPCA2 (O1S1S2) co-transfected cells ($N = 3$).

(H) Cell surface expression of ORAI1 was not changed significantly in SPCA2 co-transfected cells compared with control ($N = 2$). Capillary western blot of surface-biotinylated HeLa cells shows no significant changes of the ORAI1 expression following SPCA2 silencing. Quantification reflects normalized signal area to total protein.

(I) Western blot analysis of the coIP eluates revealed the presence of STIM1-YFP (left, anti-GFP) and SPCA2-Myc (right, anti-Myc) in the immunoprecipitated complex, confirming their association with ORAI1. Molecular weight markers are shown in kDa. Input constructs are indicated below.

See also Figure S5.

Please cite this article in press as: Kiss et al., Store-independent activation of STIM1-ORAI1 by SPCA2 determines the basal CFTR activity in secretory epithelial cells, Current Biology (2025), https://doi.org/10.1016/j.cub.2025.09.006

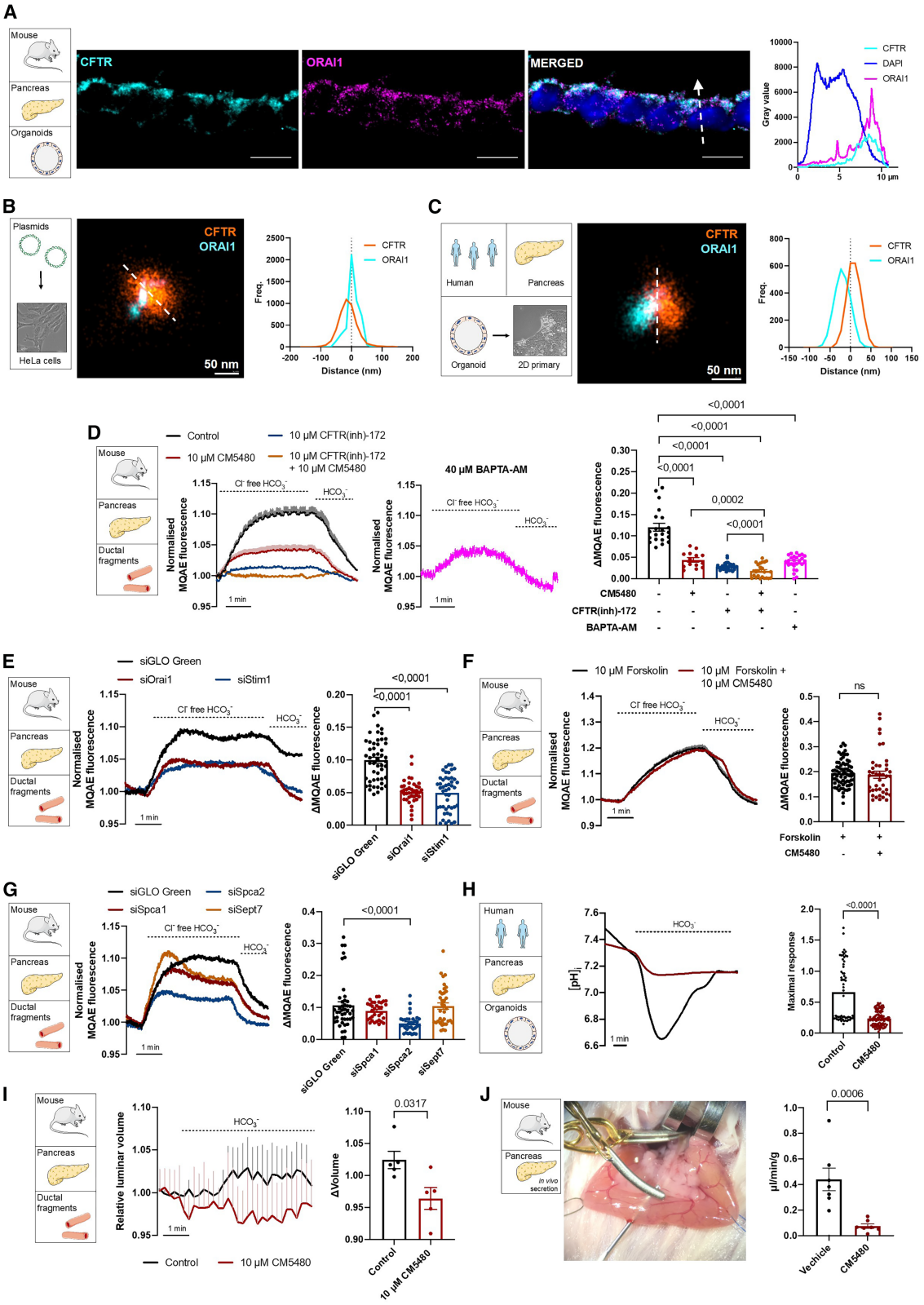

Figure 5. The SPCA2/STIM1/ORAI1 complex regulates CFTR activity in primary polarized pancreatic ductal epithelial cells

(A) Confocal pictures and line profiles demonstrate the co-localization of CFTR and ORAI1 at the apical membrane of mouse pancreatic organoids (Pearson's coefficients: r = 0.857) (scale bar: 10 µm).

(legend continued on next page)

Please cite this article in press as: Kiss et al., Store-independent activation of STIM1-ORAI1 by SPCA2 determines the basal CFTR activity in secretory epithelial cells, Current Biology (2025), https://doi.org/10.1016/j.cub.2025.09.006

pattern in cross-sections of mouse pancreatic organoids, and therefore, it was excluded as a potential interaction partner of CFTR on the apical membrane (Figure S6A). The dSTORM imaging of organoids was unsuccessful due to the high background noise and low signal-to-noise ratio. Therefore, we used transfected HeLa cells for the super-resolution localization of the ACs. Analysis of HeLa cells co-transfected with CFTR and AC1, AC3, AC6, or AC8, using dSTORM and cluster analysis, revealed that CFTR is in close physical proximity to AC1 (clusters overlapping: 62.04%), 3 (clusters overlapping: 34.3%), and 8 (clusters overlapping: 60.1%), with limited co-localization with AC6 (clusters overlapping: 14.56%) (Figure 7B). Co-localization frequency remained stable across varying expression levels of the different proteins (Figure S6B). In addition, these ACs co-localized with ORAI1 as well as in co-transfected HeLa cells (Figure 7C). Although AC6 is a prominent regulator of CFTR,[44] it is inhibited by Ca^{2+} and was therefore excluded as a potential transmitter of SICE regulation to CFTR. To visualize the signaling nanodomain, we applied three-color dSTORM in HeLa cells transfected with CFTR, ORAI1, and AC1, 3, or 8, which confirmed that these three proteins are in the same PM nanodomain (Figure 7D). To further assess the physical interaction between ORAI1 and ACs, we performed dSTORM imaging using N- or C-terminal deletion mutants of ORAI1.[45] Loss of the N-terminal domain (ΔNT) strongly reduced co-localization with AC3 and AC8, indicating its necessity for AC clustering, whereas C-terminal deletion (ΔCT) had little effect (Figure S6C). Next, we dissected isoform-specific cAMP signaling within these microdomains by utilizing FRET-based cAMP sensors targeted to raft (Lyn-H147) and non-raft (H147-Kras) membrane compartments.[46] HeLa cells co-expressing individual AC isoforms (AC1, AC3, AC6, AC8) with these sensors were stimulated with forskolin (Figure S6D). AC1 and AC3 preferentially elevated cAMP in non-raft regions, AC6 showed no difference between the regions, and AC8 showed robust activity in raft domains. Moreover, CM5480 treatment reduced cAMP levels significantly more in AC8-expressing cells than in those with AC6 (Figure S6E), suggesting a potentially predominant role for AC8 in CFTR-related cAMP signaling. Next, we knocked down the expression of AC1/3/8 using siRNA in isolated pancreatic ductal fragments, which had no effect on the apical localization of ORAI1 and CFTR (Figure S7A) but significantly impaired the CFTR-mediated Cl^- extrusion in unstimulated mouse pancreatic ductal fragments (Figure S7B). In the siAC1/3/8-treated ductal fragments, the CFTR-mediated Cl^- extrusion was not impaired further by the application of CM5480, indicating effects on the same pathway. Moreover, single knockdown experiments in apical-out human pancreatic organoids revealed that basal CFTR activity is most profoundly impaired upon silencing of AC8, as measured by MQAE fluorescence (Figure 7E), suggesting that AC8 is the key isoform maintaining constitutive secretion under resting conditions. Finally, the PKA inhibitor H-89 significantly decreased the Cl^- efflux in pancreatic ductal fragments, which was not impaired further by the inhibition of ORAI1 with CM5480 or by chelation of the intracellular Ca^{2+} with BAPTA-AM (Figure S7C). To confirm that this effect is specifically mediated by PKA, we employed the more selective PKA inhibitors PKI (5–24) (100 nM; a high-affinity peptide inhibitor) and KT5720 (1 μM; a small-molecule inhibitor). Both compounds robustly reduced Cl^- efflux in isolated pancreatic ductal fragments, supporting that CFTR activity in this context is strongly dependent on PKA-mediated phosphorylation (Figure 7F). To further characterize the spatial relationship between PKA and ORAI1, we performed dual-color dSTORM imaging in HeLa cells. ORAI1 typically formed small nanoclusters, in certain membrane regions expanding beyond 400 nm and overlapping with PKAα signals (Figures S7D and S7E). Cluster analysis showed that approximately 2% (292 of 13,884) of the ORAI1 clusters overlapped with PKAα, suggesting that a small but distinct subpopulation of ORAI1 nanodomains closely associated with PKAα, potentially facilitating localized signaling. Moreover, in HeLa cells overexpressing ORAI1, CM5480 treatment reduced AKAP79-AKAR4 FRET signal,[47] indicating that basal PKA activity depends on the SPCA2-Orai1 axis (Figure S12F). These observations suggest that the Ca^{2+}-stimulated AC1/3/8 act via PKA in a signaling nanodomain with a dominant role of the lipid raft-associated AC8 to translate the stimulatory effect of SICE via ORAI1 on cAMP elevation and increased basal CFTR activity.

DISCUSSION

CFTR Cl^- channel fundamentally determines transepithelial ion and fluid secretion and hence hydration of different organs' luminal surfaces; moreover, basal CFTR activity is required to maintain hydration of the luminal surfaces even when stimulated secretion is not activated. Therefore, proper spatiotemporal regulation of the channel activity is essential for life. This study identified and comprehensively characterized a novel regulatory

(B) Evaluated representative dSTORM picture illustrates the physical proximity of CFTR and ORAI1 in the PM of co-transfected HeLa cells and adherent culture derived from human pancreatic organoids.
(C) The frequency of blinking events was plotted as a function of the distance from the indicated white dashed lines (B and C).
(D) The intracellular Cl^- level was measured by MQAE in pancreatic ductal fragments where the quantity of intracellular Cl^- and the intensity of fluorescence are inversely proportional. Challenging the cells with Cl^--free extracellular solution resulted in a decrease in intracellular Cl^-, which was completely abolished by 10 μM CFTR(inh)-172. Inhibition of ORAI1 or global Ca^{2+} chelation with 40 μM BAPTA-AM pre-incubation significantly decreased the CFTR-mediated Cl^- efflux. The bar chart represents the maximal change of MQAE fluorescence upon extracellular Cl^- withdrawal in each investigated experimental group.
(E) Average traces of 3–4 experiments and bar chart demonstrate that *Orai1* or *Stim1* knockdown by siRNA significantly decreased CFTR-mediated Cl^- efflux.
(F) Forskolin-stimulated Cl^- efflux was not changed by 10 μM CM5480 in isolated pancreatic ducts.
(G) Among siSpca1, *siSpca2*, and *siSept7*, only knockdown of *Spca2* resulted in significantly decreased Cl^- efflux, as represented by average traces and bar chart.
Q13 (H) Intracellular pH measurements with BCECF-AM HCO_3^- extrusion in HCO_3^-/CO_2 buffered solution was significantly impaired by 10 μM CM5480.
(I) Spontaneous swelling of unstimulated ductal fragments in HCO_3^-/CO_2 buffered solution was significantly impaired by 10 μM CM5480.
(J) *In vivo* pancreatic fluid secretion was inhibited by CM5480 treatment (N = 7/group).
See also Figures S2 and S4.

Please cite this article in press as: Kiss et al., Store-independent activation of STIM1-ORAI1 by SPCA2 determines the basal CFTR activity in secretory epithelial cells, Current Biology (2025), https://doi.org/10.1016/j.cub.2025.09.006

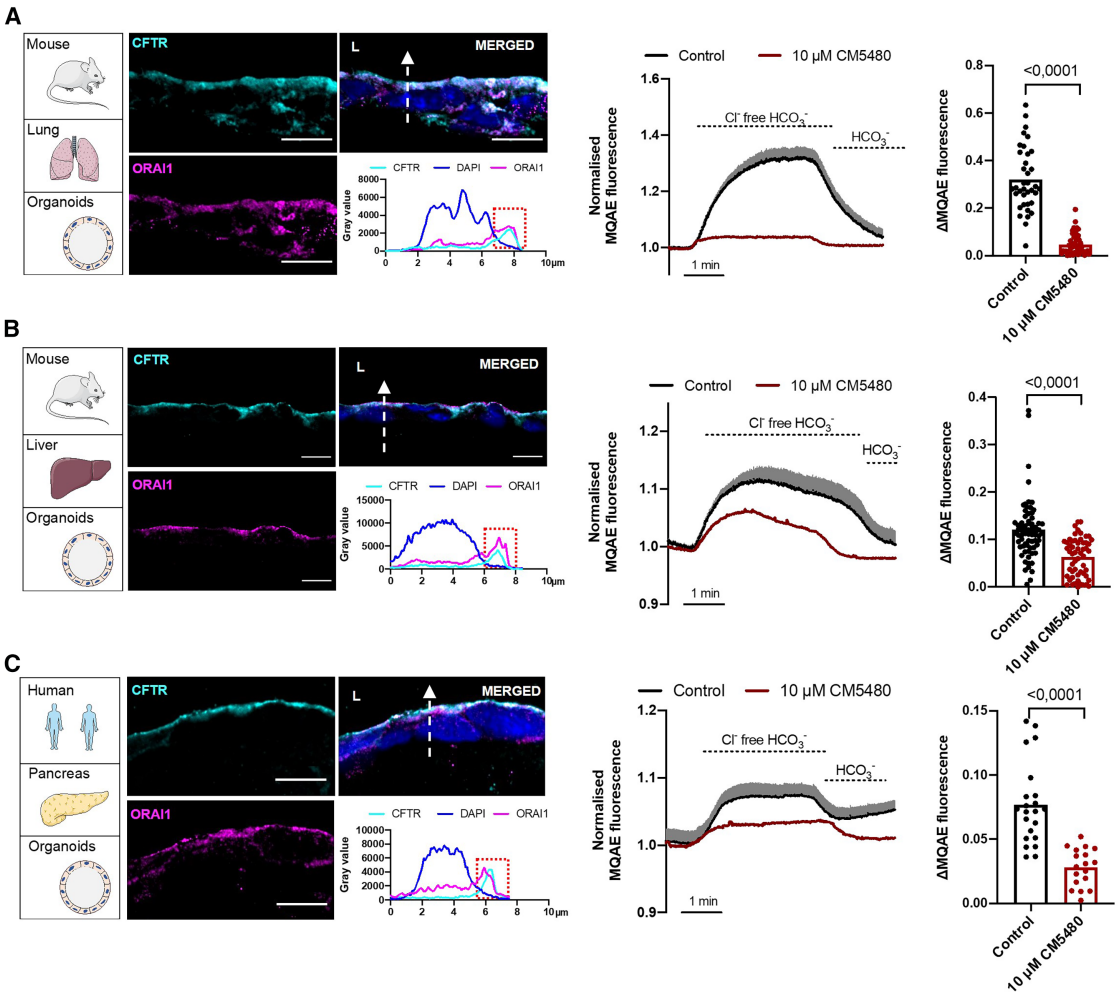

Figure 6. ORAI1 regulates CFTR activity in primary OCs derived from mouse lung, mouse liver, and human pancreatic tissue

Confocal images and their line profile analysis demonstrate the co-localization of CFTR and ORAI1 proteins at the apical membrane of OCs derived from mouse lung (A), mouse liver (B), and human pancreatic tissue (C) (Pearson's coefficients: mouse lung-derived OC r = 0.903; mouse liver-derived OC r = 0.875; human pancreas-derived OC r = 0.688) (scale bar: 10 μm). Average traces and bar charts show that ORAI1 inhibition by 10 μM CM5480 significantly decreased CFTR activity in mouse lung (A), mouse liver (B), and human pancreatic OCs (C).

mechanism determining basal CFTR activity in unstimulated primary polarized epithelial cells independently of neurohormonal stimuli. By applying state-of-the-art molecular biology and imaging techniques, we describe a highly organized signaling nanodomain on the apical PM of epithelial cells from mouse and human tissues, including the pancreas, liver, and lung. In this nanodomain, SPCA2 maintains constitutive interaction between STIM1/ORAI1 in a Ca^{2+} store-independent manner, leading to a constitutive extracellular Ca^{2+} influx. The SICE initiated by SPCA2 maintains the activity of the Ca^{2+}-dependent ACs that determine basal CFTR activity and fluid secretion in secretory epithelial cells.

The molecular components of SOCE, STIM1, and ORAI1 are ubiquitously expressed.[37,48] In this study, we showed that ORAI1 is primarily expressed on the apical membrane of polarized secretory epithelial cells in the pancreas, liver, and airway. Surprisingly, we found that ORAI1-mediated Ca^{2+} influx is constitutively active, significantly contributing to basal Ca^{2+} levels in these cells. This constitutive activity was absent in pancreatic acinar cells, where ORAI1 activates only after store depletion.[49,50] While previous studies mainly focused on the pathological roles of ORAI1,[51] the physiological functions and mechanisms of ORAI1-mediated SICE remain poorly understood. Previously, Feng et al. demonstrated that the ORAI1-SPCA2 complex elicits constitutive store- and STIM1-independent Ca^{2+} signaling that promotes tumorigenesis in breast cancer-derived cells.[10] Here, we show that the constitutive ORAI1 activity in polarized epithelial cells is independent of ER Ca^{2+} store depletion; however, it requires STIM1 and is activated by SPCA2. Previously, the overexpression of SPCA1 was also reported to induce cytosolic Ca^{2+} influx.[8] However, our knockdown experiments suggested that in primary epithelial cells, the regulation is specific to SPCA2 and is not affected by SPCA1. Unlike ubiquitously expressed SPCA1,[52] SPCA2 expression is tissue specific,[53] possibly explaining why SICE occurs in secretory epithelia but not in acinar cells. In the pancreatic

Please cite this article in press as: Kiss et al., Store-independent activation of STIM1-ORAI1 by SPCA2 determines the basal CFTR activity in secretory epithelial cells, Current Biology (2025), https://doi.org/10.1016/j.cub.2025.09.006

CellPress
OPEN ACCESS

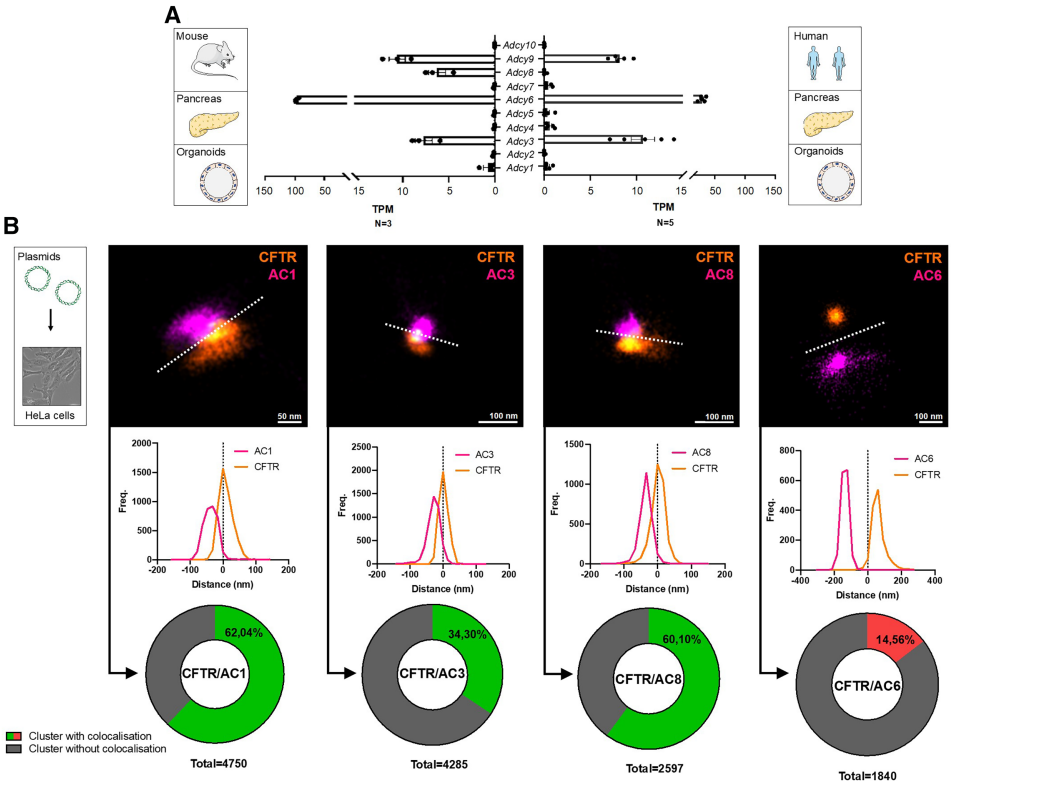

(legend on next page)

Please cite this article in press as: Kiss et al., Store-independent activation of STIM1-ORAI1 by SPCA2 determines the basal CFTR activity in secretory epithelial cells, Current Biology (2025), https://doi.org/10.1016/j.cub.2025.09.006

acinar cells, previous studies identified a specific isoform of SPCA2 (termed SPCA2C),[31] which was involved in the regulation of Ca^{2+} homeostasis, when expressed in HEK293 cells.[32] In contrast, secretory epithelial cells, including pancreatic ductal cells, express the full-length SPCA2.[33] In addition, previous studies suggest that both the N′- and C′-terminal domains of SPCA2 have important functions in the protein-protein interactions.[12]

In our experiments, SPCA2 displayed a reticular expression pattern enriched at the apical pole of polarized epithelial cells. Mechanistically, SPCA2 enhanced unstimulated puncta formation of ORAI1 and the STIM1-ORAI1 complex independently of ER Ca^{2+} depletion. However, SPCA2 did not increase basal STIM1 puncta formation without exogenous ORAI1 overexpression, suggesting that SPCA2 primarily targets ORAI1. The clustered ORAI1 can recruit and stabilize STIM1 in the puncta, as it is known that ORAI1 reduces STIM1 mobility to stabilize STIM1 clustering.[40] Notably, the activation of ORAI1 by SPCA2 did not reach the level of maximal ORAI1 activation. The FLIM-FRET measurements also revealed that SPCA2 and ORAI1 are in physical proximity in unstimulated cells, which is in line with the previous findings.[10] Of note, the ER Ca^{2+} depletion decreased co-cluster area of SPCA2 and ORAI1; however, the FRET efficiency was not increased further, which could be explained by the redistribution of the ER in response to Ca^{2+} depletion.[54] We demonstrated that SPCA2 can activate ORAI1 currents independently of its Ca^{2+} ATPase activity, even in the absence of STIM1, and can also modulate ORAI1 activity in the presence of STIM1, which may explain the similar inhibition of the constitutive Ca^{2+} influx observed upon si*STM1* and si*SPCA2* treatment. In the presence of SPCA2, the rate of slow Ca^{2+}-dependent inactivation is increased, suggesting a modulatory role of SPCA2 in the ORAI1 channel function. Moreover, the modulation of ORAI11 is even more prominent when it is not activated by STIM1. Yet, in both sets of experiments, SPCA2 independently from the Ca^{2+} ATPase activity increased the ORAI11 current density. These findings also raise the possibility that SPCA2 may function as a tether at the ER/PM junctions. From previous work, we know that the higher the Orai1 current the faster the Ca^{2+}-dependent inactivation, further indicating that SPCA2 increases the ORAI1 current.[45]

CFTR-mediated ion secretion is a critical rate-limiting step in secretory epithelial cells; thus, we examined how SPCA2-triggered SICE affects CFTR activity. Previous studies suggest that the co-localization of these proteins as mutations in CFTR affected ORAI1 channel function and enhanced ORAI1-mediated Ca^{2+} influx, leading to increased interleukin-8 (IL-8) secretion in airway cells.[26] Even more importantly, Shan et al. described that CFTR has basal activity that was inhibited by the administration of 2-APB, a non-selective inhibitor of ORAI1.[55] The authors also showed that the basal current was also markedly reduced by MDL-12330A, a membrane-bound AC antagonist, and by the PKA inhibitor Rp-cAMPS. These findings indicate that basal CFTR activity depends on local cAMP production by membrane-bound ACs activated by Ca^{2+} influx through ORAI1 channels. Moreover, a recent study showed that the nasal epithelium displays constitutive CFTR activity, which is essential to maintain viscoelastic properties of the mucus layer and to mucociliary transport.[56] Here, we directly showed that CFTR and ORAI1 closely co-localize (~20–30 nm apart) on the apical membrane of pancreatic, liver, and airway epithelial cells, providing the first direct evidence for their assembly into a signaling complex nanodomain. Functional assays revealed that both pharmacologic inhibition or gene silencing of *STIM1* and *ORAI1* impaired CFTR activity and abolished unstimulated basal fluid secretion. In contrast, forskolin-induced CFTR activity remained intact when ORAI1 was inhibited, indicating that SICE regulates basal but not stimulated CFTR activity. CFTR-mediated ion secretion is energy dependent, while SPCA2 was recently shown to regulate mitochondrial respiration and DNA damage response via SICE.[41] Additionally, SPCA2-associated SICE moderately reduced intracellular ATP levels and mitochondrial membrane potential without significantly affecting mitochondrial oxygen consumption, suggesting partial but not exclusive regulation of mitochondrial function. The presence of this mechanism across mouse and human secretory epithelia (such as the pancreas, liver, and airway), also confirmed *in vivo*, highlights the general role of the SPCA2/STIM1/ORAI1 complex in regulating basal CFTR function in secretory epithelia.

Previously, we and others showed that sustained, uncontrolled ORAI1 activation increases intracellular Ca^{2+} levels, causing cell damage in various diseases.[34,50,57] However, our results indicate that constitutive ORAI1 activity is necessary to maintain resting Ca^{2+} levels and basal CFTR activity in secretory epithelial cells. Notably, the Ca^{2+} changes due to SPCA2/ORAI1 interactions are smaller than those from stimulated responses, possibly due to limitations of the cytoplasmic dye (FURA2-AM), which average signals across the entire cell and are not accumulated at or targeted to a specific subcellular region. Large, prolonged Ca^{2+} elevations can be toxic, often leading to ER stress and cell death.[58] Thus, continuous SICE likely induces localized Ca^{2+} nanodomains

Figure 7. Ca^{2+}/calmodulin-activated ACs are involved in the formation of the protein nanodomain-regulating CFTR

(A) Expression pattern of AC family members in mouse- (N = 3) and human (N = 5) pancreas-derived OCs. All data are given in TPM.

(B) Representative dSTORM images show overlapping positions of CFTR and AC1/3/8/6 in the focal plane of the membrane of co-transfected HeLa cells. Cluster analysis results show the percentage of clusters with co-localizing fluorophores within a maximum radius of 300 nm from the centroids formed by individual blinking events.

(C) Evaluated dSTORM pictures illustrate the physical proximity of AC1/3/8 and ORAI1 in the membrane of co-transfected HeLa cells. In comparison, three-color dSTORM images demonstrate the molecular assembly of the protein nanodomain consisting of CFTR, ORAI1, and one of the AC1/3 or 8.

(D) Dashed lines indicate the zero point of the distance scale represented as a function of blinking event frequency.

(E) Average traces and summary bar charts from 4 to 6 independent experiments show that individual gene silencing of AC1, AC3, or AC8 significantly reduced CFTR-mediated anion secretion, assessed by MQAE fluorescence upon Cl^- withdrawal, in apical-out human pancreatic organoids.

(F) Average traces and corresponding bar charts show that treatment with 100 nM PKI(5–24) (red) or 1 μM KT5720 (blue) significantly reduced Cl^- efflux, compared with vehicle-treated controls (black), upon Cl^-/HCO_3^- exchange. Data are presented as mean ± SEM.

See also Figures S6 and S7.

Please cite this article in press as: Kiss et al., Store-independent activation of STIM1-ORAI1 by SPCA2 determines the basal CFTR activity in secretory epithelial cells, Current Biology (2025), https://doi.org/10.1016/j.cub.2025.09.006

near the CFTR-expressing subplasmalemmal regions, rather than widespread increases, supporting physiological functions without the depletion of ER stores and ER stress. Our findings also raise the possibility that distinct ORAI1 pools exist in specific PM nanodomains of polarized cells, regulating channel function and store-dependent or -independent activities.

Finally, we wanted to provide mechanistic insight into how SPCA2/STIM1/ORAI1-mediated SICE determines CFTR activity. Independent studies suggest synergism between cAMP and Ca^{2+} signaling that is crucial in regulating secretory epithelial cells' physiological functions.[2] One form of synergism is the divergent regulation of AC protein activities by Ca^{2+}, which can affect CFTR activity.[59] Another example is the action of IP_3R-binding protein released with $InsP_3$ (IRBIT) in pancreatic ductal epithelia,[60] which significantly improved the dose response of CFTR to forskolin or carbachol, independently of cytoplasmic Ca^{2+}. Our experiments revealed that SICE in epithelial cells controls CFTR activity in a PKA-dependent manner, which suggests that the enhanced cAMP synthesis by ACs is a critical step in the process. Whole-transcriptome analysis of mouse and human pancreatic ductal organoids revealed the expression of *Ac1*, *3*, *5*, *6*, *7*, *8*, and *9* in the ductal epithelia, and the highest expression was observed in the case of *Ac6*. Sabbatini et al. previously showed that *Ac6* knockout mice had reduced cAMP generation, PKA activation, and impaired fluid secretion after hormonal stimulation.[44] However, AC6 is inhibited by Ca^{2+} and thus unlikely to mediate SICE. Earlier studies indicated direct interactions between the amino termini AC8 and ORAI1 coordinating Ca^{2+} and cAMP signaling,[25] while STIM1 translocation upon ER Ca^{2+} depletion enhanced AC-mediated cAMP independently of cytosolic Ca^{2+} levels.[61] Previous studies in bronchial epithelial cells report that compartmentalized AC1-CFTR interaction is responsible for Ca^{2+}/cAMP cross-talk in response to purinergic stimulation that also influence the activity of TMEM16A.[62,63] Our dSTORM analysis showed that CFTR closely co-localizes with AC1, AC3, and AC8—but only moderately with AC6—in PM nanodomains containing ORAI1. Knockdown of AC1/3/8 reduced basal CFTR activity, and the most significant decrease was achieved by siAC8 treatment. We also showed that the deletion of the N-terminal domain of ORAI1 markedly reduced co-localization with AC8, whereas the AC8 had significantly higher activity in the lipid rafts. Our results also suggest that the inhibition of ORAI1 decreases CFTR activity via the impaired generation of the local cAMP pool and PKA activity. These results are in line with previous observations[25,64,65] and also highlight that CFTR is at least partially associated with lipid raft domains of the PM. A previous study identified two populations of CFTR at the cell surface distinguished based on their dynamics that were highly cholesterol dependent in the first group, providing biophysical evidence for multiple CFTR populations in the PM.[66] This observation and our finding also raise the possibility that different CFTR subpopulations play a role in basal and stimulated secretion. Moreover, our recent study revealed that epithelial secretion depends on phosphatidylserine (PtdSer) levels in the ER/PM junctions, regulated by opposing actions of lipid transfer proteins E-Syt3 and ORP5.[67] Altering junctional PtdSer by E-Syt3 disrupted CFTR and NBCe1-B activation, while E-Syt3 depletion enhanced Cl^- flux and fluid secretion in mouse epithelial tissues.

In summary, we describe a novel mechanism in which SPCA2 regulates epithelial ion secretion through STIM1/ORAI1-mediated constitutive Ca^{2+} influx, essential for basal CFTR activity in polarized secretory epithelial cells. Moreover, we identified a protein nanodomain on the apical membrane composed of SPCA2/STIM1/ORAI1, CFTR, and Ca^{2+}-activated AC1, 3, and 8, highlighting distinct regulatory mechanisms for basal versus stimulated secretion. Our model proposes that constitutive Ca^{2+} influx maintains basal CFTR activity independently of neurohormonal stimulation that adjust the ion and fluid secretion to various stimuli. Importantly, this nanodomain may also impact cancer biology, as SPCA2 promotes breast cancer progression,[68] loss of CFTR expression is linked to enhanced Wnt/β-catenin signaling and tumor risk in cystic fibrosis,[69] and ORAI1 regulates proliferation and metastasis.[70] Understanding Orai1/SPCA2 interactions may therefore uncover novel therapeutic targets for cancer.

RESOURCE AVAILABILITY

Lead contact

Further information and requests for resources and reagents should be directed to and will be fulfilled by the lead contact, József Maléth (maleth.jozsef@med.u-szeged.hu).

Materials availability

This study did not generate new unique reagents.

Data and code availability

This study includes no data deposited in external repositories. This paper does not report original code. Any additional information required to reanalyze the data reported in this paper is available from the lead contact upon request.

ACKNOWLEDGMENTS

The research was supported by the Momentum grant of the Hungarian Academy of Sciences (LP2017-18/2017 to J.M.) and the Bolyai Research Fellowship (BO/00569/17 to P.P.), by funding from the Hungarian National Research, Development and Innovation Office (FK139269 to J.M., PD116553 to P.P.); and by the National Excellence Programme (20391-3/2018/FEKUSTRAT and TKP2021-EGA-28 to J.M., UNKP-21-4-SZTE-116 to T.M., and UNKP-21-3-SZTE-94 to B.J.). This work was also supported by the Albert Szent-Györgyi Research Grant (to T.C.) from the Faculty of Medicine, University of Szeged. The project has received funding from the EU's Horizon 2020 research and innovation program under grant agreement no. 739593. The project was further supported by funding from the Hungarian Government (NTP-NFTÖ-B-0011 to Á.V., NTP-NFTÖ-21-B-0205 to A.K., and NTP-NFTÖ-21-B-0079 to V.S.). The FLIM measurements (TKP2021-NVA-19) have been implemented with support provided by the Ministry of Innovation and Technology of Hungary from the National Research, Development and Innovation Fund, financed under the TKP2021-NVA funding scheme. Q16

AUTHOR CONTRIBUTIONS

Á.V. and J.M. designed the research project. Á.V., M.G., T.M., W.Y.C., P.P., V. S., A.K., P.S., E.K.-S., D.V., P.B., I.H.S., T.C., B.J., B.T., A.B., M.E., and S.M. contributed to the acquisition, analysis, and interpretation of data for the work. Á.V. and J.M. drafted the manuscript, and all authors approved the final version of the manuscript and agreed to be accountable for all aspects of the work in ensuring that questions related to the accuracy or integrity of any part of the work are appropriately investigated and resolved. All persons designated as authors qualify for authorship, and all those who qualify for authorship are listed.

DECLARATION OF INTERESTS

The authors declare no competing interests.

STAR★METHODS

Detailed methods are provided in the online version of this paper and include the following:

- KEY RESOURCES TABLE
- EXPERIMENTAL MODEL AND STUDY PARTICIPANT DETAILS
  - Ethics
  - Animals
  - Adherent Cell cultures
- METHOD DETAILS
  - Isolation of pancreatic ductal fragments and acinar cells
  - Mouse, human and human apical-out organoid cultures
  - Constructs, transfection, and site-directed mutagenesis
  - Gene knockdown
  - End-point and qRT-PCR analysis
  - Gene expression analysis of mouse pancreatic ductal organoid cultures by RNA-Seq
  - Immunofluorescent labeling for confocal microscopy
  - Western blot, Cell Surface Biotinylation and Co-immunoprecipitation
  - Fluorescent microscopy
  - *In vitro* measurement of pancreatic fluid secretion
  - *In vivo* pancreatic fluid secretion measurement
  - Current recording
  - Measurement of mitochondrial functions
  - Direct Stochastic Optical Reconstruction Microscopy (dSTORM)
  - FLIM-FRET measurements
- QUANTIFICATION AND STATISTICAL ANALYSIS
  - Fluorescent microscopy
  - Calculation of current density and inactivation slope
  - Definition of co-clusters in dSTORM images
  - Calculation of the fluorescent lifetime
  - Statistical analysis

SUPPLEMENTAL INFORMATION

Supplemental information can be found online at https://doi.org/10.1016/j.cub.2025.09.006.

Received: September 16, 2024
Revised: July 16, 2025
Accepted: September 2, 2025

REFERENCES

1. Ahuja, M., Chung, W.Y., Lin, W.-Y., McNally, B.A., and Muallem, S. (2020). Ca2+ Signaling in Exocrine Cells. Cold Spring Harb. Perspect. Biol. *12*, a035279. https://doi.org/10.1101/cshperspect.a035279.
2. Ahuja, M., Jha, A., Maléth, J., Park, S., and Muallem, S. (2014). cAMP and Ca^{2+} signaling in secretory epithelia: crosstalk and synergism. Cell Calcium *55*, 385–393. https://doi.org/10.1016/j.ceca.2014.01.006.
3. Liou, J., Kim, M.L., Heo, W.D., Jones, J.T., Myers, J.W., Ferrell, J.E., and Meyer, T. (2005). STIM is a Ca2+ sensor essential for Ca2+-store-depletion-triggered Ca2+ influx. Curr. Biol. *15*, 1235–1241. https://doi.org/10.1016/j.cub.2005.05.055.
4. Prakriya, M., Feske, S., Gwack, Y., Srikanth, S., Rao, A., and Hogan, P.G. (2006). Orai1 is an essential pore subunit of the CRAC channel. Nature *443*, 230–233. https://doi.org/10.1038/nature05122.
5. Concepcion, A.R., Vaeth, M., Wagner, L.E., Eckstein, M., Hecht, L., Yang, J., Crottes, D., Seidl, M., Shin, H.P., Weidinger, C., et al. (2016). Store-operated Ca2+ entry regulates Ca2+-activated chloride channels and eccrine sweat gland function. J. Clin. Invest. *126*, 4303–4318. https://doi.org/10.1172/JCI89056.
6. Schober, R., Waldherr, L., Schmidt, T., Graziani, A., Stilianu, C., Legat, L., Groschner, K., and Schindl, R. (2019). STIM1 and Orai1 regulate Ca2+ microdomains for activation of transcription. Biochim. Biophys. Acta Mol. Cell Res. *1866*, 1079–1091. https://doi.org/10.1016/j.bbamcr.2018.11.001.
7. Yeung, P.S.-W., Yamashita, M., and Prakriya, M. (2023). A pathogenic human Orai1 mutation unmasks STIM1-independent rapid inactivation of Orai1 channels. eLife *12*, e82281. https://doi.org/10.7554/eLife.82281.
8. Smaardijk, S., Chen, J., Kerselaers, S., Voets, T., Eggermont, J., and Vangheluwe, P. (2018). Store-independent coupling between the Secretory Pathway Ca2+ transport ATPase SPCA1 and Orai1 in Golgi stress and Hailey-Hailey disease. Biochim. Biophys. Acta Mol. Cell Res. *1865*, 855–862. https://doi.org/10.1016/j.bbamcr.2018.03.007. Q14
9. Cross, B.M., Hack, A., Reinhardt, T.A., and Rao, R. (2013). SPCA2 regulates Orai1 trafficking and store independent Ca2+ entry in a model of lactation. PLoS One *8*, e67348. https://doi.org/10.1371/journal.pone.0067348.
10. Feng, M., Grice, D.M., Faddy, H.M., Nguyen, N., Leitch, S., Wang, Y., Muend, S., Kenny, P.A., Sukumar, S., Roberts-Thomson, S.J., et al. (2010). Store-independent activation of Orai1 by SPCA2 in mammary tumors. Cell *143*, 84–98. https://doi.org/10.1016/j.cell.2010.08.040.
11. Peretti, M., Badaoui, M., Girault, A., Van Gulick, L., Mabille, M.P., Tebbakha, R., Sevestre, H., Morjani, H., and Ouadid-Ahidouch, H. (2019). Original association of ion transporters mediates the ECM-induced breast cancer cell survival: Kv10.1-Orai1-SPCA2 partnership. Sci. Rep. *9*, 1175. https://doi.org/10.1038/s41598-018-37602-7.
12. Girault, A., Peretti, M., Badaoui, M., Hémon, A., Morjani, H., and Ouadid-Ahidouch, H. (2021). The N and C-termini of SPCA2 regulate differently Kv10.1 function: role in the collagen 1-induced breast cancer cell survival. Am. J. Cancer Res. *11*, 251–263.
13. Jentsch, T.J., Stein, V., Weinreich, F., and Zdebik, A.A. (2002). Molecular structure and physiological function of chloride channels. Physiol. Rev. *82*, 503–568. https://doi.org/10.1152/physrev.00029.2001.
14. Widdicombe, J.H., and Wine, J.J. (2015). Airway Gland Structure and Function. Physiol. Rev. *95*, 1241–1319. https://doi.org/10.1152/physrev.00039.2014.
15. Hegyi, P., Wilschanski, M., Muallem, S., Lukacs, G.L., Sahin-Tóth, M., Uc, A., Gray, M.A., Rakonczay, Z., and Maléth, J. (2016). CFTR: A New Horizon in the Pathomechanism and Treatment of Pancreatitis. Rev. Physiol. Biochem. Pharmacol. *170*, 37–66. https://doi.org/10.1007/112_2015_5002.
16. Quinton, P.M. (2007). Cystic fibrosis: lessons from the sweat gland. Physiology (Bethesda) *22*, 212–225. https://doi.org/10.1152/physiol.00041.2006.
17. Madácsy, T., Varga, Á., Papp, N., Tél, B., Pallagi, P., Szabó, V., Kiss, A., Fanczal, J., Rakonczay, Z., Tiszlavicz, L., et al. (2022). Impaired regulation of PMCA activity by defective CFTR expression promotes epithelial cell damage in alcoholic pancreatitis and hepatitis. Cell. Mol. Life Sci. *79*, 265. https://doi.org/10.1007/s00018-022-04287-1.
18. Baker, J.M.R., Hudson, R.P., Kanelis, V., Choy, W.Y., Thibodeau, P.H., Thomas, P.J., and Forman-Kay, J.D. (2007). CFTR regulatory region interacts with NBD1 predominantly via multiple transient helices. Nat. Struct. Mol. Biol. *14*, 738–745. https://doi.org/10.1038/nsmb1278.
19. Chong, P.A., Kota, P., Dokholyan, N.V., and Forman-Kay, J.D. (2013). Dynamics intrinsic to cystic fibrosis transmembrane conductance regulator function and stability. Cold Spring Harb. Perspect. Med. *3*, a009522. https://doi.org/10.1101/cshperspect.a009522.
20. Gadsby, D.C., Vergani, P., and Csanády, L. (2006). The ABC protein turned chloride channel whose failure causes cystic fibrosis. Nature *440*, 477–483. https://doi.org/10.1038/nature04712.

21. Hwang, T.-C., and Sheppard, D.N. (2009). Gating of the CFTR Cl- channel by ATP-driven nucleotide-binding domain dimerisation. J. Physiol. *587*, 2151–2161. https://doi.org/10.1113/jphysiol.2009.171595.

22. Mense, M., Vergani, P., White, D.M., Altberg, G., Nairn, A.C., and Gadsby, D.C. (2006). In vivo phosphorylation of CFTR promotes formation of a nucleotide-binding domain heterodimer. EMBO J. *25*, 4728–4739. https://doi.org/10.1038/sj.emboj.7601373.

23. Musheshe, N., Schmidt, M., and Zaccolo, M. (2018). cAMP: From Long-Range Second Messenger to Nanodomain Signalling. Trends Pharmacol. Sci. *39*, 209–222. https://doi.org/10.1016/j.tips.2017.11.006.

24. Arige, V., and Yule, D.I. (2022). Spatial and temporal crosstalk between the cAMP and Ca2+ signaling systems. Biochim. Biophys. Acta Mol. Cell Res. *1869*, 119293. https://doi.org/10.1016/j.bbamcr.2022.119293.

25. Willoughby, D., Everett, K.L., Halls, M.L., Pacheco, J., Skroblin, P., Vaca, L., Klussmann, E., and Cooper, D.M.F. (2012). Direct binding between Orai1 and AC8 mediates dynamic interplay between Ca2+ and cAMP signaling. Sci. Signal. *5*, ra29. https://doi.org/10.1126/scisignal.2002299.

26. Balghi, H., Robert, R., Rappaz, B., Zhang, X., Wohlhuter-Haddad, A., Evagelidis, A., Luo, Y., Goepp, J., Ferraro, P., Roméo, P., et al. (2011). Enhanced Ca2+ entry due to Orai1 plasma membrane insertion increases IL-8 secretion by cystic fibrosis airways. FASEB J. *25*, 4274–4291. https://doi.org/10.1096/fj.11-187682.

27. Molnár, R., Madácsy, T., Varga, Á., Németh, M., Katona, X., Görög, M., Molnár, B., Fanczal, J., Rakonczay, Z., Hegyi, P., et al. (2020). Mouse pancreatic ductal organoid culture as a relevant model to study exocrine pancreatic ion secretion. Lab. Invest. *100*, 84–97. https://doi.org/10.1038/s41374-019-0300-3.

28. Varga, Á., Madácsy, T., Görög, M., Kiss, A., Susánszki, P., Szabó, V., Jójárt, B., Dudás, K., Farkas, G., Szederkényi, E., et al. (2023). Human pancreatic ductal organoids with controlled polarity provide a novel ex vivo tool to study epithelial cell physiology. Cell. Mol. Life Sci. *80*, 192. https://doi.org/10.1007/s00018-023-04836-2.

29. Palmer, A.E., Jin, C., Reed, J.C., and Tsien, R.Y. (2004). Bcl-2-mediated alterations in endoplasmic reticulum Ca2+ analyzed with an improved genetically encoded fluorescent sensor. Proc. Natl. Acad. Sci. USA *101*, 17404–17409. https://doi.org/10.1073/pnas.0408030101.

30. Deb, B.K., Pathak, T., and Hasan, G. (2016). Store-independent modulation of Ca(2+) entry through Orai by Septin 7. Nat. Commun. *7*, 11751. https://doi.org/10.1038/ncomms11751.

31. Fenech, M.A., Sullivan, C.M., Ferreira, L.T., Mehmood, R., MacDonald, W. A., Stathopulos, P.B., and Pin, C.L. (2016). Atp2c2 Is Transcribed From a Unique Transcriptional Start Site in Mouse Pancreatic Acinar Cells. J. Cell. Physiol. *231*, 2768–2778. https://doi.org/10.1002/jcp.25391.

32. Fenech, M.A., Carter, M.M., Stathopulos, P.B., and Pin, C.L. (2020). The pancreas-specific form of secretory pathway calcium ATPase 2 regulates multiple pathways involved in calcium homeostasis. Biochim. Biophys. Acta Mol. Cell Res. *1867*, 118567. https://doi.org/10.1016/j.bbamcr.2019.118567.

33. Uhlén, M., Fagerberg, L., Hallström, B.M., Lindskog, C., Oksvold, P., Mardinoglu, A., Sivertsson, Å., Kampf, C., Sjöstedt, E., Asplund, A., et al. (2015). Proteomics. Tissue-based map of the human proteome. Science *347*, 1260419. https://doi.org/10.1126/science.1260419.

34. Pallagi, P., Görög, M., Papp, N., Madácsy, T., Varga, Á., Crul, T., Szabó, V., Molnár, M., Dudás, K., Grassalkovich, A., et al. (2022). Bile acid- and ethanol-mediated activation of Orai1 damages pancreatic ductal secretion in acute pancreatitis. J. Physiol. *600*, 1631–1650. https://doi.org/10.1113/JP282203.

35. Wu, M.M., Buchanan, J., Luik, R.M., and Lewis, R.S. (2006). Ca2+ store depletion causes STIM1 to accumulate in ER regions closely associated with the plasma membrane. J. Cell Biol. *174*, 803–813. https://doi.org/10.1083/jcb.200604014.

36. Mercer, J.C., Dehaven, W.I., Smyth, J.T., Wedel, B., Boyles, R.R., Bird, G. S., and Putney, J.W. (2006). Large store-operated calcium selective currents due to co-expression of Orai1 or Orai2 with the intracellular calcium sensor, Stim1. J. Biol. Chem. *281*, 24979–24990. https://doi.org/10.1074/jbc.M604589200.

37. Prakriya, M., and Lewis, R.S. (2015). Store-Operated Calcium Channels. Physiol. Rev. *95*, 1383–1436. https://doi.org/10.1152/physrev.00020.2014.

38. Jha, A., Chung, W.Y., Vachel, L., Maleth, J., Lake, S., Zhang, G., Ahuja, M., and Muallem, S. (2019). Anoctamin 8 tethers endoplasmic reticulum and plasma membrane for assembly of Ca2+ signaling complexes at the ER/PM compartment. EMBO J. *38*, e101452. https://doi.org/10.15252/embj.2018101452.

39. Chung, W.Y., Ahuja, M., McNally, B.A., Leibow, S.R., Ohman, H.K.E., Movahed Abtahi, A., and Muallem, S. (2023). PtdSer as a signaling lipid determined by privileged localization of ORP5 and ORP8 at ER/PM junctional foci to determine PM and ER PtdSer/PI(4)P ratio and cell function. Proc. Natl. Acad. Sci. USA *120*, e2301410120. https://doi.org/10.1073/pnas.2301410120.

40. Wu, M.M., Covington, E.D., and Lewis, R.S. (2014). Single-molecule analysis of diffusion and trapping of STIM1 and Orai1 at endoplasmic reticulum-plasma membrane junctions. Mol. Biol. Cell *25*, 3672–3685. https://doi.org/10.1091/mbc.E14-06-1107.

41. Makena, M.R., Ko, M., Mekile, A.X., Senoo, N., Dang, D.K., Warrington, J., Buckhaults, P., Talbot, C.C., Claypool, S.M., and Rao, R. (2022). Secretory pathway Ca2+-ATPase SPCA2 regulates mitochondrial respiration and DNA damage response through store-independent calcium entry. Redox Biol. *50*, 102240. https://doi.org/10.1016/j.redox.2022.102240.

42. Maléth, J., Venglovecz, V., Rázga, Z., Tiszlavicz, L., Rakonczay, Z., and Hegyi, P. (2011). Non-conjugated chenodeoxycholate induces severe mitochondrial damage and inhibits bicarbonate transport in pancreatic duct cells. Gut *60*, 136–138. https://doi.org/10.1136/gut.2009.192153.

43. Park, S., Shcheynikov, N., Hong, J.H., Zheng, C., Suh, S.H., Kawaai, K., Ando, H., Mizutani, A., Abe, T., Kiyonari, H., et al. (2013). Irbit mediates synergy between ca(2+) and cAMP signaling pathways during epithelial transport in mice. Gastroenterology *145*, 232–241. https://doi.org/10.1053/j.gastro.2013.03.047.

44. Sabbatini, M.E., D'Alecy, L., Lentz, S.I., Tang, T., and Williams, J.A. (2013). Adenylyl cyclase 6 mediates the action of cyclic AMP-dependent secretagogues in mouse pancreatic exocrine cells via protein kinase A pathway activation. J. Physiol. *591*, 3693–3707. https://doi.org/10.1113/jphysiol.2012.249698.

45. Maléth, J., Choi, S., Muallem, S., and Ahuja, M. (2014). Translocation between PI(4,5)P2-poor and PI(4,5)P2-rich microdomains during store depletion determines STIM1 conformation and Orai1 gating. Nat. Commun. *5*, 5843. https://doi.org/10.1038/ncomms6843.

46. Averaimo, S., Assali, A., Ros, O., Couvet, S., Zagar, Y., Genescu, I., Rebsam, A., and Nicol, X. (2016). A plasma membrane microdomain compartmentalizes ephrin-generated cAMP signals to prune developing retinal axon arbors. Nat. Commun. *7*, 12896. https://doi.org/10.1038/ncomms12896.

47. Musheshe, N., Lobo, M.J., Schmidt, M., and Zaccolo, M. (2018). Targeting FRET-Based Reporters for cAMP and PKA Activity Using AKAP79. Sensors (Basel) *18*, 2164. https://doi.org/10.3390/s18072164.

48. Parekh, A.B., and Putney, J.W. (2005). Store-operated calcium channels. Physiol. Rev. *85*, 757–810. https://doi.org/10.1152/physrev.00057.2003.

49. Ahuja, M., Schwartz, D.M., Tandon, M., Son, A., Zeng, M., Swaim, W., Eckhaus, M., Hoffman, V., Cui, Y., Xiao, B., et al. (2017). Orai1-Mediated Antimicrobial Secretion from Pancreatic Acini Shapes the Gut Microbiome and Regulates Gut Innate Immunity. Cell Metab. *25*, 635–646. https://doi.org/10.1016/j.cmet.2017.02.007.

50. Szabó, V., Csákány-Papp, N., Görög, M., Madácsy, T., Varga, Á., Kiss, A., Tél, B., Jójárt, B., Crul, T., Dudás, K., et al. (2023). Orai1 calcium channel inhibition prevents progression of chronic pancreatitis. JCI Insight *8*, e167645. https://doi.org/10.1172/jci.insight.167645.

51. Pallagi, P., Madácsy, T., Varga, Á., and Maléth, J. (2020). Intracellular Ca2+ Signalling in the Pathogenesis of Acute Pancreatitis: Recent

Advances and Translational Perspectives. Int. J. Mol. Sci. *21*, 4005. https://doi.org/10.3390/ijms21114005.

52. Sorin, A., Rosas, G., and Rao, R. (1997). PMR1, a Ca2+-ATPase in yeast Golgi, has properties distinct from sarco/endoplasmic reticulum and plasma membrane calcium pumps. J. Biol. Chem. *272*, 9895–9901. https://doi.org/10.1074/jbc.272.15.9895.
53. Vanoevelen, J., Dode, L., Van Baelen, K., Fairclough, R.J., Missiaen, L., Raeymaekers, L., and Wuytack, F. (2005). The secretory pathway Ca2+/Mn2+-ATPase 2 is a Golgi-localized pump with high affinity for Ca2+ ions. J. Biol. Chem. *280*, 22800–22808. https://doi.org/10.1074/jbc.M501026200.
54. Chang, C.-L., Hsieh, T.-S., Yang, T.T., Rothberg, K.G., Azizoglu, D.B., Volk, E., Liao, J.-C., and Liou, J. (2013). Feedback Regulation of Receptor-Induced Ca2+ Signaling Mediated by E-Syt1 and Nir2 at Endoplasmic Reticulum-Plasma Membrane Junctions. Cell Rep. *5*, 813–825. https://doi.org/10.1016/j.celrep.2013.09.038.
55. Shan, J., Liao, J., Huang, J., Robert, R., Palmer, M.L., Fahrenkrug, S.C., O'Grady, S.M., and Hanrahan, J.W. (2012). Bicarbonate-dependent chloride transport drives fluid secretion by the human airway epithelial cell line Calu-3. J. Physiol. *590*, 5273–5297. https://doi.org/10.1113/jphysiol.2012.236893.
56. Balázs, A., Rubil, T., Wong, C.K., Berger, J., Drescher, M., Seidel, K., Stahl, M., Graeber, S.Y., and Mall, M.A. (2025). The potentiator ivacaftor is essential for pharmacological restoration of F508del-CFTR function and mucociliary clearance in cystic fibrosis. JCI Insight *10*, e187951. https://doi.org/10.1172/jci.insight.187951.
57. Wen, L., Voronina, S., Javed, M.A., Awais, M., Szatmary, P., Latawiec, D., Chvanov, M., Collier, D., Huang, W., Barrett, J., et al. (2015). Inhibitors of ORAI1 Prevent Cytosolic Calcium-Associated Injury of Human Pancreatic Acinar Cells and Acute Pancreatitis in 3 Mouse Models. Gastroenterology *149*, 481–92.e7. https://doi.org/10.1053/j.gastro.2015.04.015.
58. Gidalevitz, T., Prahlad, V., and Morimoto, R.I. (2011). The stress of protein misfolding: from single cells to multicellular organisms. Cold Spring Harb. Perspect. Biol. *3*, a009704. https://doi.org/10.1101/cshperspect.a009704.
59. Halls, M.L., and Cooper, D.M.F. (2011). Regulation by Ca2+-signaling pathways of adenylyl cyclases. Cold Spring Harb. Perspect. Biol. *3*, a004143. https://doi.org/10.1101/cshperspect.a004143.
60. Park, H.W., Nam, J.H., Kim, J.Y., Namkung, W., Yoon, J.S., Lee, J.S., Kim, K.S., Venglovecz, V., Gray, M.A., Kim, K.H., et al. (2010). Dynamic regulation of CFTR bicarbonate permeability by [Cl-]i and its role in pancreatic bicarbonate secretion. Gastroenterology *139*, 620–631. https://doi.org/10.1053/j.gastro.2010.04.004.
61. Lefkimmiatis, K., Srikanthan, M., Maiellaro, I., Moyer, M.P., Curci, S., and Hofer, A.M. (2009). Store-operated cyclic AMP signalling mediated by STIM1. Nat. Cell Biol. *11*, 433–442. https://doi.org/10.1038/ncb1850.
62. Namkung, W., Finkbeiner, W.E., and Verkman, A.S. (2010). CFTR-adenylyl cyclase I association responsible for UTP activation of CFTR in well-differentiated primary human bronchial cell cultures. Mol. Biol. Cell *21*, 2639–2648. https://doi.org/10.1091/mbc.E09-12-1004.
63. Lérias, J., Pinto, M., Benedetto, R., Schreiber, R., Amaral, M., Aureli, M., and Kunzelmann, K. (2018). Compartmentalized crosstalk of CFTR and TMEM16A (ANO1) through EPAC1 and ADCY1. Cell. Signal. *44*, 10–19. https://doi.org/10.1016/j.cellsig.2018.01.008.
64. Cooper, D.M.F. (2015). Store-operated Ca^{2+}-entry and adenylyl cyclase. Cell Calcium *58*, 368–375. https://doi.org/10.1016/j.ceca.2015.04.004.
65. Johnstone, T.B., Agarwal, S.R., Harvey, R.D., and Ostrom, R.S. (2018). cAMP Signaling Compartmentation: Adenylyl Cyclases as Anchors of Dynamic Signaling Complexes. Mol. Pharmacol. *93*, 270–276. https://doi.org/10.1124/mol.117.110825.
66. Abu-Arish, A., Pandzic, E., Goepp, J., Matthes, E., Hanrahan, J.W., and Wiseman, P.W. (2015). Cholesterol modulates CFTR confinement in the plasma membrane of primary epithelial cells. Biophys. J. *109*, 85–94. https://doi.org/10.1016/j.bpj.2015.04.042.

67Sarkar, P., Lüscher, B.P., Ye, Z., Chung, W.Y., Abtahi, A.M., Zheng, C., Lee, M.G., Varga, Á., Pallagi, P., Maléth, J., et al. (2025). Lipid transporters E-Syt3 and ORP5 regulate epithelial ion transport by controlling phosphatidylserine enrichment at ER/PM junctions. EMBO J. *44*, 3697–371910.1038/s44318-025-00470-9.

68. Cross, B.M., Breitwieser, G.E., Reinhardt, T.A., and Rao, R. (2014). Cellular calcium dynamics in lactation and breast cancer: from physiology to pathology. Am. J. Physiol. Cell Physiol. *306*, C515–C526. https://doi.org/10.1152/ajpcell.00330.2013.
69. Strubberg, A.M., Liu, J., Walker, N.M., Stefanski, C.D., MacLeod, R.J., Magness, S.T., and Clarke, L.L. (2018). Cftr Modulates Wnt/β-Catenin Signaling and Stem Cell Proliferation in Murine Intestine. Cell. Mol. Gastroenterol. Hepatol. *5*, 253–271. https://doi.org/10.1016/j.jcmgh.2017.11.013.
70. Hammad, A.S., and Machaca, K. (2021). Store Operated Calcium Entry in Cell Migration and Cancer Metastasis. Cells *10*, 1246. https://doi.org/10.3390/cells10051246.
71. Maléth, J., Balázs, A., Pallagi, P., Balla, Z., Kui, B., Katona, M., Judák, L., Németh, I., Kemény, L.V., Rakonczay, Z., et al. (2015). Alcohol disrupts levels and function of the cystic fibrosis transmembrane conductance regulator to promote development of pancreatitis. Gastroenterology *148*, 427–39.e16. https://doi.org/10.1053/j.gastro.2014.11.002.
72. Fanczal, J., Pallagi, P., Görög, M., Diszházi, G., Almássy, J., Madácsy, T., Varga, Á., Csernay-Biró, P., Katona, X., Tóth, E., et al. (2020). TRPM2-mediated extracellular Ca2+ entry promotes acinar cell necrosis in biliary acute pancreatitis. J. Physiol. *598*, 1253–1270. https://doi.org/10.1113/JP279047.
73. Boj, S.F., Hwang, C.-I., Baker, L.A., Chio, I.I.C., Engle, D.D., Corbo, V., Jager, M., Ponz-Sarvise, M., Tiriac, H., Spector, M.S., et al. (2015). Organoid models of human and mouse ductal pancreatic cancer. Cell *160*, 324–338. https://doi.org/10.1016/j.cell.2014.12.021.
74. Huch, M., Dorrell, C., Boj, S.F., van Es, J.H., Li, V.S.W., van de Wetering, M., Sato, T., Hamer, K., Sasaki, N., Finegold, M.J., et al. (2013). In vitro expansion of single Lgr5+ liver stem cells induced by Wnt-driven regeneration. Nature *494*, 247–250. https://doi.org/10.1038/nature11826.
75. Kiss, A., Farkas, A., Ayaydin, F., Lázár, G., Varga, Á., and Maléth, J. (2024). Human Pancreas-Derived Organoids with Controlled Polarity: Detailed Protocols and Experimental Timeline. Curr. Protoc. *4*, e70045. https://doi.org/10.1002/cpz1.70045.
76. Bozoky, Z., Ahmadi, S., Milman, T., Kim, T.H., Du, K., Di Paola, M., Pasyk, S., Pekhletski, R., Keller, J.P., Bear, C.E., et al. (2017). Synergy of cAMP and calcium signaling pathways in CFTR regulation. Proc. Natl. Acad. Sci. USA *114*, E2086–E2095. https://doi.org/10.1073/pnas.1613546114.
77. Pallagi, P., Balla, Z., Singh, A.K., Dósa, S., Iványi, B., Kukor, Z., Tóth, A., Riederer, B., Liu, Y., Engelhardt, R., et al. (2014). The role of pancreatic ductal secretion in protection against acute pancreatitis in mice*. Crit. Care Med. *42*, e177–e188. https://doi.org/10.1097/CCM.0000000000000101.
78. Komlódi, T., Sobotka, O., Krumschnabel, G., Bezuidenhout, N., Hiller, E., Doerrier, C., and Gnaiger, E. (2018). Comparison of Mitochondrial Incubation Media for Measurement of Respiration and Hydrogen Peroxide Production. Methods Mol. Biol. *1782*, 137–155. https://doi.org/10.1007/978-1-4939-7831-1_8.
79. Nászai, A., Terhes, E., Kaszaki, J., Boros, M., and Juhász, L. (2019). Ca(2+) N It Be Measured? Detection of Extramitochondrial Calcium Movement With High-Resolution FluoRespirometry. Sci. Rep. *9*, 19229. https://doi.org/10.1038/s41598-019-55618-5.

Please cite this article in press as: Kiss et al., Store-independent activation of STIM1-ORAI1 by SPCA2 determines the basal CFTR activity in secretory epithelial cells, Current Biology (2025), https://doi.org/10.1038/s44318-025-00470-9

STAR★METHODS

KEY RESOURCES TABLE

REAGENT or RESOURCE	SOURCE	IDENTIFIER
Adherent Cell cultures		
HeLa cell line	ATCC	ATCC-CCL-2
HEK-293 cell line	ATCC	CRL-1573
DMEM	Gibco	41965
FBS	Gibco	10500064
Kanamycin Sulfate	Gibco	15160054
Antibiotic-Antimycotic Solution	Gibco	15240062
Penicillin/Streptomycin	Gibco	15070063
GlutaMax™	Gibco	3505006
L-WRN cell line	ATCC	ATCC-CRL-3276
ATCC-formulated DMEM	ATCC	ATCC-30-2002
G-418	Gibco	11811031
Hygromycin B	Invitrogen	10687010
Constructs, transfection and site-directed mutagenesis		
Cover glass	VWR	ECN 631–1583
ADCY1-myc-DDK	ORIGENE	RC237562
ADCY3-myc-DDK	ORIGENE	RC220272
ADCY6-myc-DDK	ORIGENE	RC214902
ADCY8-myc-DDK	ORIGENE	RC211815
pcDNA-D1ER	Addgene	36325
SPCA2-myc-DDK	ORIGENE	RC212990
SPCA2-tGFP	ORIGENE	RG239585
Lipofectamine 2000	Invitrogen	11668019
Opti-MEM	Gibco	31985070
Q5 Site-Directed Mutagenesis Kit	New England BioLabs	E0554S
Gene knockdown		
siGLO Green transfection indicator	Horizon	D-001630-01
Lipofectamine 2000	Invitrogen	11668019
Opti-MEM	Gibco	31985070
Stim1 siRNA	Dharmacon	L-062376-00-0005
Cftr siRNA	Dharmacon	L-042164-00-0005
Orai1 siRNA	Dharmacon	L-056431-02-0005
Spca1 siRNA	Dharmacon	L-041293-00-0005
Spca2 siRNA	Dharmacon	L-065820-01-0005
SPCA2 siRNA	Dharmacon	L-006280-00-0005
Septin7 siRNA	Dharmacon	L-042160-01-0005
Immunofluorescent labeling for confocal microscopy		
Shandon Cryomatrix	ThermoFisher S.	6769006
Cryostat	Leica	CM 1860 UV
Microscope slides	ThermoFisher S.	J3800AMNZ
PFA	Alfa Aesar	43368
PBS	Sigma	P4417-100TAB
Sodium Citrate	Sigma	71402
Tween-20	Sigma	P1379
Goat Serum	Sigma	G9023

(*Continued on next page*)

Please cite this article in press as: Kiss et al., Store-independent activation of STIM1-ORAI1 by SPCA2 determines the basal CFTR activity in secretory epithelial cells, Current Biology (2025), https://doi.org/10.1038/s44318-025-00470-9

Continued

REAGENT or RESOURCE	SOURCE	IDENTIFIER
Bovine Serum Albumin (BSA)	Pan Biotech	P061391100
Recombinant Anti-ADCY9/AC9 antibody	Abcam	ab191423
Anti-CFTR antibody	Abcam	ab2784
Extracellular Anti-Orai1 Antibody	Alomone labs	ACC-062
Orai1 Antibody	Alomone labs	ACC-060
Cytokeratin 19 Antibody	ThermoFisher S.	MA5-31977ATP
ATP2C1 monoclonal antibody (SPCA1)	Novus Biologicals	H00027032-M01
ATP2C2 polyclonal antibody (SPCA2)	Invitrogen	PA567396
ATP2C2 antibody	Invitrogen	PA521127
Anti-STIM1 antibody	Cell Signaling Tech.	5668
SEPTIN7 polyclonal antibody	ThermoFisher S.	13818-0-AP
Calreticulin	Invitrogen	PA3-900
SERCA2 ATPase Monoclonal antibody	Invitrogen	MA3-919
Golgin-97	Invitrogen	PA530048
Lamp1	Invitrogen	53-1079-42
Goat anti-Rabbit Alexa 488	ThermoFisher S.	A11034
Donkey anti-Mouse Alexa 647	ThermoFisher S.	A31571
Western blot, Cell Surface Biotinylation and Co-immunoprecipitation		
1X DPBS	ThermoFisher Scientific	14190250
Cell Scraper	Greiner	54170
RIPA lysis buffer (10X)	EMD Millipore Corp.	20–188
cOmplete ULTRA Tablets, Mini, EASYpack	Roche	05892970001
30% Acrylamide/Bis Solution 29:1	Bio-Rad	1610156
UltraPure™ TEMED	Invitrogen	15524-010
NuPAGE LDS Sample Buffer (4X)	Invitrogen	NP0007
10X TG	Bio-Rad	161-0771
10X TGS	Bio-Rad	161-0772
Immun-Blot PVDF Membrane	Bio-Rad	1620177
anti-GAPDH	Cell Signalling Technology	5174S
anti-HA-Tag	Cell Signalling Technology	3724
ClarityTM Western ECL Substrate	Bio-Rad	1705060
Goat anti-Rabbit peroxidase conjugate	Merck Millipore	A8275
Pierce™ Cell Surface Biotinylation and Isolation Kit	ThermoFisher Scientific	A44390
12–230 kDa Separation Module, 8 x 25 capillary cartridges	Biotechne	SM-W004
Anti-Rabbit Detection Module	Biotechne	DM-001
Anti-Mouse Detection Module	Biotechne	DM-002
Total Protein Detection Module	Biotechne	DM-TP01
RePlex™ Module	Biotechne	RP-001
20X Anti-Rabbit HRP Conjugate	Biotechne	043-426
Dynabeads™ Protein A for Immunoprecipitation	ThermoFisher Scientific	10002D
Myc Tag Polyclonal antibody	Thermo Scientific	A21281
Anti- HA-tag antibody	Cell Signaling Technology	3724S
Fluorescent microscopy		
Poly-L-lysine	Sigma	P8920-100ML
Cover glass	VWR	ECN 631-1583
Fura2-AM	Invitrogen	F1201
MQAE	Invitrogen	E3101
Mag-Fluo-4	Invitrogen	M14206
BCECF-AM	Invitrogen	B1170

(*Continued on next page*)

Please cite this article in press as: Kiss et al., Store-independent activation of STIM1-ORAI1 by SPCA2 determines the basal CFTR activity in secretory epithelial cells, Current Biology (2025), https://doi.org/10.1038/s44318-025-00470-9

Continued

REAGENT or RESOURCE	SOURCE	IDENTIFIER
CPA	Tocris	1235
CM5480	Provided by CalciMedica	
GSK-7975A	Sigma	5.34351
Carbamylcholine chloride (Carbachol)	Sigma	PHR1511
Forskolin	Tocris	1099
CFTRinh-172	Biotechne	3430
BAPTA-AM	Sigma	A1076
Direct Stochastic Optical Reconstruction Microscopy (dSTORM)		
Methanol	Sigma	34860
Two-component adhesive	Picodent	1300 7100
Cavity slides	Sigma	BR475505-50EA
Myc Tag Polyclonal antibody	Thermo Scientific	A21281
Anti- HA-tag antibody	Cell Signaling Technology	3724S
Anti- CFTR antibody	Abcam	ab2784
Extracellular Anti-Orai1 Antibody	Alomone labs	ACC-062
PKA alpha polyclonal antibody	Invitrogene	PA517626
Donkey anti-Mouse Alexa 647	ThermoFisher S.	A31571
Goat anti-Chicken Alexa 647	Thermo Scientific	A32933
Goat anti-Rabbit Alexa 568	Thermo Scientific	A11011
Goat anti-Mouse Alexa 488	Thermo Scientific	A11001

EXPERIMENTAL MODEL AND STUDY PARTICIPANT DETAILS

Ethics

The NIH rules and the EU Directive 2010/63/EU were followed while using animals. The National Scientific Ethical Committee on Animal Experimentation granted the study license number XXI./1541/2020. The collection and use of human samples, including cadaver donor pancreas, was carried out following EU norms and was approved by the Hungarian Medical Research Council's Regional Committee of Research Ethics under license number 37/2017-SZTE.

Animals

8- to 12-week-old and 20-25-gram weighted FVB/N mice were used during all the experiments. Animals were kept at a constant room temperature (22-24°C) with a 12-hour light-dark cycle. Mice were allowed free access to rodent chow. The gender ratio was 1:1 for all investigated groups.

Adherent Cell cultures

HeLa, and HEK293 cells were cultured according to the provider's protocol and were used for transient transfection and subsequent measurements. L-WRN cell line (ATCC-CRL-3276) was utilized to produce conditioned medium required for organoid cultures. HeLa cells were grown in DMEM containing 10% fetal bovine serum (FBS), 1% Kanamycin Sulfate, 1% Antibiotic-Antimycotic solution, and 1% GlutaMax™ supplement. Conditioned medium for organoid cultures has been provided by L-WRN cell line grown in selection medium containing 10% FBS and 0.5-0.5 mg/ml G418 and Hygromycin B in ATCC-formulated DMEM. Conditioned medium (10% FBS and 1-1% Kanamycin Sulfate and Antibiotic-Antimycotic solution were applied in ATCC-formulated DMEM) has been collected a total of three times every three days and pooled before further applications (Table S1).

METHOD DETAILS

Isolation of pancreatic ductal fragments and acinar cells

Pancreatic ductal fragments were isolated as described previously.[71,72] Briefly, terminal anesthesia with pentobarbital was followed by surgical removal of the pancreas. Pancreatic tissue was partially digested in a vertical shaker with an enzymatic solution containing 100 U/ml collagenase, 0.1 mg/ml trypsin inhibitor, 1 mg/ml bovine serum albumin (BSA) in DMEM/F12 for 30 mins at 37°C. Small intra-/interlobular ducts were identified and isolated by microdissection under a stereomicroscope. The tissue was minced into 1-3 mm^3 pieces for pancreatic acinar cell isolation and placed in ice-cold HBSS. Lipids and fats were removed by centrifugation at 450 RCF (Rotor radius: 180 mm) for 2 min. Tissue pieces were digested in a freshly prepared solution containing 10 mM HEPES (Table S1), 200 units/ml collagenase, and 0.25 mg/ml trypsin inhibitor at 37°C for 20 min as described previously.[72] Digested

tissue was washed by HBSS at 4°C containing 10 mM HEPES, 0.25 mg/ml soybean trypsin inhibitor, and 5% FBS. The supernatant was centrifuged for 2 min at 450 RCF (Rotor radius: 180 mm), and the pellet was resuspended in DMEM/F12 with 2.5% FBS, 2 mM glutamine, and 0.25 mg/ml soybean trypsin inhibitor. Materials are listed in Table S1.

Mouse, human and human apical-out organoid cultures

Mouse pancreatic, liver lung and human pancreatic organoids were generated by using enzymatic solutions and maintained in L-WRN conditioned media supplemented by growth factors as described earlier.[28,73,74] Human pancreatic tissue samples were collected from cadaver donors. For mouse organoid cultures (OCs), after terminal anesthesia by pentobarbital, pancreatic, liver, and lung tissue were removed from the animals surgically and placed in splitting media (listed in Table S2). Mouse and human tissues were minced into small fragments and incubated at 37°C in a digestion solution (detailed in Table S2) in a vertical shaker for approximately 1h, depending on tissue density. The efficiency of the digestion process was verified by stereomicroscopy every 10 minutes. Cells were collected (200 RCF, 10 min, 4°C, Rotor radius: 180 mm) and washed twice by Wash Media (detailed in Table S3). Resuspended cells in Wash media were mixed with Matrigel in a ratio of 1:5. Matrigel domes (10 μl) were placed in one well of a 24-well cell culture plate. After 10 minutes of solidification at 37°C, 500 μl Feeding Media (listed in Table S2) were applied in each well. Feeding media was changed every second day. For OC passaging, domes were pooled and collected (200 RCF, 10 min, 4°C, Rotor radius: 180 mm). Matrigel removal and cell separation were performed simultaneously by using TrypLE™ Express Enzyme at 37°C for 15 minutes in a vertical shaker, followed by washing and plating the cells in Matrigel as described above. Apical-out pancreatic organoids were generated as previously described.[28,75] Briefly, we enzymatically removed the Matrigel surrounding the mature organoids using TrypLE™ Express. The released organoids were subsequently transferred into low-attachment culture plates and maintained in suspension culture for 48–72 hours to allow for spontaneous polarity inversion. This method was adapted from our previously published protocol.[75] Details of the materials used can be found in Table S2.

Constructs, transfection, and site-directed mutagenesis

HeLa cells were grown on cover glass and transfected with the following plasmid DNA constructs: Lyn-H147 and H147-Kras constructs were provided by Xavier Nicol,[46] ORA1-HA, ORAI1-mCherry, ORAI1ΔCT, ORAI1ΔNT and YFP-STIM1 were described before,[45] mCherry-CFTR was a generous gift from Julie Forman-Kay,[76] ADCY and SPCA2 carrying constructs (ADCY1-myc-DDK, ADCY3-myc-DDK, ADCY6-myc-DDK, ADCY8-myc-DDK, and ATP2C2-myc-DDK) were purchased from ORIGENE while pcDNA-D1ER was purchased from Addgene. Transfection was carried out using Lipofectamine 2000 according to the manufacturer's protocol. For *in vitro* mutagenesis, Q5 high-fidelity, thermostable DNA polymerase was applied along with sequence-specific primers in PCR reactions according to the attached protocol. A common concern with experiments derived from heterologous expression of multiple proteins is the altered endogenous stoichiometry of the proteins. To compensate for this, we performed a high number of experiments to buffer and reduce outliers and we tried to confirm the crucial results in primary cells expressing endogenous proteins without overexpression. Details of constructs and materials are listed in Table S3.

Gene knockdown

Isolated mouse ductal fragments were transfected with 50 nM siRNA or siGLO Green transfection indicator and Lipofectamine 2000 in Feeding media (Table S3) for 24h. siGLO Green Transfection Indicator is a fluorescent oligonucleotide duplex that localizes to the nucleus, thus concentrating its signal to permit unambiguous visual assessment of uptake into mammalian cells. It is ideal for use in optimization experiments to determine optimal siRNA transfection conditions and for monitoring relative delivery efficiency. In this control experiments the isolated ductal fragments were incubated with siGLO Green and used for experiments under the same conditions to provide proper controls as previously.[28] In general, to increase the efficiency of gene silencing and reduce off-target effects, pre-validated and pre-designed siRNA pools were applied (SMARTpool siRNAs provided by Dharmacon) in all the experiments and the duration of gene silencing was set at 48 hours, taking into account the half-life of the target proteins. Pre-designed and validated siRNA sets used for gene-specific knockdown are listed in Table S3. The efficiency of gene knock downs was tested with real-time PCR measurements to determine the mRNA levels in the siRNA treated samples, immunofluorescent stainings and capillary Western blot (Figures S1 and S5). In addition, we performed immunostainings to confirm the changes in the protein expression.[28] Overall, these controls showed a marked decrease in the expressions of the proteins of interest.

End-point and qRT-PCR analysis

Total mRNA was isolated from mouse pancreatic ductal fragments by NucleoSpin RNA XS kit according to the manufacturer's instructions. The mRNA concentrations were measured by NanoDrop™ One/One^{C} Microvolume UV-Vis Spectrophotometer. 1 μg purified mRNA was used for the cDNA synthesis step. The efficiency of the pre-validated siRNA pools on the target genes' expression was verified at the level of mRNA by qRT-PCR. Products of polymerase chain reactions were separated in agarose gel prior image acquisition. All qRT-PCR raw data was analyzed by the ΔΔCq method. Applied materials for the qRT-PCR and conventional PCR amplification are indicated in Table S4.

Gene expression analysis of mouse pancreatic ductal organoid cultures by RNA-Seq

RNA was extracted from the collected cell pellet separated from Matrigel described above by NucleoSpin RNA Plus kit according to the manufacturer's protocol (Table S4). RNA-sequencing was performed by Illumina NextSeq 500 instrument, and data analysis

Please cite this article in press as: Kiss et al., Store-independent activation of STIM1-ORAI1 by SPCA2 determines the basal CFTR activity in secretory epithelial cells, Current Biology (2025), https://doi.org/10.1038/s44318-025-00470-9

process services were provided by DeltaBio2000 Ltd. Gene expression pattern was determined according to TPM (transcript/million) values (Data S1). As plasma membrane proteins display relatively low expression levels compared to other genes, such as transcription factors, the threshold for non-expressing genes was TPM<1. The TPM values of the human *CFTR* gene was published previously.[28]

Immunofluorescent labeling for confocal microscopy

Immunofluorescent labeling on sectioned ductal fragments was performed as previously described.[27] Briefly, isolated pancreatic ductal fragments and organoids were frozen in Shandon™ Cryomatrix™ at -20 °C. The 7 μm thick cut sections were placed on microscope slides. The fixation step was done with 4% PFA-PBS for 20 minutes, followed by washing for 3x5 minutes in PBS. After antigen retrieval, sections were blocked with 0.1% goat serum and 10% BSA in PBS for 2 h. The samples were incubated overnight with primary antibodies at 4°C and 2h at room temperature with secondary antibodies. A list of antibodies applied is provided in Table S5. Nuclear staining and mounting are carried out simultaneously by ProLong™ Gold Antifade mounting medium with DAPI. Images were captured by a Zeiss LSM880 confocal microscope using a 40X oil immersion objective (Zeiss, NA: 1.4) and analyzed by Fiji ImageJ software (Version: 2.3.0/1.53f).

Western blot, Cell Surface Biotinylation and Co-immunoprecipitation

HeLa cells were transfected with ORAI1, STIM1, and SPCA2-carrying constructs. After 18 h, cells were washed with 1X DPBS, collected with a cell scraper, and lysed with RIPA buffer supplemented with protease inhibitors. Protein electrophoresis was carried out in 10% acrylamide gels, and, after blotting, the primary antibodies were used at the following dilutions: anti-GAPDH 1:10000; anti-HA 1:1000. Secondary peroxidase-conjugated antibody was used at a dilution of 1:10000. For cell surface protein measurements PierceTM Cell Surface Biotinylation and Isolation Kit was applied according to the attached protocol. Blot picture analysis and quantification were computed by ImageJ software. In selected experiments, protein expression changes were validated using automated capillary Western blotting (Abby, ProteinSimple) in Replex mode. Sample preparation, antibody incubation, and data acquisition were performed according to the protocol provided by the manufacturer. This method enabled multiplexed detection and normalization to total protein within the same capillary. Signal quantification was performed using Compass software, and total protein normalization was applied throughout the analysis. At the same time, uncropped blot images are shown in Figures S5A and S5B. In additional experiments, co-immunoprecipitation was performed to confirm protein-protein interactions. HeLa cells were transfected with ORAI1-HA, STIM1-YFP, and SPCA2-Myc constructs. Dynabeads® Protein A magnetic beads were incubated with 5 μg rabbit anti-HA antibody in 0.1 M sodium phosphate buffer (pH 8.0) for 30–60 minutes at room temperature. After washing, the bead–antibody complex was incubated with 500 μg of clarified cell lysate at 4 °C for overnight. Protein complexes were eluted with 0.1 M glycine-HCl (pH 2.8), and immediately neutralized with 1/10 volume of 1 M Tris-HCl (pH 8.0). Eluted proteins were analyzed by capillary western blott with anti-GFP and anti-Myc antibodies to detect STIM1 and SPCA2 co-precipitation with ORAI1-HA. Applied materials are described in Table S5.

Fluorescent microscopy

Isolated pancreatic ductal fragments or organoids were attached to a poly-L-lysine coated cover glass and were incubated in HEPES solution (Table S6) for 30 min at 37 °C with 5% CO_2. BCECF-AM (1.5 μmol/L) Fura2-AM (5 μmol/L), MQAE (2 μmol/L) fluorescent dye were applied for intracellular pH, Ca^{2+} and Cl^- measurements. Intracellular Ca^{2+} content of the ER was measured with Mag-Fluo-4 (5 μmol/L) fluorescent dye. Olympus IX73 inverted microscopes were used during experiments. Dye-loaded samples were excited with an Olympus CoolLED PE-4000 illumination system. The filter combination for each fluorescent dye was described previously.[27] Hamamatsu Orca-Flash 4.0 sCMOS camera and 20X water immersion objective (Olympus; NA: 0.8) with a temporal resolution of 1 s were used for capturing fluorescent signals. Reagents and inhibitors applied in experiments are listed in Table S5. FRET imaging and data analysis were performed with the same hardware setup extended with a motorized emission filter wheel (Olympus CMR-U-FFWO). The filers were used as follows: 436/20 nm and 504/12 nm excitation filters, a dual-band polychroic mirror for CFP and YFP, and 483/32 nm and 542/27 nm emission filters. Olympus Excellence software was used for fluorescent image analysis while maximum FRET responses (ratio of YFP/CFP) were computed, drift corrected, and normalized to the initial unstimulated values.

In vitro measurement of pancreatic fluid secretion

Isolated pancreatic ductal fragments were attached to poly-L-lysine coated cover glasses and perfused with HEPES or HCO_3^--buffered solutions at 37°C (Table S6). Changes in intraluminal volume were monitored by transmitted video microscopy with Olympus IX73 inverted microscope. The relative intraluminal volume was evaluated with Scion Image software as described earlier.[77]

In vivo pancreatic fluid secretion measurement

CM5480 (i.p.; 20 mg/bwkg) or vehicle was administered twice every 24 hours (total treatment duration 48 hours) before direct *in vivo* pancreatic fluid collection.[50] Mice were anaesthetized with a ketamine/xylazine cocktail (respectively 125 and 12.5 mg/bwkg, i.p.) and placed on a heated pad to maintain body temperature. Following stimulation with secretin (0.75 clinical unit/bwkg, i.p.), the pancreatic juice was collected for 30 min and the secretory rate was calculated as μl/body weight (in g)/1 h. Applied materials are indicated in Table S5.

Please cite this article in press as: Kiss et al., Store-independent activation of STIM1-ORAI1 by SPCA2 determines the basal CFTR activity in secretory epithelial cells, Current Biology (2025), https://doi.org/10.1038/s44318-025-00470-9

Current recording

Ion currents were recorded by Axopatch 200B amplifier with low-pass filtering at 1 kHz in HEK293 cells using the whole-cell configuration of the patch-clamp technique, as detailed before.[38] Pipettes were pulled from glass capillaries (Warner Instruments) using a vertical puller and had a resistance of 5–7 MΩ when filled with the pipette solution. HEK293 cells were maintained in DMEM medium supplemented with 10% fetal bovine serum and 1% Pen/Strep (Table S1). Cells were transfected with the required plasmids using Lipofectamine 2000 (Table S4) and used after for 24h at 37°C. On the day of experiments, the cells were released and re-plated on coverslips and allowed to reattach and recover for at least 2h at 37°C. The pipette solution contained (mM) 135 Cs-methanesulfonate, 6 $MgCl_2$, 2 MgATP, 10 HEPES and 10 BAPTA, pH 7.4 (with CsOH). When the cells were transfected with ORAI1(V102C), the recording started with 15 sec of establishing the whole cell configuration. When the cells were transfected with ORAI1+STIM1, after establishing the whole cell configuration, the cells were kept in Ca^{2+}-free bath solution for 3 min to allow store depletion by BAPTA before exposing the cells to bath solution containing 10 mM Ca^{2+}. The bath solution contained (mM) 130 NaCl, 5 KCl, 1 $MgCl_2$, and 10 HEPES with or without 10 $CaCl_2$ (pH 7.4 with NaOH). The whole cell current was recorded using an Axopatch 200B amplifier with low-pass filtering at 1 kHz. The currents were digitized at a sampling frequency of 5 kHz using Digidata 1440A and stored. Applied materials are indicated in Table S5.

Measurement of mitochondrial functions

Determination of the Intracellular ATP with Cell Viability Assay

Mouse pancreatic ductal organoids (mPOCs) were grown in Matrigel until passage number 3. mPOCs were collected and digested with 25% TrypLE Express for around 15 min in 37°C horizontal shaker (165 rpm) until the Matrigel digested and organoids broke down into individual cells. Pellet was washed with 3 ml wash solution, then cells were regenerated in pre-warmed feeding medium for 30 min in 37°C humidified incubator. Six technical parallels were used in case of each sample (10,000 cells/ well/ in 100 μl final volume) and transferred into 96-well Lumitrac microplate. Standard feeding medium were used as control, DMSO as vehicle control, 10 μM CM5480 as test sample and 50% 12N HCl as positive control. Every treatment was applied for 10 min at 37°C in a humidified incubator before the measurement. CellTiter-Glo® 3D cell viability assay was carried out according the manufacturer's protocol. Briefly, a volume (100 μl) of CellTiter-Glo® 3D Reagent was added equal to the volume of each well. Contents were mixed for 5 minutes in CLARIOstar Plus plate reader (BMG Labtech). Plate was allowed to incubate at room temperature for an additional 25 minutes. Luminescence was recorded in CLARIOstar Plus plate reader and data was analyzed with 4-parameter fit probe. Total protein amount was determined using by BCA assay in CLARIOstar Plus plate reader. Blank corrected data was normalized to the total protein amount. Applied materials are indicated in Table S5.

Mitochondrial membrane potential measurements via JC-10

Changes in mitochondrial membrane potential following CM5480 treatment was assessed by JC-10 assay on mouse (FVB/N) pancreatic ductal epithelial organoids in passage number 3. After organoids were collected, they were split into a single cell state for the assay, using 25% TrypLE™ Express Enzyme in PBS. Samples were washed 3 times after the digestion step then cells were counted on a Bürker chamber. For the assay 200 cells/ 0,1 μL solution were used. Cells received either 10 μM CM5480, 100 μM carbonyl cyanide m-chlorophenyl hydrazone (CCCP) or no treatment for 10 minutes in a 37°C, 5% CO2 incubator. Cells were then collected again and resuspended in warm 1xPBS and plated onto a 96 well, glass bottom plate. JC-10 protocol was carried out by the manufacturer's instructions, briefly, cells were incubated with JC-10 dye-loading solution at 37°C, 5% CO2 incubator, protected from light for 30 minutes, then Assay Buffer B was added to the wells before the reding of the fluorescent intensity by CLARIOstar Plus plate reader. Fluorescent intensity was measured at 490/525 nm and 540/590 for ration analysis. Applied materials are indicated in Table S5.

Measurement of mitochondrial oxygen consumption using High-Resolution Respirometry

mPOCs were propagated and used at passage number 4, when organoids were collected and digested for around 15 min in 37°C horizontal shaker (165 rpm) until the Matrigel digested and organoids broke down into individual cells. Pellet was washed with 3 ml wash solution, then cells were regenerated in pre-warmed feeding medium for 30 min in 37°C humidified incubator. For the assessment of respiration following 10 minutes of CM5480 treatment, ductal epithelial cells ($1x10^6$ cells) were carefully suspended and pipetted into Oxygraph chambers (Oxygraph-2k; Oroboros Instruments). Before measurement instrument was calibrated to feeding medium. The measurements were conducted in a 2 mL feeding medium with continuous magnetic stirring at 750 rpm and a temperature of 37°C. In order to prevent the impact of low oxygen levels on mitochondrial respiration, the O2 concentrations in the chamber were maintained between 50–200 μM without reoxygenation, as described by [78,79]. Following a consistent pattern of respiration (without external substances and ADP), ATP synthase was hindered using oligomycin (2.5 μM; leak respiration). By titrating a protonophore (carbonyl cyanide m-chlorophenylhydrazone [CCCP]; final concentration: 0.75 μM/step), the electron transport system's (ETS) capacity was maximized. ETS-independent respiration (also known as residual oxygen consumption, or ROX) was measured in the presence of complex III inhibitor antimycin A (2.5 μM) after complex I inhibition (with 0.5 μM rotenone). We utilized the DatLab 7.3 software from Oroboros Instruments for online display, respirometry data acquisition, and analysis.

Direct Stochastic Optical Reconstruction Microscopy (dSTORM)

HeLa cells were grown on cover glass and co-transfected by plasmid DNA constructs described above. Primary cells from human pancreatic ductal organoids were plated on cover glass after cell separation by TrypLE™ Express Enzyme in the same way as subculturing OCs. Fixation and antigen retrieval were carried out by ice-cold methanol treatment at -20°C for 5 minutes on both cell

Please cite this article in press as: Kiss et al., Store-independent activation of STIM1-ORAI1 by SPCA2 determines the basal CFTR activity in secretory epithelial cells, Current Biology (2025), https://doi.org/10.1038/s44318-025-00470-9

types. Further steps were the same as described for immunofluorescent labeling. At the end of the process, cover glasses were placed in blinking buffer, and dSTORM images were captured by Nanoimager S (Oxford Nanoimaging ONI Ltd.). Cluster analysis of the dSTORM images was performed with the CODI software (Oxford Nanoimaging ONI Ltd.). Applied antibodies, reagents, and other components are listed in Table S7.

FLIM-FRET measurements

YFP or GFP (donor) and mCherry (acceptor) tagged protein constructs were used during the experiments. Fluorescence lifetime (FLIM) measurements were performed using a PicoQuant LSM upgrade kit installed into a Nikon C2+ confocal unit. A special beam splitter unit was designed to easily switch between TCSPC-based FLIM and traditional confocal modes. Picosecond laser diodes operating at 485 nm and 560 nm were used to excite donor and acceptor molecules, respectively. The repetition rate was set to 20 MHz, and a neutral filter with OD1 was used in the excitation path. Images were captured with a 60x, high numerical aperture objective (Nikon CFI Plan Apo Lambda 60x Oil, NA:1.4) to reduce the measurement time and enhance the spatial resolution. First, the donor lifetimes were measured in the 520/35 emission channel in the presence of the acceptor. Then, we bleached the acceptor with a 561 nm wavelength CW laser and measured the donor lifetime in the absence of the acceptor.

QUANTIFICATION AND STATISTICAL ANALYSIS

Fluorescent microscopy

For each curve read from ROI in Ca^{2+} measurements, we calculated the baseline fluorescence ratio (average of the first 20 datapoints of F340/F380 values in each ROI), which were averaged to gain information about the basal Ca^{2+} levels. The extent of the change of the F340/F380 ratio after CM5480 administration was determined and was represented as ΔF340/F380. Correction for bleaching due to the chemical properties of the dyes during the fluorescent microscopy was compensated by drift correction for all curves (and all type of experiments) throughout the data analysis. Leak and bleaching were determined using untreated cells. Each ROIs represent one experiment and the number of samples of different experiments is shown in the bar chart.

Calculation of the basal Ca^{2+} levels and the maximal responses

For each curve read from ROI in Ca^{2+} measurements, we calculated the baseline fluorescence ratio (average of the first 20 datapoints of F340/F380 values in each ROI), which were averaged to gain information about the basal Ca^{2+} levels (Figure S2F). The extent of the change of the F340/F380 ratio after CM5480 administration was determined and was represented as ΔF340/F380. Correction for bleaching due to the chemical properties of the dyes during the fluorescent microscopy was compensated by drift correction for all curves (and all type of experiments) throughout the data analysis. Leak and bleaching were determined using untreated cells. Each ROIs represent one experiment and the number of samples of different experiments is shown in the bar chart.

Calculation of current density and inactivation slope

Current recording was done with PClamp 10 software, and analysis was done with Clampfit software. The ORAI1 current was recorded by 400-ms rapid alterations of membrane potential (RAMP) from -100 to +100 mV from a holding potential of 0 mV. RAMPs were spaced at 4-s intervals. The current recorded at -100 mV was used to calculate current density as pA/pF. When relevant, the inactivation slope was calculated as before.[38]

Definition of co-clusters in dSTORM images

According to the geometry of the ER-plasma membrane junctions membrane contact sites are generally under 300 nm in length in linear profiles.[35] Therefore, in this manuscript we determined the criteria for co-localization clusters with a maximal size of 300 nanometers. The co-clusters were quantified as histograms that indicate information about the blinking frequency and distance of a representative cluster - which is also presented in the image format - showing colocalization of the two proteins of interest within 300 nm. The pie charts show the proportion of clusters, defined as colocalization clusters, within the threshold value as a function of all clusters that have recorded blinking events from only one of these proteins within 300 nm of the cluster centromere.

Calculation of the fluorescent lifetime

The average lifetimes were determined by fitting the arrival time distributions using the Tail Fit method (SymPhoTime 64, PicoQuant). FRET efficiency was calculated for each cell based on the changes in the average donor lifetime ($E = 1 - \tau_{DA}/\tau_D$).

Statistical analysis

All data are expressed as means ± SEM. Shapiro-Wilk normality test was applied. Both parametric (Unpaired t-test or one-way analysis of variance with Tukey's multiple comparisons test) and nonparametric (Mann-Whitney test and Kruskal-Wallis test) tests were used based on the normality of data distribution. P value below 0.05 was considered statistically significant. All statistical analyses were carried out by GraphPad Prism software (Version 8.3.1.).

Current Biology, Volume *35*

Supplemental Information

Store-independent activation of STIM1-ORAI1 by SPCA2 determines the basal CFTR activity in secretory epithelial cells

Aletta Kiss, Árpád Varga, Marietta Görög, Tamara Madácsy, Woo Young Chung, Petra Pallagi, Viktória Szabó, Petra Susánszki, Enikő Kúthy-Sutus, Dániel Varga, Péter Bíró, Ingrid Hegnes Sendstad, Tim Crul, Boldizsár Jójárt, Bálint Tél, Zsófia Horváth, Szintia Barnai, Anita Balázs, György Lázár, Miklós Erdélyi, Shmuel Muallem, and József Maléth

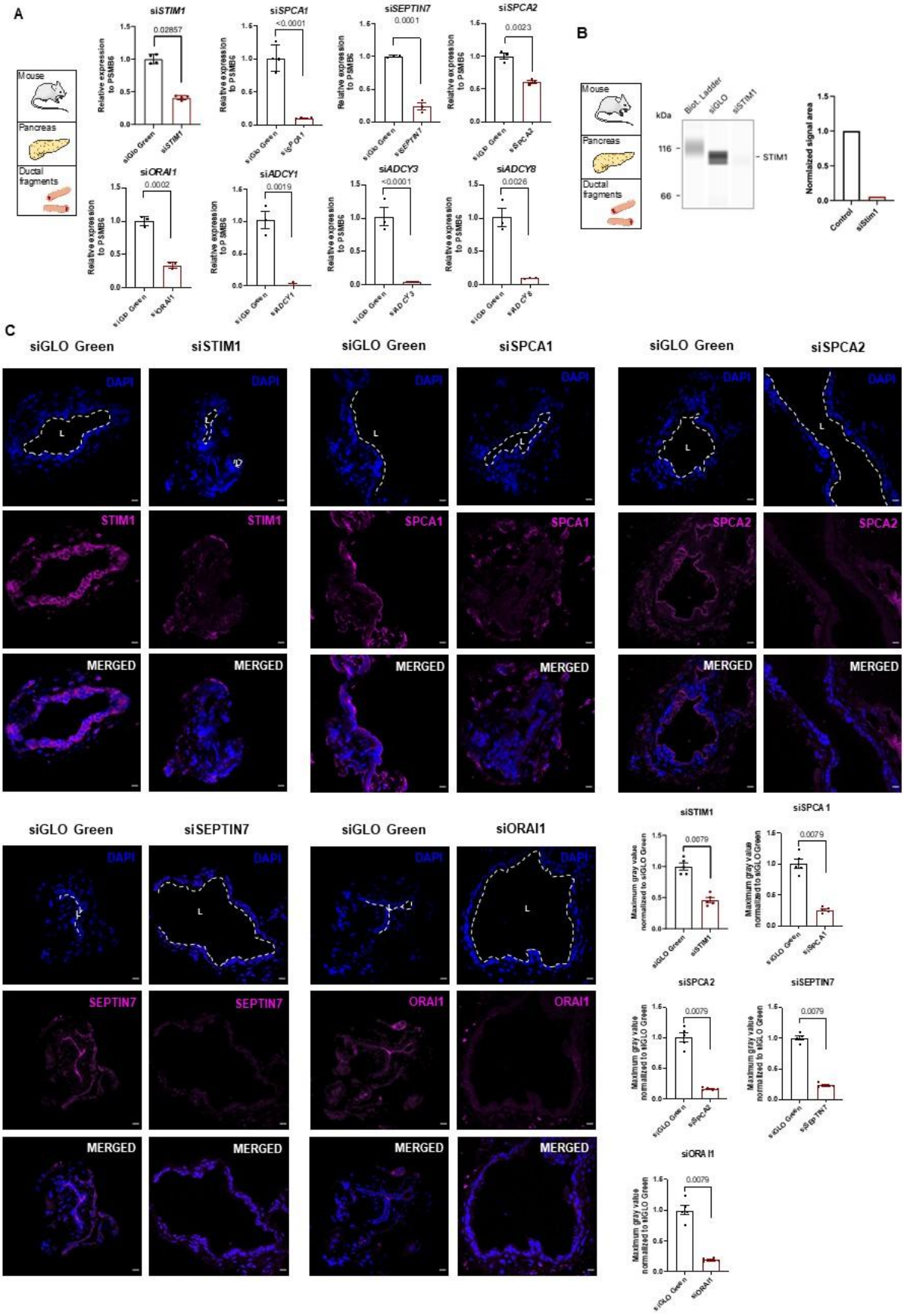
A
Mouse
Pancreas
Ductal fragments
siSTIM1
0.02857
siSPCA1
<0.0001
siSEPTIN7
0.0001
siSPCA2
0.0023
siORAI1
0.0002
siADCY1
0.0019
siADCY3
<0.0001
siADCY8
0.0026
Relative expression to PSMB6
siGlo Green
siSTIM1
siSPCA1
siSEPTIN7
siSPCA2
siORAI1
siADCY1
siADCY3
siADCY8
B
Mouse
Pancreas
Ductal fragments
kDa
Biot. Ladder
siGLO
siSTIM1
116
66
STIM1
Normalized signal area
Control
siStim1
C
siGLO Green
siSTIM1
siSPCA1
siSPCA2
siSEPTIN7
siORAI1
DAPI
STIM1
SPCA1
SPCA2
SEPTIN7
ORAI1
MERGED
L
D
Maximum gray value normalized to siGLO Green
0.0079

Figure S1. Validation of the siRNA mediated gene silencing in mouse isolated ductal fragments. Related to STAR Methods. Isolated ductal fragments were incubated with siRNA for 48 hours (**A-C)**. The efficiency of the pre-validated ON-TARGETplus siRNA SMARTpools on the target genes' expression was verified at the level of mRNA by qRT-PCR (**A.**), by capillary western blotting in the case of STIM1 knockdown (**B.**), and at the protein level by immunofluorescent labelling (**C**.). Due to the high degree of sequence similarity among adenylyl cyclase isoforms, specific antibodies are not available; therefore, validation was performed at the RNA level only. All qRT-PCR raw data were analyzed using the ΔΔCq method. In confocal images, intensity data were collected from three distinct membrane regions per condition, and the maximum values of three independent intensity profiles are plotted in bar charts (scale bar: 10 μm; L: luminal/apical side).

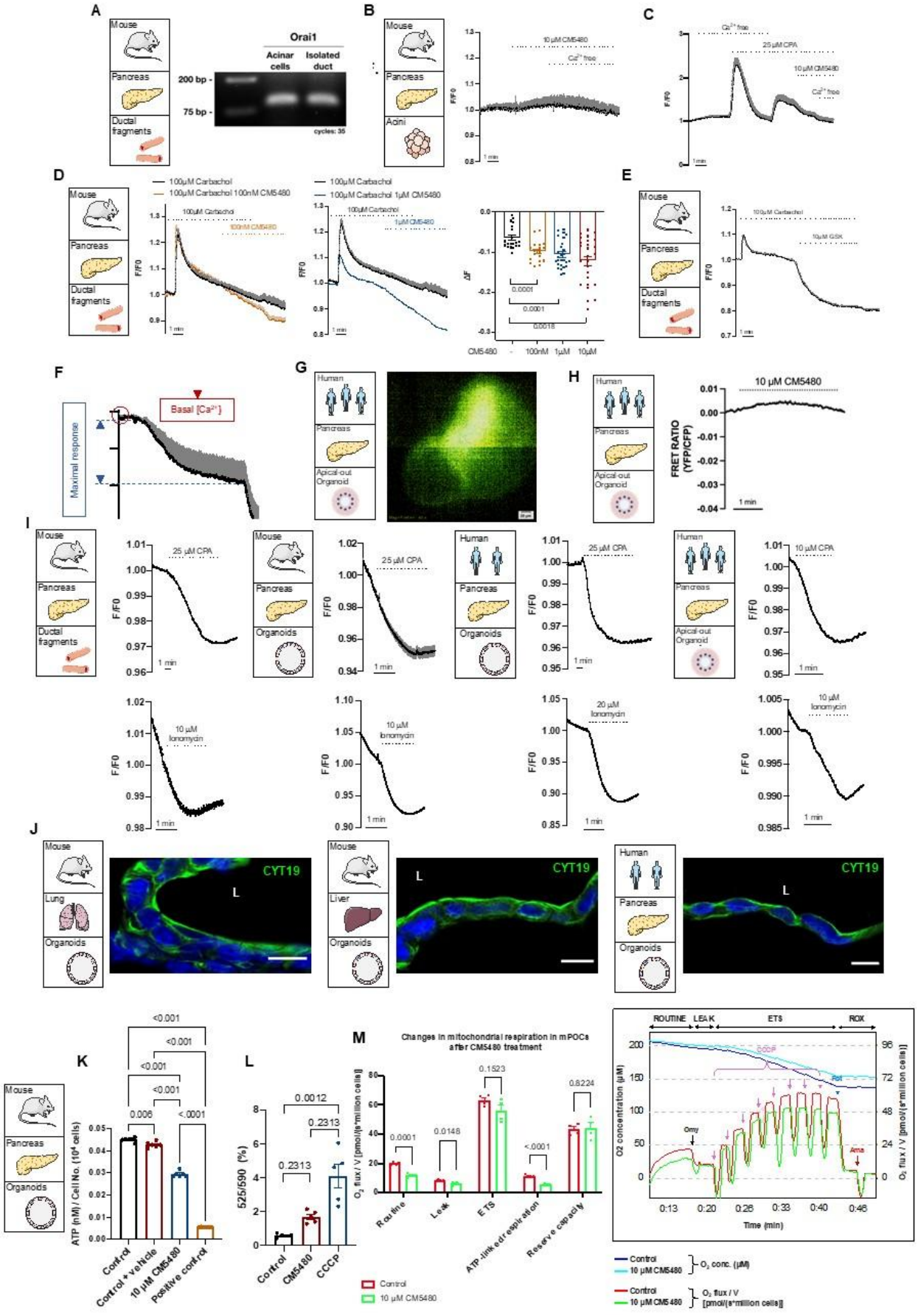
A
Mouse
Pancreas
Ductal fragments
Orai1
Acinar cells
Isolated duct
200 bp
75 bp
cycles: 35
B
Mouse
Pancreas
Acini
10 µM CM5480
Ca2+ free
C
Ca2+ free
25 µM CPA
10 µM CM5480
Ca2+ free
D
Mouse
Pancreas
Ductal fragments
100µM Carbachol
100µM Carbachol 100nM CM5480
100µM Carbachol 1µM CM5480
1µM CM5480
ΔF
0.0001
0.0001
0.0018
CM5480 - 100nM 1µM 10µM
E
Mouse
Pancreas
Ductal fragments
100µM Carbachol
10µM GSK
F
Basal [Ca2+]
Maximal response
G
Human
Pancreas
Apical-out Organoid
H
Human
Pancreas
Apical-out Organoid
10 µM CM5480
FRET RATIO (YFP/CFP)
I
Mouse
Pancreas
Ductal fragments
Organoids
Human
Apical-out Organoid
25 µM CPA
10 µM CPA
10 µM Ionomycin
20 µM Ionomycin
J
Mouse
Lung
Liver
Organoids
Human
Pancreas
CYT19
L
K
Mouse
Pancreas
Organoids
ATP (nM) / Cell No. (10^4 cells)
<0.001
<0.001
<0.001
<0.001
0.006
<.0001
Control
Control + vehicle
10 µM CM5480
Positive control
L
525/590 (%)
0.0012
0.2313
0.2313
Control
CM5480
CCCP
M
Changes in mitochondrial respiration in mPOCs after CM5480 treatment
O2 flux / V [pmol/(s*million cells)]
0.0001
0.0148
0.1523
<.0001
0.8224
Routine
Leak
ETS
ATP-linked respiration
Reserve capacity
Control
10 µM CM5480
ROUTINE
LEAK
ETS
ROX
O2 concentration (µM)
O2 flux / V [pmol/(s*million cells)]
FCCP
Rot
Omy
Ama
0:13
0:20
0:26
0:33
0:40
0:46
Time (min)
Control
10 µM CM5480
O2 conc. (µM)
Control
10 µM CM5480
O2 flux / V [pmol/(s*million cells)]

Figure S2. A. Expression and functional activity of Orai1. Related to Figure 1, 5, and STAR Methods. Agarose gel image of PCR products generated from cDNA templates derived from isolated acini and ductal fragments confirm that the expression of *Orai1* is present in murine exocrine pancreas. **B.** The administration of CM5480 had no effect on the intracellular Ca^{2+} level in the absence of ER depletion in pancreatic acinar cells indicated by the steady fura2-AM signal (N=3). **C.** An average trace of 3 independent experiments demonstrates that the inhibition of ORAI1 significantly decreases the store-operated Ca^{2+} entry in pancreatic acinar cells. **D.** Representation of the dose-dependent effect of CM5480 ORAI1 inhibitor in pancreatic ductal cells. Ductal fragments were stimulated with 100 μM carbachol. The administration of 100 nM, 1 μM and 10 μM CM5480 disrupted the plateau phase of the signal as demonstrated by average traces and bar chart. The plotted data points represent measurement samples (ROIs) from 3 independent experiments. **E.** Average trace shows the effect of GSK-7975A CRAC channel inhibitor on pancreatic ductal epithelial cells upon 100 μM carbachol stimulation. **F.** A schematic explanation of the calculations used in physiological measurements. The site for reading basal intracellular Ca^{2+} is marked in red, while the site for calculating the maximum change in the intracellular Ca^{2+} level is marked in blue. **G.** Epifluorescent image of human apical-out pancreatic organoids following D1ER FRET sensor transfection. **H.** Apical-out human pancreatic organoids transfected with the D1ER FRET sensor showed that 10 μM CM5480 had no effect on ER Ca^{2+} store level. The plotted data points represent measurement samples (ROIs) from 3 independent experiments. **I.** ER Ca^{2+} measurements. The figure show ER calcium depletion in various biological samples. Our findings indicate that the endoplasmic reticulum calcium depletion of isolated ductal fragments, mouse or human pancreatic organoids, and even human apical-out organoids could be similarly triggered by CPA or Ionomycin. Intracellular Ca^{2+} content of the ER was measured using the Mag-Fluo-4 fluorescent dye. Cells were loaded with 5 μM Mag-Flou-4 in HEPES solution. The plotted data points represent measurement samples from 3 independent experiments. **J.** Multiple immunofluorescent labeling of CYT19 protein demonstrates the epithelial identity of mouse lung, liver and human pancreas derived organoids (scale bar: 10 μm; L: luminal/apical side). **K.** The effect of Orai1 inhibition in mitochondrial function. Bar chart show the effect of 10 μM CM5480 on the intracellular ATP content measured by CellTiter-Glo® 3D cell viability assay (N=6). Results are indicated the normalized result to 10^6 cells. **L.** Changes in mitochondrial membrane potential following CM5480 treatment was assessed by JC-10 assay. Fluorescent intensity was measured for ration analysis (N=5). **M.** Bar charts includes measurements of routine respiration, leak state, maximal electron transport system (ETS) capacity, reserve capacity, and ATP-linked respiration, which are presented as O_2 flux/V (pmol/[s × million cells]). All measuring points were adjusted to residual oxygen consumption (ROX) = ETS-independent respiration, therefore the ROX data is not displayed on a separate bar chart. The bar charts display the average values along with their standard error of the mean (mean±SEM). The experimental figures display the chamber O_2 concentrations in control and CM5480-treated cells, providing a representation of the mitochondrial respiration measurements. The maximal capacity of the ETS was reached by gradually adding an uncoupler (carbonyl cyanide m-chlorophenylhydrazone - CCCP). Abbreviations: OMY - oligomycin, CCCP - carbonyl cyanide m-chlorophenylhydrazone, ROT – rotenone, AMA - antimycin A.

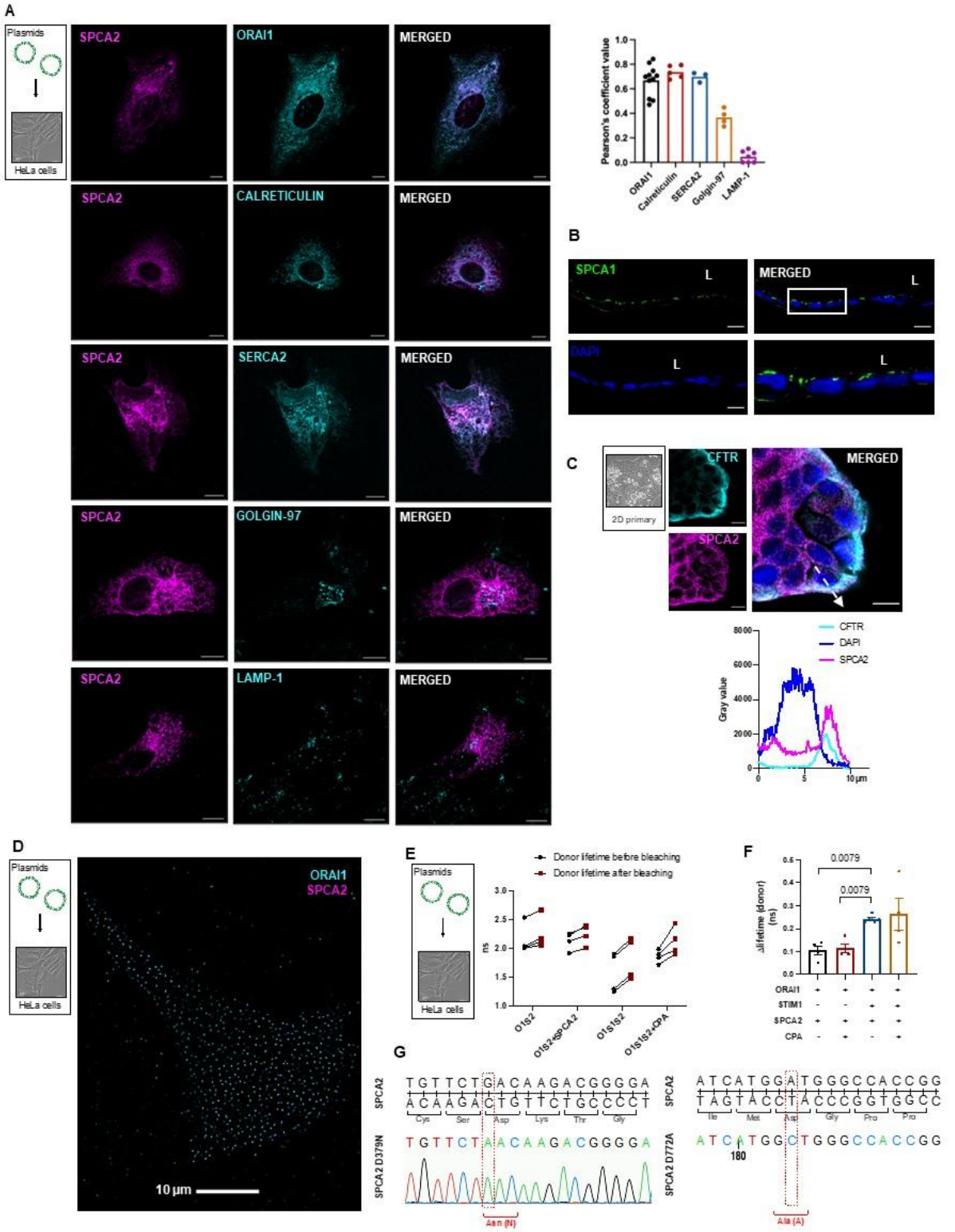

Figure S3. A. Colocalization of SPCA2 with organellar markers. Related to Figure 2. Representative images of transiently transfected HeLa cells co-stained for SPCA2 (magenta) and ORAI1, Calreticulin, SERCA2, Golgin, or Lamp1 (cyan), illustrating partial co-localization of SPCA2 with ER and ORA1. Quantification of Pearson's correlation coefficients is shown in the graph. Scale bars = 10 µm. **B.** Immunofluorescent labeling demonstrates the perinuclear localization of SPCA1 protein in human pancreas derived organoid (scale bar: 10 µm; L: luminal/apical side). **C.** Representative confocal image and line profile analysis demonstrate the localization of CFTR and SPCA2 in human pancreatic organoid culture-derived adherent 2D culture (scale bar: 10 µm).

D. Whole-cell super-resolution (dSTORM) image of a transiently transfected HeLa cell with ORAI1 and SPCA2 immunofluorescent labeling. **E-F.** Donor lifetime changes upon acceptor photobleaching indicating significant elevation in triple transfected (ORAI1, STIM1, SPCA2) group which could not be enhanced further by CPA treatment. **G.** Sanger-sequencing results of *SPCA2* carrying plasmid DNA shows single nucleotide substitutions resulting in amino acid exchange (D379N and D772A).

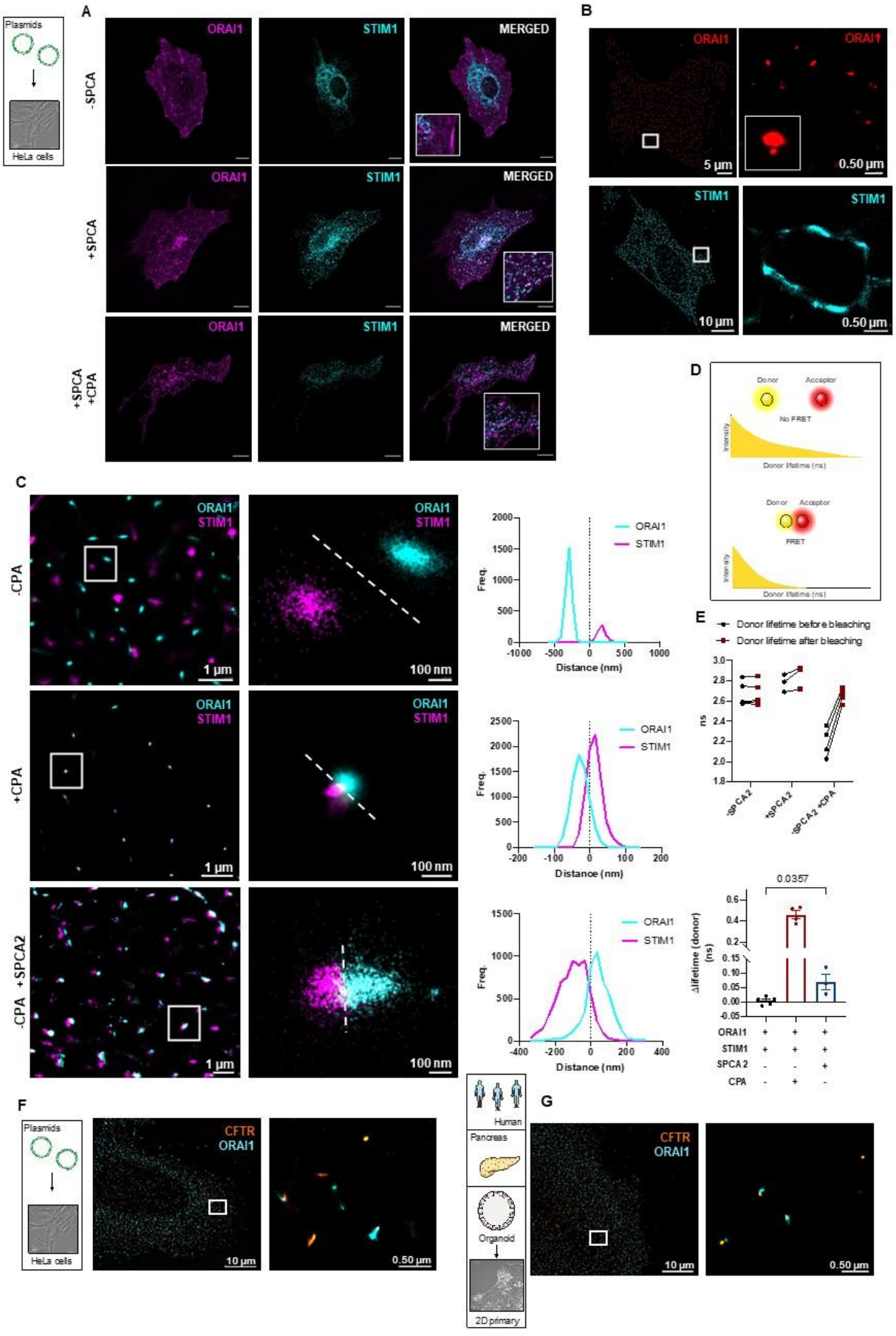
A
Plasmids
HeLa cells
-SPCA
+SPCA
+SPCA +CPA
ORAI1
STIM1
MERGED
B
ORAI1
STIM1
5 µm
0.50 µm
10 µm
C
-CPA
+CPA
-CPA +SPCA2
1 µm
100 nm
Freq.
Distance (nm)
D
Donor
Acceptor
No FRET
FRET
Intensity
Donor lifetime (ns)
E
Donor lifetime before bleaching
Donor lifetime after bleaching
ns
-SPCA2
+SPCA2
-SPCA2 +CPA
0.0357
Δlifetime (donor) (ns)
ORAI1
STIM1
SPCA 2
CPA
F
CFTR
ORAI1
G
Human
Pancreas
Organoid
2D primary

Figure S4. Colocalization of ORAI1 and STIM1. Related to Figure 4 and 5. A. Representative confocal images demonstrate that co-expression of SPCA2 with ORAI1 and STIM1 in HeLa cells changed the localization pattern of ORAI1and STIM1 to a puncta-like distribution which could be further enhanced by 10 μM CPA (scale bar: 10 μm). Merged versions of confocal images also presented in **Figure 4. C. B.** Representative dSTORM images show distributional differences between the membrane localized ORAI1 channels (single focuses) and STIM1 proteins located in the ER membrane resulting in a reticular signal in an unstimulated state. **C.** dSTORM image shows the effect of 25 μM CPA treatment or the presence of SPCA2 in which STIM1 and ORAI1 proteins condense into well demarcated interactional foci in the membrane. **D.** Schematic depiction of the FLIM-FRET measurements and the individual value chart shows the lifetime of the donor fluorophores in nanoseconds recorded during FLIM measurements before and after photobleaching of the acceptor. Individual dots represent single cells. **E.** The bar chart of the calculated change in donor lifetime upon acceptor photobleaching shows significant differences between the double transfected (ORAI1, STIM1) control and the CPA treated or triple transfected (ORAI1, STIM1, SPCA2) but CPA untreated groups. **F.** Images show overlapping distribution of CFTR and ORAI1 proteins in co-transfected HeLa cells **G.** and human pancreas organoid derived 2D adherent culture.

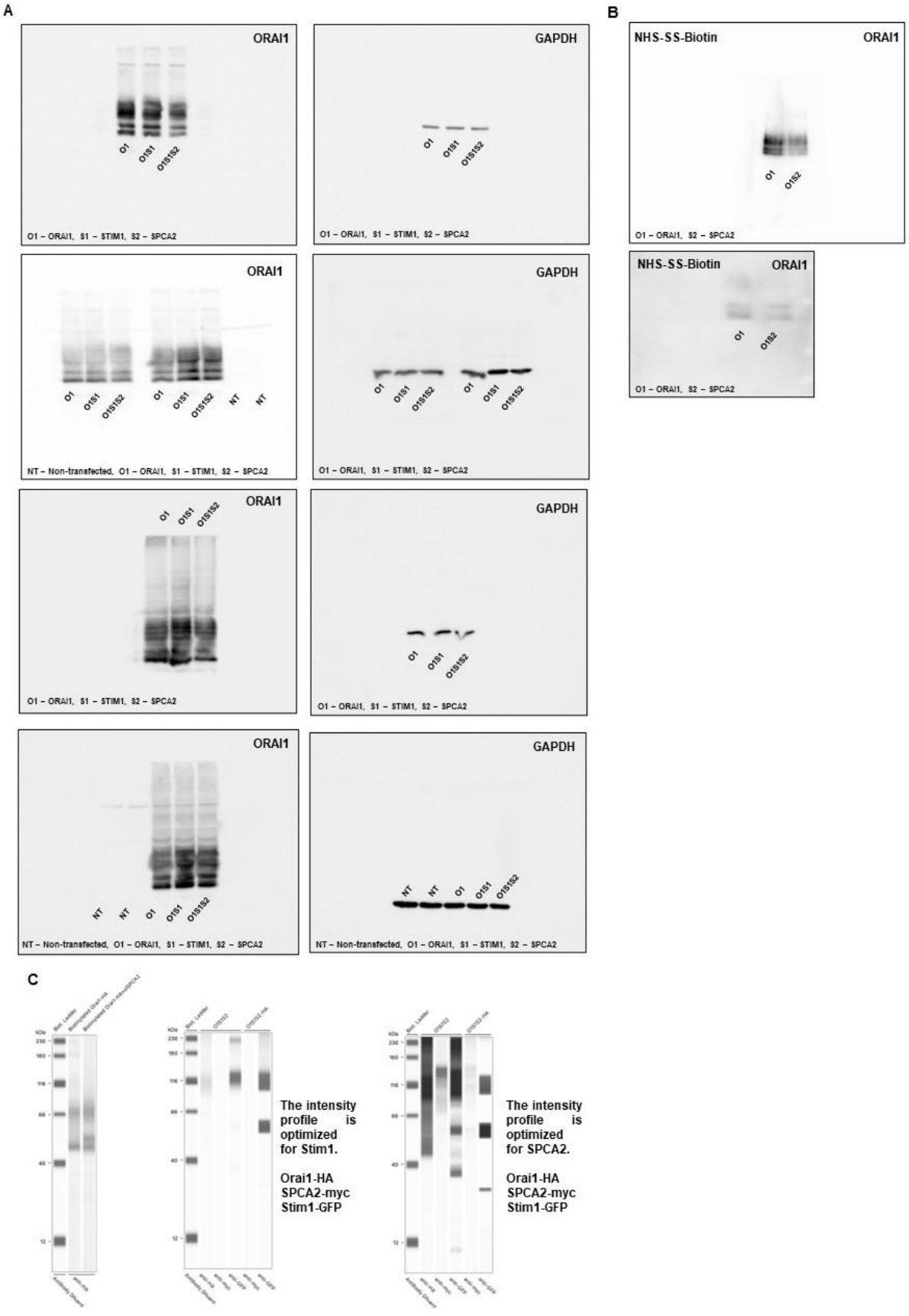
A
ORAI1
GAPDH
O1
O1S1
O1S1S2
O1 – ORAI1, S1 – STIM1, S2 – SPCA2
NT – Non-transfected, O1 – ORAI1, S1 – STIM1, S2 – SPCA2
NT
B
NHS-SS-Biotin
ORAI1
O1S2
O1 – ORAI1, S2 – SPCA2
C
The intensity profile is optimized for Stim1.
Orai1-HA
SPCA2-myc
Stim1-GFP
The intensity profile is optimized for SPCA2.
Orai1-HA
SPCA2-myc
Stim1-GFP

Figure S5. Full-length unedited blot images. Related to Figure 4 and STAR Methods. **A.** Blots of Figure 4.G. **B.** Full-length blot of Figure 4.H. **C.** Full length capillary Western blot images.

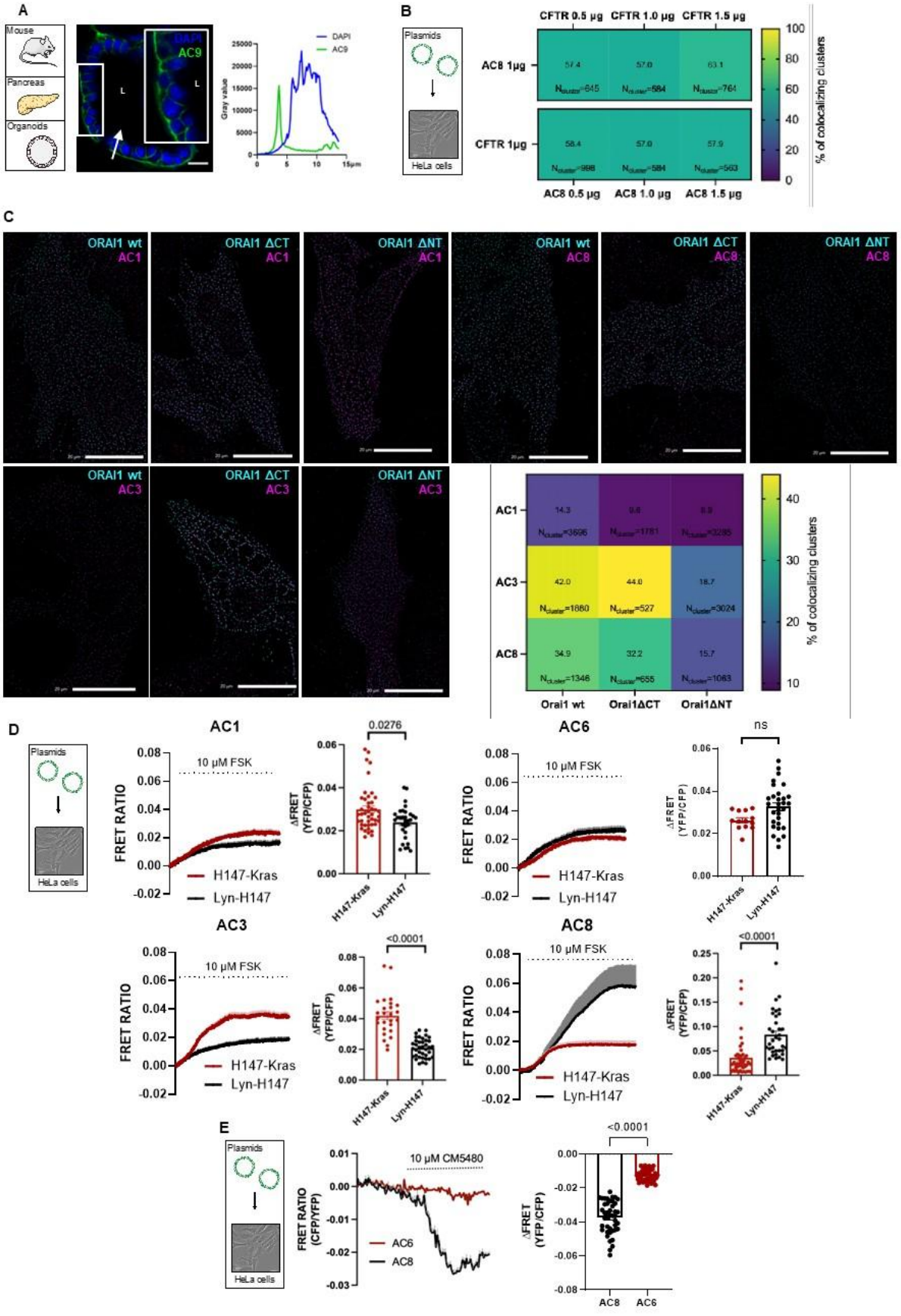

Figure S6. The interaction of Orai1 with ACs. Related to Figure 7. A. Confocal imaging and line profile analysis indicate the basolateral membrane localization of AC9 in mouse pancreatic organoids. (L: luminal side, scale bar: 10 µm).

B. HeLa cells were transfected with constant amounts of one plasmid (either CFTR or AC8 at 1 μg) and increasing concentrations (0.5, 1.0, or 1.5 μg) of the corresponding co-transfected partner (AC8 or CFTR, respectively). Dual-color dSTORM imaging followed by cluster-based colocalization analysis revealed that the proportion of CFTR-AC8 colocalizing clusters (% of total clusters) remained consistent across varying expression levels. The numbers inside each tile of the heatmap indicate the percentage of colocalizing clusters, while $N_{cluster}$ denotes the total number of clusters analyzed under each condition. **C.** dSTORM images and heatmap visualization of nanodomain colocalization between ORAI1 (WT, ΔNT, ΔCT) and adenylyl cyclase isoforms (AC1, AC3, AC8) based on dSTORM imaging. Each square displays the percentage of colocalized clusters relative to total clusters for the respective condition. The $N_{cluster}$ values within each tile indicate the total number of detected clusters. **D.** Average traces and quantification of YFP/CFP ratio changes measured using Lyn-H147 (raft) and H147-Kras (non-raft) cAMP sensors upon forskolin stimulation in cells expressing AC1, AC3, or AC8. For visualization the curves were inverted to represent the increase of cAMP production. Bar graph shows pooled quantification of maximal FRET ratio change (mean ± SEM); statistical analysis was performed using Mann-Whitney test (indicated p-values). Data were derived from 3-4 independent experiments. **E.** Average FRET ratio traces (YFP/CFP) measured with the Lyn-H147 cAMP sensor upon 10 μM CM5480 treatment. For visualization the curves were inverted to represent the decrease of cAMP production. Right: Bar graph quantifying ΔFRET response shows significantly greater cAMP reduction in AC8-versus AC6-expressing cells.

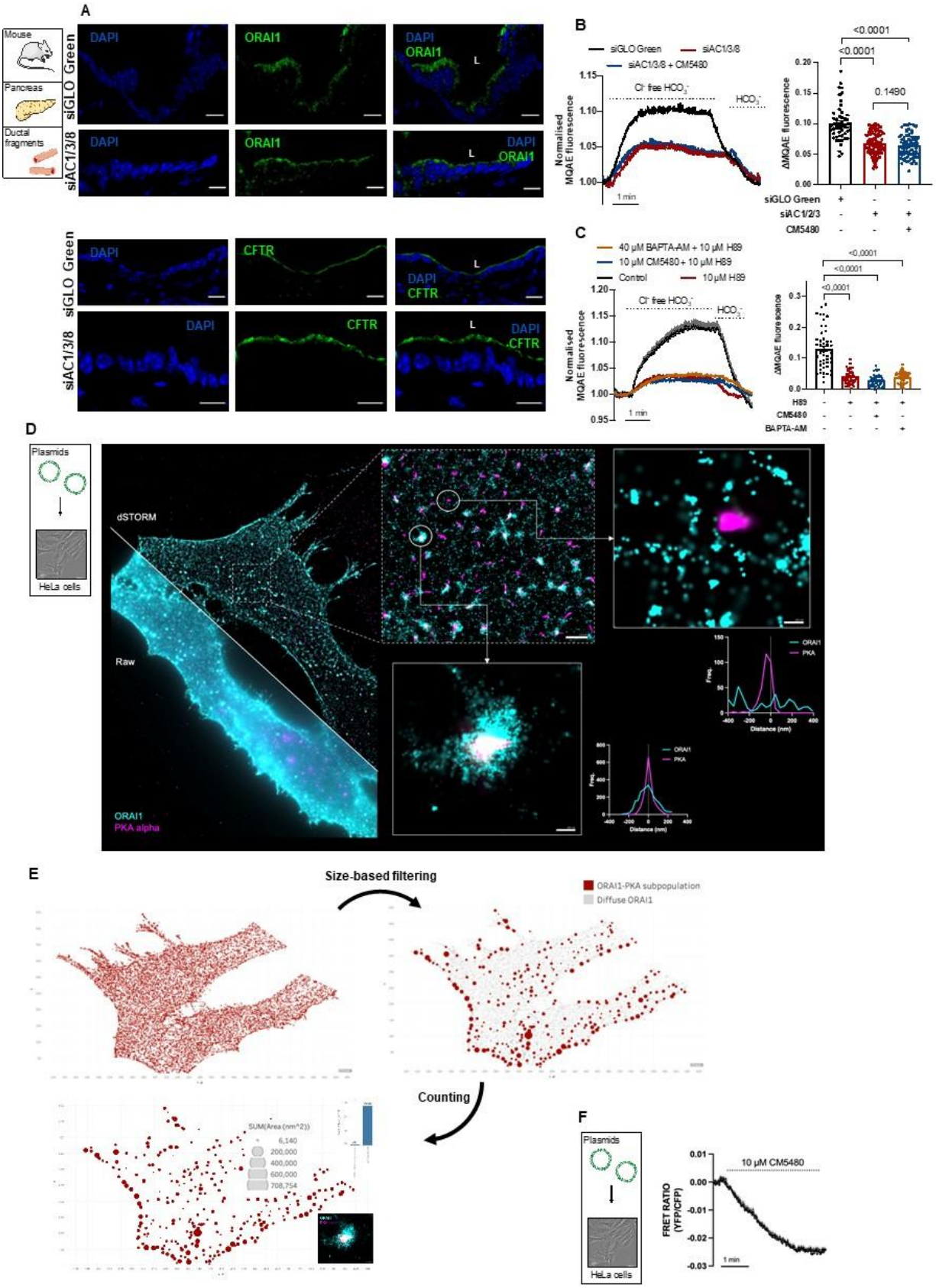

Figure S7. The expression and interaction of ACs with Orai1 in ductal cells. Related to Figure 7. A. Apical localization of CFTR and ORAI1 proteins is retained after 24 h of siAC1/3/8 gene knockdown in isolated mouse pancreatic ductal fragments. **(**L: luminal/apical side, scale bar: 10 μm) **B.** Average traces and summary bar charts from 4-6 independent experiments show that simultaneous gene silencing of AC1, AC3, or AC8 significantly

reduced CFTR-mediated anion secretion, assessed by MQAE fluorescence upon Cl^- withdrawal, in mouse isolated ductal fragments. **C.** Average traces and bar chart demonstrate that CFTR mediated Cl^- efflux was significantly decreased by 10 μM H89 PKA inhibitor and in combination with 40 μM BAPTA-AM Ca^{2+} chelator or 10 μM CM5480. Data are presented as mean ± SEM. **D.** Representative dual-color dSTORM image showing the subcellular distribution of ORAI1 (cyan) and PKAα (magenta) in HeLa cells. Raw and super-resolution images reveal heterogeneous ORAI1 cluster organization, including large focal aggregates that colocalize with PKAα. Insets show two levels of zoom highlighting distinct ORAI1 distribution patterns and their overlap with PKAα. The blinking frequency distribution plots represent localization density as a function of distance from the cluster center for ORAI1 and PKA. **E.** Cluster segmentation and analysis were performed using the CODI pipeline. Cluster coordinates were imported into Tableau Public software for visualization. Size-based filtering excluded clusters smaller than 4000 nm^2, a threshold established by re-identifying clusters in the raw data to distinguish diffuse and focal ORAI1 populations. The remaining clusters were classified as either ORAI1-PKA overlapping (red) or non-overlapping (grey), and are represented with dot size proportional to area. Quantification shows that ~2.1% of all detected ORAI1 clusters colocalize with PKAα. **F.** In HeLa cells transfected with ORAI1, application of 10 μM CM5480 induced a robust decrease in AKAP79-AKAR4 FRET ratio, indicating reduced PKA activity.

Adherent Cell cultures		
Component	Manufacturer	Cat.No.
HeLa cell line	ATCC	ATCC-CCL-2
HEK-293 cell line	ATCC	CRL-1573
DMEM	Gibco	41965
FBS	Gibco	10500064
Kanamycin Sulfate	Gibco	15160054
Antibiotic-Antimycotic Solution	Gibco	15240062
Penicillin/Streptomycin	Gibco	15070063
GlutaMax™	Gibco	3505006
L-WRN cell line	ATCC	ATCC-CRL-3276
ATCC-formulated DMEM	ATCC	ATCC-30-2002
G-418	Gibco	11811031
Hygromycin B	Invitrogen	10687010
Isolation of pancreatic ductal fragments and acinar cells		
DMEM/F12	Sigma	D6421
Collagenase purified	Worthington	LS005273
Soybean Trypsin Inhibitor	ThermoFisher Scientific	17075029
Bovine Serum Albumin (BSA)	Pan-Biotech	P061391100
HBSS	Sigma	H9269
FBS	Gibco	10500-064
L-Glutamine	Gibco	25030149
Mouse and human organoid cultures (OCs)		
Matrigel	Corning	354234
24-well plate	Greiner	662160
TrypLE™ Express Enzyme	Gibco	12605028

Table S1. List of consumables used for cell culture and primary cell isolation. Related to STAR Methods.

Mouse and human organoid cultures (OCs)		
Spitting Media		
Component	Manufacturer/Cat.No.	Final cc/volume
Advanced DMEM/F-12	Gibco, Catalog No.: 12634-010	500 ml
1 M HEPES	Gibco, Catalog No.: 15630080	5 ml (10 mM)
GlutaMax Supplement (100X)	Gibco, Catalog No.: 35050061	5ml (1X)
Primocin (400X)	Invivogen, Catalog No.: ant-pm-2	1,25 ml (1X)
Digestion Media		
Splitting media	-	19,0984 ml
Collagenase IV.	Worthington, Catalog No.: LS004188	1250 U/ml

Dispase	Sigma-Aldrich, Catalog No: D4693-1G	0,5 U/ml
FBS	Gibco, Catalog No: 10500064	0,5 ml 2,5%
Soybean Trypsin Inhibitor	Sigma-Aldrich, Catalog No: T9128-1G	1mg/ml
Kanamycin Sulfate	Gibco, Catalog No: 15160054	200 µl 1X
Antibiotic-Antimycotic Solution	Gibco, Catalog No: 15240062	200 µl 1X
Voriconazole (25mg/ml)	Tocris, Catalog No: 3760/10	1,6 µl (cc:2 µg/ml)
Wash Media		
Splitting media	-	47,7484 ml
FBS	Gibco, Catalog No: 10500064	1,25 ml (2,5%)
Kanamycin Sulfate	Gibco, Catalog No: 15160054	500 µl (1X)
Antibiotic-Antimycotic Solution	Gibco, Catalog No: 15240062	500 µl (1X)
Voriconazole (25mg/ml)	Tocris, Catalog No: 3760/10	4 µl (cc:2 µg/ml)
Feeding Medium		
Splitting media	-	22,808 ml
A-83	TOCRIS, Catalog No: 2939	500 nM (50 µl)
EGF	Gibco, Catalog No: PMG8041	50 ng/ml (5 µl)
FGF	Gibco, Catalog No: PHG0360	100 ng/ml (5 µl)
Gastrin I	TOCRIS, Catalog No: 3006	0.01 µM (5 µl)
N-acetylcytsteine	Sigma-Aldrich, Catalog No: A9165-56	1.25 mM (125 µl)
Nicotinamide	Sigma-Aldrich, Catalog No: NO636-100G	10 mM (500 µl)
B-27 Supplement (50X)	Gibco, Catalog No: 17504001	1X (1ml)
L-WRN conditioned media	-	25 ml
Y-27632 Rho-Kinase Inhibitor	TOCRIS, Catalog No: 1254	10.5 µM (50 µl)
Prostaglandin E2 (PGE2)	TOCRIS, Catalog No: 2296	1 µM (50 µl)
Kanamycin Sulfate	Gibco, Catalog No: 15160054	1X (500 µl)
Antibiotic-Antimycotic Solution	Gibco, Catalog No: 15240062	1X (500 µl)
Voriconazole (25mg/ml)	Tocris, Catalog No: 3760/10	4 µl (cc:2 µg/ml)

Table S2. List and composition of solutions used for organoid generation. Related to STAR Methods.

Constructs, transfection and site-directed mutagenesis		
Component	Manufacturer	Cat.No.
Cover glass	VWR	ECN 631-1583
ADCY1-myc-DDK	ORIGENE	RC237562
ADCY3-myc-DDK	ORIGENE	RC220272
ADCY6-myc-DDK	ORIGENE	RC214902
ADCY8-myc-DDK	ORIGENE	RC211815
pcDNA-D1ER	Addgene	36325
SPCA2-myc-DDK	ORIGENE	RC212990
SPCA2-tGFP	ORIGENE	RG239585
Lipofectamine 2000	Invitrogen	11668019
Opti-MEM	Gibco	31985070
Q5 Site-Directed Mutagenesis Kit	New England BioLabs	E0554S
Gene knockdown		
siGLO Green transfection indicator	Horizon	D-001630-01
Lipofectamine 2000	Invitrogen	11668019
Opti-MEM	Gibco	31985070
Stim1 siRNA	Dharmacon	L-062376-00-0005
Cftr siRNA	Dharmacon	L-042164-00-0005
Orai1 siRNA	Dharmacon	L-056431-02-0005
Spca1 siRNA	Dharmacon	L-041293-00-0005
Spca2 siRNA	Dharmacon	L-065820-01-0005
SPCA2 siRNA	Dharmacon	L-006280-00-0005
Septin7 siRNA	Dharmacon	L-042160-01-0005

Table S3. List of commercially available plasmids, siRNA pools and consumables used for gene expression manipulations. Related to STAR Methods.

Constructs, transfection and site-directed mutagenesis				
Primers for site-directed mutagenesis				
Name	5’-3’			
SPCA2 D379N Fwd. mut. primer	TGTTCTAACAAGACGGGGA			
SPCA2 D379N Rev. primer	GAGAACGCTGCAGCAAC			
SPCA2 D379N Fwd. Seq. primer	TCATTGGCTGGTCGCAAGG			
SPCA2 D772A Fwd. mut. primer	ATCATGGCTGGGCCACC			
SPCA2 D772A Rev. primer	GATGTTGATCCATAGGATCTGC			
SPCA2 D772A Fwd. Seq. primer	GCCGCCAACATGATCCTG			
qRT-PCR Primers				
Name	5’-3’	Target NCBI	Position	Product
Orai1 Fwd	CTTCGCCATGGTAGCGAT	NM_175423.3	484-501	91 bp
Orai1 Rev	TGTGGTGCAGGCACTAAAGA		574-555	
Psmb6 Fwd	CTGACAAGCTGACCCCTATC	NM_008946.4	298-317	106 bp
Psmb6 Rev	TGGAAACCAAGCTGGTAAGT		403-384	
Adcy1 Fwd	CCCAGCCTAAGACGGATCAC		1190-1209	

Adcy1 Rev	CAGCCACGGATGTGATGGTA	NM_009622.1	1267-1248	78 p
Adcy3 Fwd	GGACTCTCCTATGGTGGCCT	NM_001159537.1	2982-3001	70 bp
Adcy3 Rev	CCTGTCAGTGCCATTGAGCC		3051-3032	
Adcy8 Fwd	GGAGGAATCCCTGGGAGGAT	NM_009623.2	2812-2831	179 bp
Adcy8 Rev	ACGATGTCTTCAGGCAAGCA		2990-2971	
Septin7 Fwd	AAAGACTGTACAGGTGGAGCA	NM_001359736.1	649-669	101 bp
Septin7 Rev	CCACTGCATCTCCAAATCCTG		749-729	
Atp2c1 Fwd	CTGCAATTGCCATCGCTAGTC	NM_001359822	2154-2174	71 bp
Atp2c1 Rev	GACTTCTTCCCCAGACACGG		2224-2205	
Atp2c2 Fwd	CTGTCGCTCTCAGACCAAGC	NM_026922.1	2718-2737	81 bp
Atp2c2 Rev	AGGGACCCAAGGACTGAGTA		2798-2779	
SPCA2 Fwd	GAAGAAACTCGGCTTCTCGG	NM_001286527.3	108-127	86 bp
SPCA2 Rev	CACTCTGTTCATCAATCAAGGCT		193-171	
SPCA2C Fwd	GGGAGCGCTTGATTTGCTG	NM_001286527.3	2877-2895	113 bp
SPCA2C Rev	GCATCTGGACTCTCTTGGGG		2989-2970	

End-point and qRT-PCR analysis		
Component	Manufacturer	Cat.No.
NucleoSpin RNA XS kit	Macherey-Nagel	740902.50
iScriptTM cDNA Synthesis kit	Bio-Rad	1708890
DreamTaq Hot Start DNA Polymerase	ThermoFisher Scientific	EP1702
Gene expression analysis of mouse pancreatic ductal organoid culture by RNA-Seq		
NucleoSpin RNA Plus kit	Macherey-Nagel	740984.250

Table S4. List of primers and consumables for site-directed mutagenesis, end-point PCR and RNAseq. Related to STAR Methods.

Immunofluorescent labeling for confocal microscopy		
Component	Manufacturer	Cat.No.
Shandon Cryomatrix	ThermoFisher S.	6769006
Cryostat	Leica	CM 1860 UV
Microscope slides	ThermoFisher S.	J3800AMNZ
PFA	Alfa Aesar	43368
PBS	Sigma	P4417-100TAB
Sodium Citrate	Sigma	71402
Tween-20	Sigma	P1379
Goat Serum	Sigma	G9023
Bovine Serum Albumin (BSA)	Pan-Biotech	P061391100
Recombinant Anti-ADCY9/AC9 antibody	Abcam	ab191423
Anti-CFTR antibody	Abcam	ab2784
Extracellular Anti-Orai1 Antibody	Alomone labs	ACC-062
Orai1 Antibody	Alomone labs	ACC-060
Cytokeratin 19 Antibody	ThermoFisher S.	MA5-31977ATP
ATP2C1 monoclonal antibody (SPCA1)	Novus Biologicals	H00027032-M01
ATP2C2 polyclonal antibody (SPCA2)	Invitrogen	PA567396

ATP2C2 antibody	Invitrogen	PA521127
Anti-STIM1 antibody	Cell Signaling Tech.	5668
SEPTIN7 polyclonal antibody	ThermoFisher S.	13818-0-AP
Calreticulin	Invitrogen	PA3-900
SERCA2 ATPase Monoclonal antibody	Invitrogen	MA3-919
Golgin-97	Invitrogen	PA530048
Lamp1	Invitrogen	53-1079-42
Goat anti-Rabbit Alexa 488	ThermoFisher S.	A11034
Donkey anti-Mouse Alexa 647	ThermoFisher S.	A31571
Western blot, Cell Surface Biotinylation and Co-immunoprecipitation		
1X DPBS	ThermoFisher Scientific	14190250
Cell Scraper	Greiner	54170
RIPA lysis buffer (10X)	EMD Millipore Corp.	20-188
cOmplete ULTRA Tablets, Mini, EASYpack	Roche	05892970001
30% Acrylamide/Bis Solution 29:1	Bio-Rad	1610156
UltraPure™ TEMED	Invitrogen	15524-010
NuPAGE LDS Sample Buffer (4X)	Invitrogen	NP0007
10X TG	Bio-Rad	161-0771
10X TGS	Bio-Rad	161-0772
Immun-Blot PVDF Membrane	Bio-Rad	1620177
anti-GAPDH	Cell Signalling Technology	5174S
anti-HA-Tag	Cell Signalling Technology	3724
ClarityTM Western ECL Substrate	Bio-Rad	1705060
Goat anti-Rabbit peroxidase conjugate	Merck Millipore	A8275
Pierce™ Cell Surface Biotinylation and Isolation Kit	ThermoFisher Scientific	A44390
12-230 kDa Separation Module, 8 x 25 capillary cartridges	Biotechne	SM-W004
Anti-Rabbit Detection Module	Biotechne	DM-001
Anti-Mouse Detection Module	Biotechne	DM-002
Total Protein Detection Module	Biotechne	DM-TP01
RePlex™ Module	Biotechne	RP-001
20X Anti-Rabbit HRP Conjugate	Biotechne	043-426
Dynabeads™ Protein A for Immunoprecipitation	ThermoFisher Scientific	10002D
Myc Tag Polyclonal antibody	Thermo Scientific	A21281
Anti- HA-tag antibody	Cell Signaling Technology	3724S
Fluorescent microscopy		
Poly-L-lysine	Sigma	P8920-100ML
Cover glass	VWR	ECN 631-1583
Fura2-AM	Invitrogen	F1201
MQAE	Invitrogen	E3101
Mag-Fluo-4	Invitrogen	M14206
BCECF-AM	Invitrogen	B1170
CPA	Tocris	1235
CM5480	Provided by CalciMedica	
GSK-7975A	Sigma	5.34351
Carbamylcholine chloride (Carbachol)	Sigma	PHR1511
Forskolin	Tocris	1099

CFTRinh-172	Biotechne	3430
BAPTA-AM	Sigma	A1076
In vivo fluid secretion		
Ketamine	-	-
Xylazine	-	-
Secretin	Sigma-Aldrich	S7147
Current recording		
1X DPBS	ThermoFisher Scientific	14190250
Vertical puller	Narishige	PC-10
Amplifier	Molecular Devices	Axopatch 200B
Digitalizer	Axon Instruments	Digidata 1440A
Cell viability assay		
96-well Lumitrac microplate	Greiner	655075
CellTiter-Glo® 3D cell viability assay	Promega Corporation	G9681
Mitochondrial membrane potential measurements via JC-10		
JC-10 assay	Abcam	ab112134
TrypLE™ Express Enzyme	Gibco	12605028
96-well glassed bottom plate	VWR	734-1609

Table S5. List of consumables of the applied experiments. Related to STAR Methods.

Fluorescent microscopy					
		Applied solutions			
Component	Manufacturee Cat.No.	Standard HEPES pH=7.5	Ca^{2+} free HEPES pH=7.5	Standard HCO_3^-	Cl^- free HCO_3^-
NaCl	Sigma, S9888	140 mM	142 mM	115 mM	-
KCl	Sigma, P3911	5 mM	5 mM	5 mM	-
$MgCl_2$	Sigma, M2670	1 mM	1 mM	1 mM	-
$CaCl_2$	Sigma, 223506	1 mM	-	1 mM	-
HEPES	Sigma, H3375	10 mM	10 mM	-	-
Glucose	Sigma, G8270	10 mM	10 mM	10 mM	10 mM
$NaHCO_3^-$	Sigma, S6014	-	-	25 mM	25 mM
EGTA	Sigma, E4378	-	1 mM	-	-
Na-gluconate	Sigma, S2054	-	-	-	115 mM
K_2SO_4	Sigma, P9458	-	-	-	2.5 mM
Mg-gluconate	Sigma, M7554	-	-	-	1 mM
Ca-gluconate	Sigma, C8231	-	-	-	6 mM

Table S6. Composition of the solutions used in fluorescent microscopy. Related to STAR Methods.

Direct Stochastic Optical Reconstruction Microscopy (dSTORM)		
Component	Manufacturer	Cat.No.
Methanol	Sigma	34860
Two-component adhesive	Picodent	1300 7100

Cavity slides	Sigma	BR475505-50EA
Myc Tag Polyclonal antibody	Thermo Scientific	A21281
Anti- HA-tag antibody	Cell Signaling Technology	3724S
Anti- CFTR antibody	Abcam	ab2784
Extracellular Anti-Orai1 Antibody	Alomone labs	ACC-062
PKA alpha polyclonal antibody	Invitrogene	PA517626
Donkey anti-Mouse Alexa 647	ThermoFisher S.	A31571
Goat anti-Chicken Alexa 647	Thermo Scientific	A32933
Goat anti-Rabbit Alexa 568	Thermo Scientific	A11011
Goat anti-Mouse Alexa 488	Thermo Scientific	A11001
Blinking buffer		
Glucose Oxidase	Sigma, G2133-50KU	100 U
Catalase	Sigma, C100	2000 U
Glucose	Sigma, G8270	55,56mM
Cysteamine hydrochloride	Sigma, M6500	100 mM
PBS	Sigma, P4417-100TAB	Final volume: 1 mL

Table S7. List of consumables and solutions used in dSTORM experiments. Related to STAR Methods.